Application of CFD in Membrane Technique

Der Fakultät für Ingenieurwissenschaften, Abteilung Maschinenbau der

Universität Duisburg-Essen

zur Erlangung des akademischen Grades

DOKTOR-INGENIEUR

genehmigte Dissertation

von

Wei Ding

aus

Shuyang, Jiang Su, V.R.China

Referent: Prof. Dr.-Ing. habil. Rolf Gimbel

Korreferent: Prof. Dr.-Ing. Thomas Melin

Tag der mündlichen Prüfung: 11.10.2012

Acknowledgements

This work was created during my study and work as a research assistant at the Universität Duisburg Essen, Institute für Maschinenbau, Verfahrenstechnik Wassertechnik. I am deeply indebted to the following people for their help throughout the project.

In particular, I am deeply indebted to my doctoral advisor Prof. Dr. –Ing Rolf Gimbel. He always was supported my work and gave me enough patience. He has decisively promoted my work by his critical suggestions and sharing his experience during the research.

I am deeply indebted to Prof. Dr. –Ing Thomas Melin from Aachener Verfahrenstechnik (AVT) RWTH Aachen, for being my second examiner and for his critical contributions and suggestions to my dissertation.

I am deeply indebted to Dr. –Ing. Stefan Panglisch from IWW Rheinisch-Westfälisches Institut für Wasserforschung gGmbH in Mühlheim a. d. Ruhr (IWW Water Center) and present at Inge AG. He was always interested in my work and gave me valuable and critical suggestions which bring this work to a successful end.

Gratitude is expressed to all my former research teammates at the Universität Duisburg Essen. They let me participate in a lot of research experience, theoretical knowledge and practical know-how.

And last, but not least, thanks goes to my immediate family and friends who have been an important and indispensable source of spiritual support. Special thanks to my wife Xiaowang, Wang. She gave me love and support all the time.

Contents

Abstract

Recently the use of low pressure membrane filtration systems, i.e. ultra- and microfiltration membrane filters, increases rapidly in the water technology field. The performance of a membrane filtration system is strongly influenced and limited by its design. German membrane manufacturers inge AG and Microdyn-Nadir GmbH designed special membrane filtration systems recently: a ultrafiltration membrane filtration system built by series of in/out capillary modules and a submerged microfiltration membrane filtration system built by series of pillow-shaped membrane plates. Both of these two new designs are as compact and flexible as possible. However a compact and flexible design can be in trouble with the performance of the filtration system. There is a need to do the optimization between the compact, flexible design and the performance of the filtration system.

Computational Fluid Dynamics (CFD) involves the solution of governing laws of fluid dynamics numerically. CFD models can be used to analyze different influencing parameters of a hydraulic system like the membrane filtration system. These influencing parameters can be geometry parameters or operation conditions. In the conventional CFD simulations, membrane filtration systems are considered on the microscopic scale and the CFD models were well developed. However on the macroscopic scale, the conventional CFD models have extremely high time and computer hardware strength requirement. In this work, with help of several methods, a new macroscopic scale membrane simulation tool will be developed and introduced.

A **Calibration-Library-Interpolation** method is employed which successfully solves the conflict between accuracy and time/hardware strength requirement of the simulation. The CFD tool becomes simple, easy, highly flexible and economical with the help of this method compared with the traditional CFD models.

The scale method is also applied in this work due to the special dimension problem of membranes. The CFD simulation is based on the discretized meshes of geometry. The mesh quality determines the performance of the simulation. Equilateral geometry mesh has the best quality. The pillow-shaped membrane plate has a thickness of millimeter-range, a length and a height of meter-range and the capillary membrane has a diameter of millimeter-range and a length of meter-range. If the membrane geometry is discretized with high quality mesh, then the mesh number will be too large to be simulated and the time and hardware strength requirement will be too high. The scale method can be applied here to solve the problem of the high time/hardware strength requirement of simulation caused by the high quality mesh. In some certain systems, like in the microfiltration system built by Microdyn-Nadir, because of the pressure difference at different sides of membrane plate, the geometry of membrane plate can be compressed. This scale model can solve the problem caused by this kind of geometry change like compression too.

The pillow-shaped membrane plate consists of two membrane sheets and one spacer to support and prevent the sticking of these two sheets. The spacer is built by porous fiber networks, which has very complex geometry which is difficult to simulate with traditional CFD tools. For simplification, **porous media approximation** method based on Modified Navier Stokes equation is employed in this work instead of complex geometry simulation.

After the validation by experiments, this CFD tool is very useful to help the designer of the membrane system. It can be used to find the optimal solution between the design and performance of membrane system. This new CFD model can be also applied for other membrane systems that the systems are built up of identical substructures with just a slight adaptation. Using the new CFD model saves time and money as expensive tests don't have to be conducted.

Keywords: *Computational Fluid Dynamics; Membrane Filtration System; Friction Loss; Calibration-Library-Interpolation Method; Optimization of Design; T-rack; BioCel®;*

1. Introduction

1.1 Introduction and Objective

In the recent decades, membrane technology has been used more and more widely in water treatment processes. The advantage of membrane technology is its reliability, low energy consumption, high efficiency and also it is relatively easy to operate and maintain, since there is no phase transition like in evaporation. More and more membrane filtration systems built up from single elements and modules are designed and produced by different companies at present. In order to be more competitive in the market, the membrane filtration system becomes more and more compact and flexible. However the compact and flexible design can be in trouble with the performance of the filtration system which causes a necessity to optimize, between the compaction, flexibility and the performance of the system. Depending on the design of the membrane elements or modules respectively their arrangement in a filtration system including the pipes can cause a significant additional pressure loss, which can be possibly avoided by a better design.

Company inge designed a new ultrafiltration capillary membrane system named T-rack system (see Figure 1.1.1). According to the manufacturer, T-rack system has 50% less installation space requirement and 5% lower cost than the conventional rack systems. A basic T-rack unit is constructed with four feed (inflow) pipes, one permeate pipe and eight capillary modules named *Dizzer 5000 plus* which are also produced by inge (see Figure 1.1.2). *Dizzer 5000 plus* has a membrane surface area of 50 m^2 and is able to produce about 5 m^3/h high quality water. The standard diameter of feed pipes is 142 mm, and the standard diameter of permeate pipe is 235 mm. Customers can decide to use several basic T-rack units to build their own systems according to their individual demand and local conditions. The details of T-rack system are introduced in Chapter

3.8.1.

Figure 1.1.1 T-rack system built by inge AG

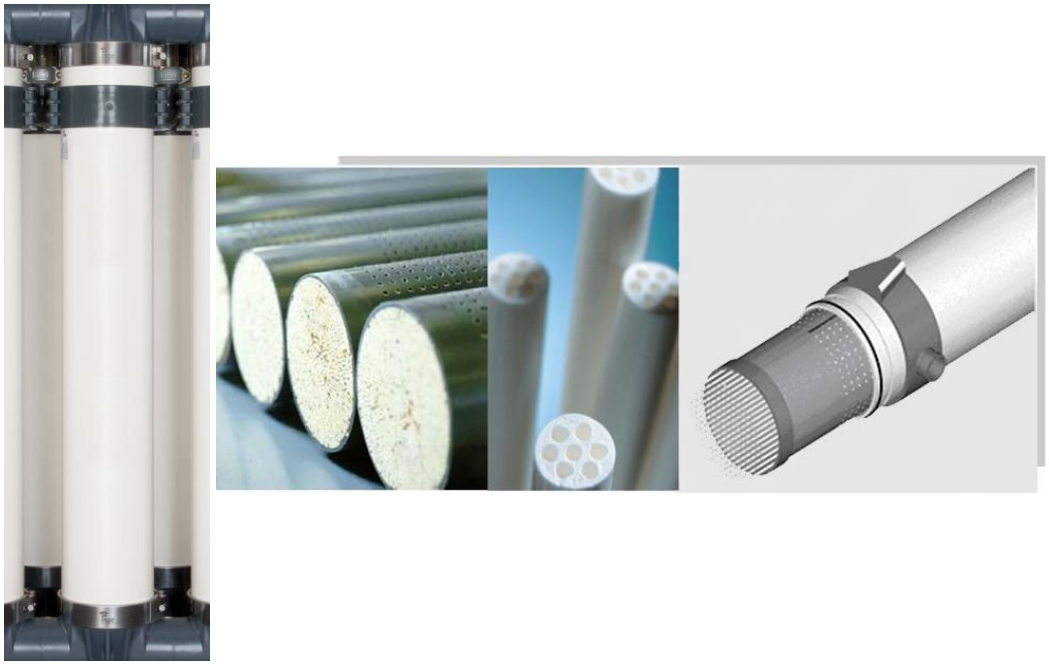

Figure 1.1.2 *Dizzer 5000 plus* and multi-pore® capillary fibers in the module (from inge AG)

Dizzer 5000 plus module is 1680 mm in height and constructed with an inner cylinder and an outer cylinder. The inner cylinder is designed to optimize the pressure distribution

in the module (especially in backwash process) and it supports the capillaries in the module. The inner diameter of inner cylinder is 225 mm and the distance between inner and outer cylinder is on average 6 mm. The Multibore® capillary membrane used in *Dizzer 5000 plus* is also produced by inge. One fiber has 7 capillaries of each 0.9 mm inner diameter (see Figure 1.1.2). In order to directly connect the feed pipes to the modules, a special T-connector was designed (see Figure 1.1.3).

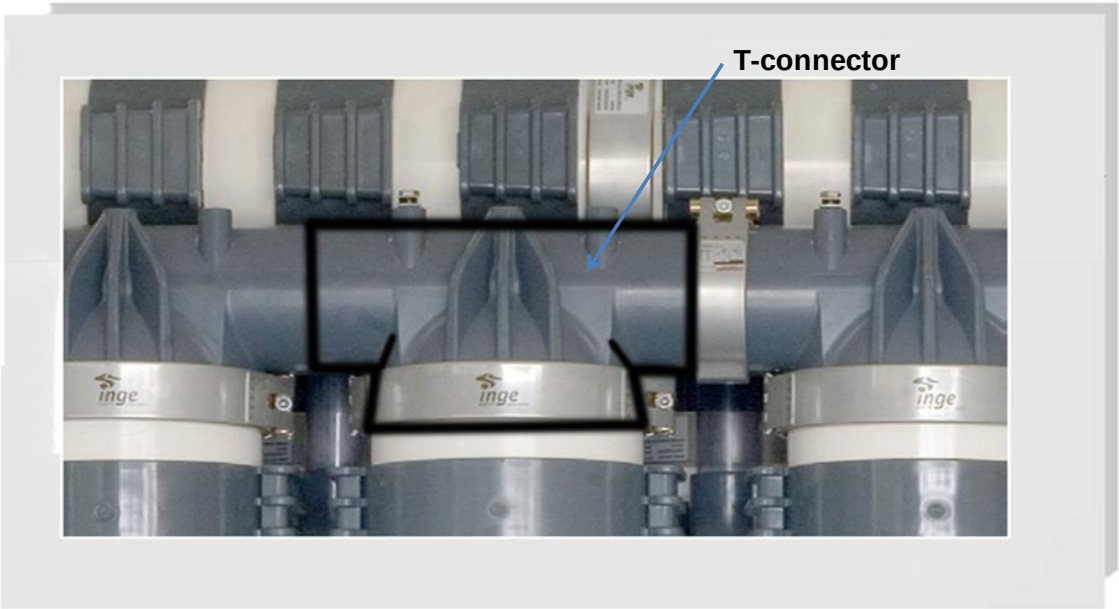

Figure 1.1.3 *Dizzer 5000 plus* with T-connectors

Microdyn-Nadir GmbH also designed a new special membrane filtration system in order to get more market share. They successfully build a compact system named BioCel® membrane filtration system with microfiltration pillow-shaped membrane plates. Membranes with a pure water permeability of around 500 l/(m²hbar) are used. Pillow-shaped membrane plates are constructed by two flat sheet membranes and one permeate spacer between them. The membrane plates are used in a submerged mode with negative pressure. One or more suction pipes are integrated on both sides of one element (see Figure 1.1.4). A basic membrane filtration module consists of several plates connected with seals and arranged in a box with an aeration chamber at the bottom. The box has one dead-end side and one suction port where the connection to the piping

system takes place (see Figure 1.1.4). Geometry, number, installation location of the suction pipe and geometry of the pipe connector between suction pipe and external piping system should be optimized by the CFD tool. The details of the simulation, prediction, and optimization of the BioCel® system are introduced in the Appendix A.

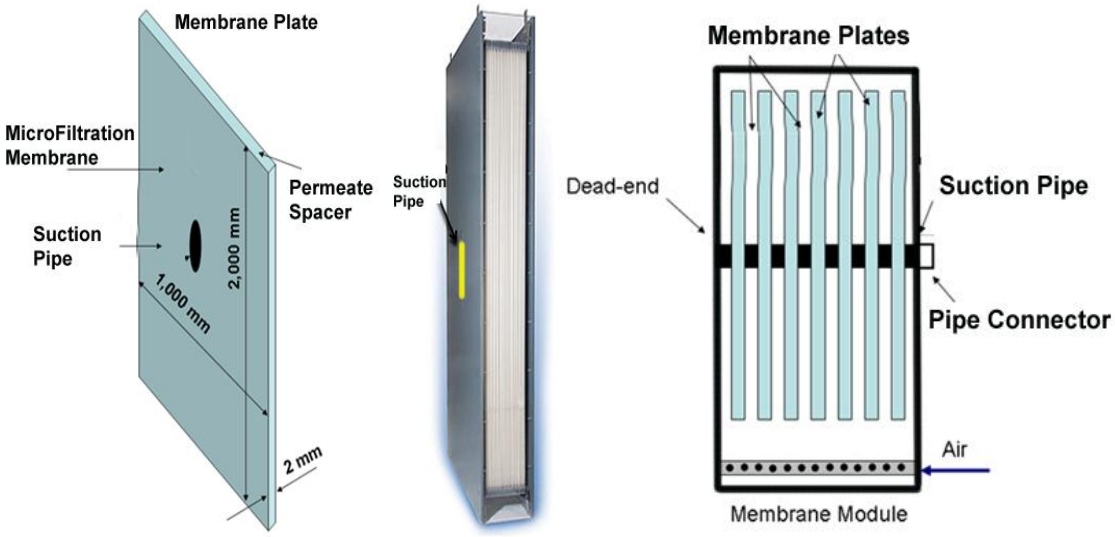

Figure 1.1.4 BioCel® membrane filtration system with quasi-ellipsoid suction pipe built by Microdyn-Nadir GmbH

In order to save investment costs and easy to be constructed and operated by customers, both T-rack and BioCel® membrane filtration systems are designed to be as compact and flexible as possible. However especially the compactness may conflict with the efficiency of the system. Therefore the geometry design of different parts of the system and operational parameters which can influence the performance homogeneity, the energy consumption and productivity of the system should be known and understood. The performance homogeneity can show whether the permeation flows of different modules in one system are of the same quality. In this work, the required driving pressure of the system (pump pressure) is used to stand for the energy consumption. The productivity is defined as the ratio of the volume of permeation flow to the consumed energy.

For low pressure driven membrane systems, filtration performance is very sensitive to

the driving pressure. In fluid dynamics, when fluid flows through a piping system smaller pipe size will lead to higher pressure loss with same flow volume[1]. Especially when the piping system causes turbulences, the pressure loss of fluid increases strongly (see Figure 1.1.7).

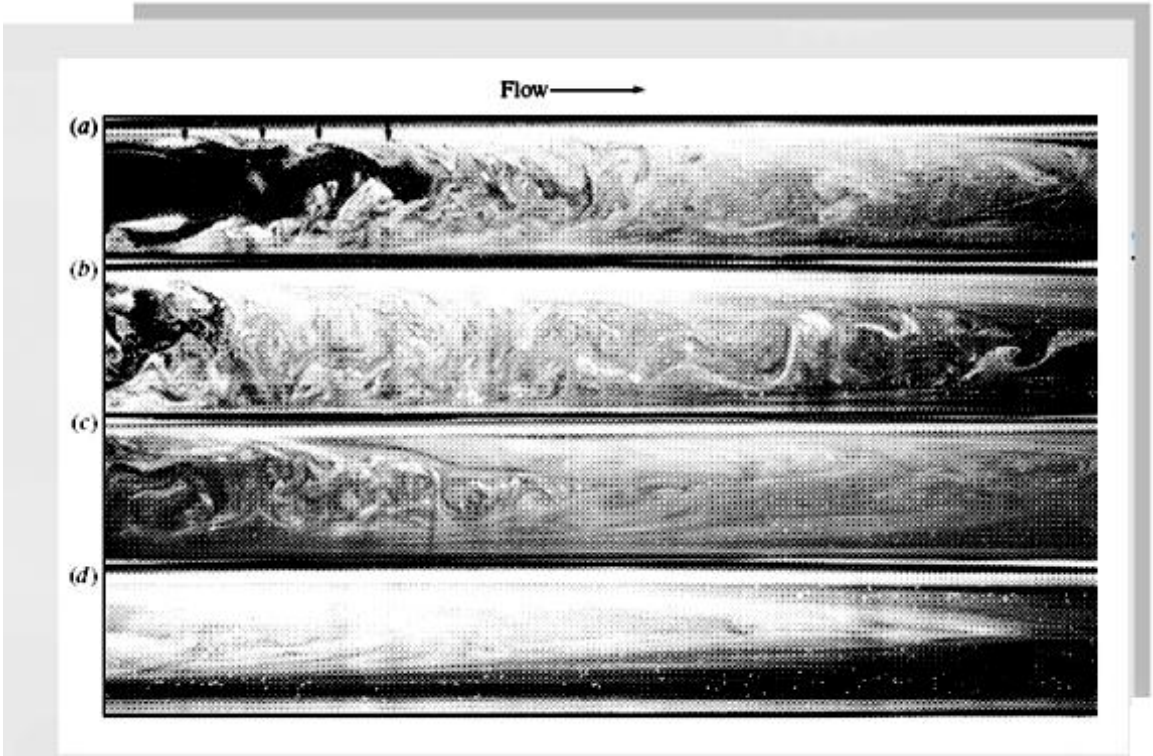

Figure 1.1.7 Formation of a turbulent puff in pipe flow; a) and b) near the entrance; c) somewhat down-stream; d) far downstream [4]

Furthermore, the complex geometry of pipe connectors or valves, where fluid velocity value or direction is changed, will cause more pressure loss which can be quantified with K-value (see Table 1.1.1) [1]. K-value or so called Pressure Loss Coefficient relates the geometry and roughness of system components (see Chapter 3.3.2).

Table 1.1.1 Pressure Loss Coefficient for Open Valves, Elbows and Tees [1]

Nominal diameter [in]									
	Screwed				Flanged				
	½	1	2	4	1	2	4	8	20
Valves (fully open):									
Globe	14	8.2	6.9	5.7	13	8.5	6.0	5.8	5.5
Gate	0.3	0.24	0.16	0.11	0.80	0.35	0.16	0.07	0.03
Swing check	5.1	2.9	2.1	2.0	2.0	2.0	2.0	2.0	2.0
Angle	9.0	4.7	2.0	1.0	4.5	2.4	2.0	2.0	2.0
Elbows:									
45° regular	0.39	0.32	0.30	0.29					
45° long radius					0.21	0.20	0.19	0.16	0.14
90° regular	2.0	1.5	0.95	0.64	0.50	0.39	0.30	0.26	0.21
90° long radius	1.0	0.72	0.41	0.23	0.40	0.30	0.19	0.15	0.10
180° regular	2.0	1.5	0.95	0.64	0.41	0.35	0.30	0.25	0.20
180° long radius					0.40	0.30	0.21	0.15	0.10
Tees:									
Line flow	0.90	0.90	0.90	0.90	0.24	0.19	0.14	0.10	0.07
Branch flow	2.4	1.8	1.4	1.1	1.0	0.8	0.64	0.58	0.41

Hence, the objective of my study is to identify a suitable CFD tool to simulate and analyze the most significant parameters such as geometry of different parts (pipe, connectors etc.) and operational parameters (pressure, inlet position, etc.) which impact the pressure loss or efficiency respectively of the inge T-rack and Microdyn-Nadir BioCel® membrane filtration system, and then to find out the influencing mechanisms of these parameters. By the simulation, the membrane filtration system can be optimally designed and the operational parameters can be identified which can satisfy both

customers' demand and local conditions. The developed CFD tool had to be easy to apply with the regular computers and the time for simulation had to be shortened as much as possible.

2. Theoretical Background

2.1 Membrane Technology

2.1.1 Membrane and Membrane Classification

A membrane is a thin semi-permeable layer typically less than 1 mm-thick, which has different permeability for substances that pass through it. Membranes have very closed relationship with our life, for example, bio-membrane exists in every living body and it is the basis of life. The application of membrane in industry began from the recent decades. Figure 2.1.1 displays a magnification picture of capillary membrane, and shows that a membrane consists of very thin skin layer and a support layer.

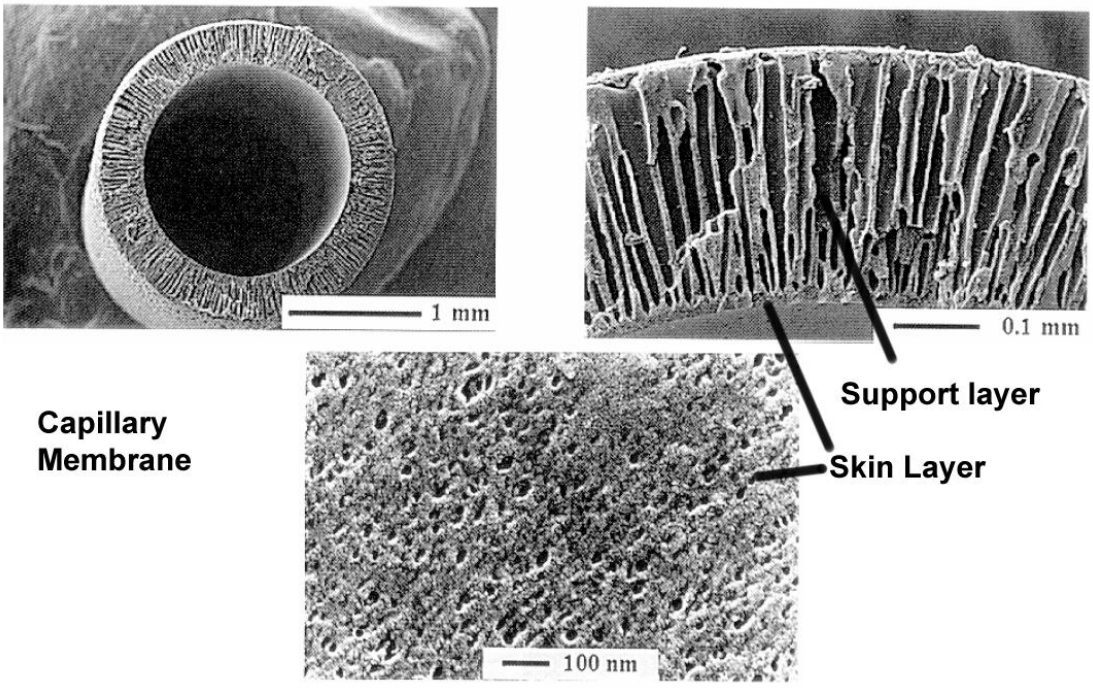

Figure 2.1.1 Structure of capillary membrane from IWW

Membrane filtration process is a modern separation technique, which usually uses pressure as the driving force. The separation mechanism is to use different permeabilities of species to them from each other.

There are many ways to classify membrane and membrane processes, for example by the flow regime, mechanism, operation mode, membrane materials and so on [9]. For membranes, one can classify e.g. porous and non-porous membranes by their porosity; symmetric and asymmetric membranes by their structures; organic and inorganic membranes by their materials. For membrane processes, one can classify e.g. low pressure or high pressure membranes by their driving pressure; cross flow and dead-end by operation mode.

Low pressure membrane filtration processes like micro- and ultrafiltration (MF and UF) are very efficient and many different substances can be separated, such as solid particles, algae, bacteria, colloids, protozoa, and so on [9, 12]. High pressure membrane filtration processes as reverse osmosis (RO) and nanofiltration (NF) are used to remove specific dissolved contaminants (e.g. pesticides, nitrate, radionuclides). RO and NF are widely applied to produce potable water from brackish or sea water, which is not involved in our project.

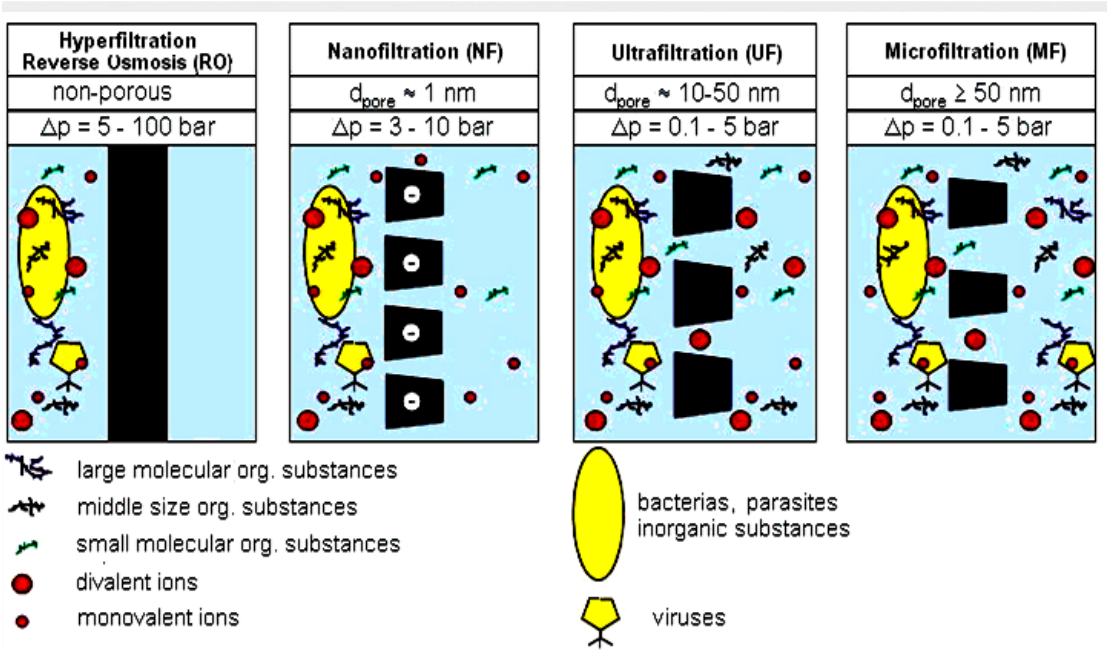

Figure 2.1.2 Membranes: reverse osmosis, nanofiltration, ultrafiltration and microfiltration [9]

Figure 2.1.2 shows the distinction of different membranes. Reverse osmosis (RO)

membrane is non-porous. This is one reason that the driving pressure for RO is the highest and almost all substances in water are rejected except water molecules. The other reason for the high driving pressure in RO membrane filtration process is to overcome the high osmotic pressure [9, 12]. According to the different pore size of membranes, further membrane filtration processes are classified into microfiltration (MF), ultrafiltration (UF) and nanofiltration (NF). MF membrane has the largest pore size among these three membranes, therefore, it needs the lowest driving force and only large substances like bacteria or parasites can be rejected. NF membrane has pore size around 1 nm and the driving force is higher than for UF and MF membranes. With NF membranes many substances in water can be rejected, e.g. viruses, dissolved organic substances and a part of divalent ions. UF membrane has properties between NF and MF membranes. It is widely used in water treatment plants.

Figure 2.1.3 shows two common operation forms of membrane processes which are called dead-end filtration and cross flow. In the filtration process, the flow entering into the process is named feed, the flow passing the membrane is named permeate.

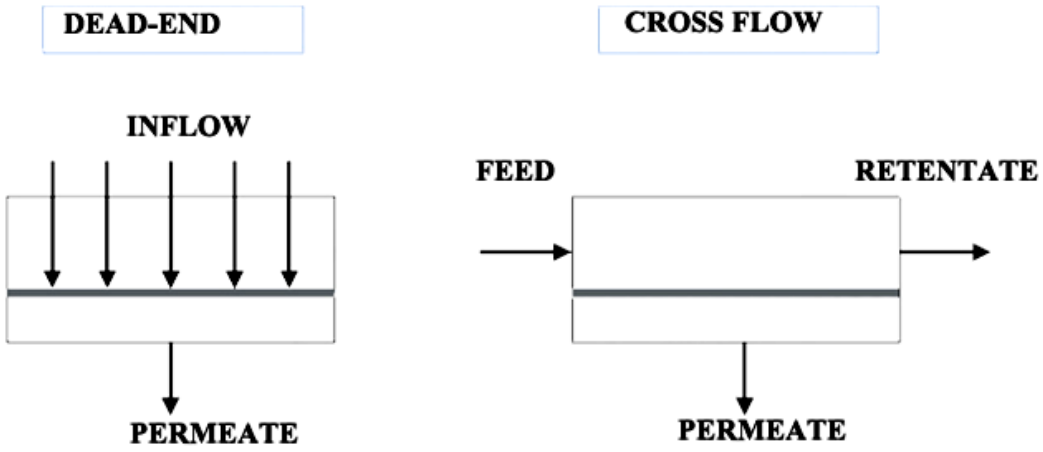

Figure 2.1.3 Dead-end and cross flow filtration [12]

In dead-end filtration, the flow direction is perpendicular to the membrane surface. Under the driving pressure all of the fluid passes the membrane and all of the particles

that cannot pass through the pores of the membrane are rejected. So all solids accumulate on the membrane surface during the filtration cycle and have to be removed by the backwash process. Backwash process is an important process in membrane technique which is used to maintain the filtration capacity of the membrane. In the backwash process, fluid flows through the membrane against the flow direction in the filtration process and takes the accumulated solids formed during filtration process away.

Compared to the dead-end filtration process, the cross flow filtration process has a different flow profile. The feed flow direction in the retentate side is parallel to the membrane surface. The concentrated flow on the membrane surface will be diluted by the feed flow which is helpful to maintain the filtration efficiency and reduce fouling. The flow with concentrated solution will flow out of the module parallel to the membrane surface which is named retentate or concentrate. The retentate can be returned to the feed line and re-circulated. As the shear stress created by the parallel flow is proportional to the quantity of cross flow velocity, sufficient cross flow velocity should be kept to carry solids away instead of accumulating on the membrane surface.

The dead-end filtration is easier in operation and it usually needs lower energy and therefore it has higher productivity; but periodic backwash cycles are essential to remove particles accumulated on the membrane surface. The cross flow filtration must be operated under a sufficient flow velocity, so it needs more energy to re-circulate the retentate. During the filtration process particles are removed with retentate, so the interval between backwashes is longer [12].

2.1.2 Membrane Filtration Systems

In recent years, a lot of different membrane filtration systems have been built in order to apply the membrane technique in water treatment plant. The choice for a certain kind of membrane system is determined by a great number of aspects, such as costs, permeation

demand, packing density, feed water qualities and operation conditions. Membrane filtration systems are preferred to enable large surface area membrane in a unit volume. There are two main types, called the flat sheet membrane system and the tube membrane system. Flat sheet membrane systems may consist of spiral wound membranes or pillow-shaped membranes [12]. Tube membrane systems may consist of tubular, capillary or hollow fiber membranes.

Spiral wound membrane system consists of two layers of membrane, placed onto a permeate collector fabric named spacer normally. This membrane flat sheet is wrapped around a centrally placed permeate pipe shown in Figure 2.1.4. With this structure, the system can have high packing density of the membranes. The feed channel is filled with a certain height feed spacer which is used to prevent sticking of the membrane unit. Spiral wound membrane system is commonly only used for NF and Reverse Osmosis (RO) applications.

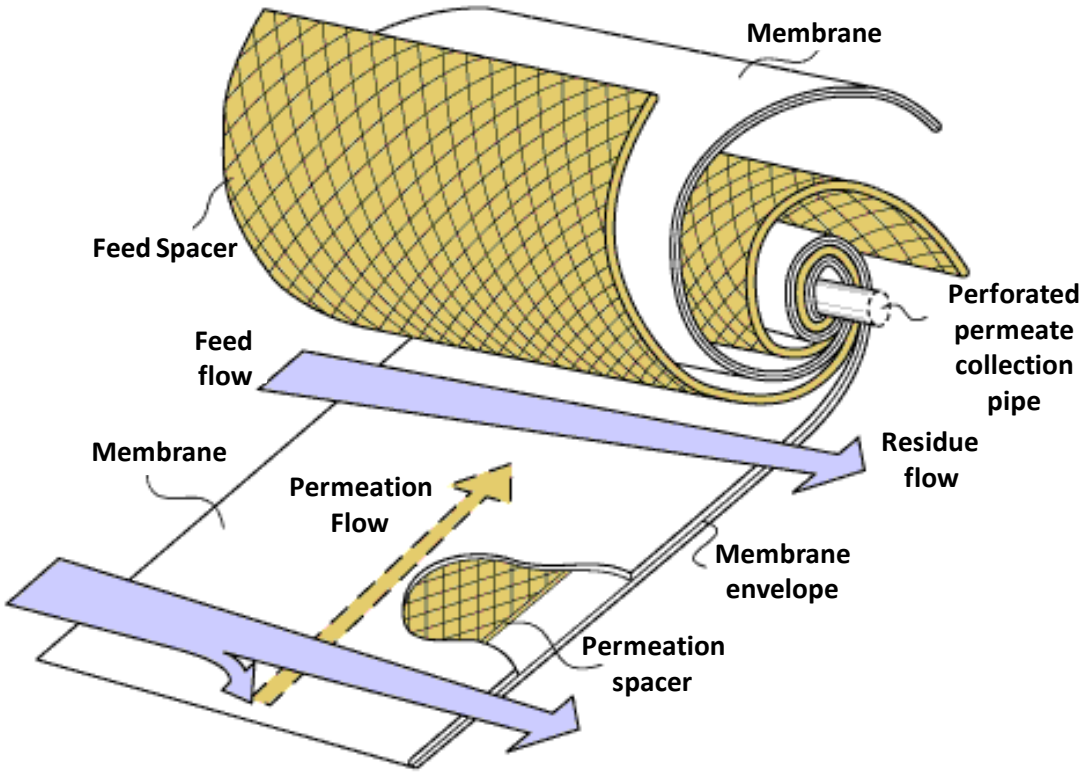

Figure 2.1.4 Spiral wound membrane system built by MTR (from MTR®)

Pillow-shaped membrane system that consists of flat sheet membranes and supporting spacer is also called membrane plate system. The name pillow-shaped membrane comes from the pillow-like look that two membranes have when they are packed together in a module. In the plates there is a spacer preventing the two membrane sheets sticking together. Within a module, multiple pillows are placed with a certain distance between them, which depends on the dissolved solids content of the water. The water flows through the membranes by “out/in”, then the permeate is directly collected by the suction pipe and carried away. The BioCel® membrane filtration system which is produced by Microdyn Nadir is built by these kinds of membrane plates.

From the size of tube diameter, the tube membrane system can be classified into tubular membrane system with diameter of the tube between 5 to 15 mm, capillary membrane system with diameter between 0.5 to 5 mm and hollow fiber membrane system with diameter less than 0.5 mm. The tubular membrane system (see Figure 2.1.5) is usually built by non self-supporting membranes. The membranes are located inside a tube, where a special kind of material as the supporting layer is placed. The flow in a tubular membrane system is usually “in/out” (fluid permeates from the inside through membrane to the outside). The main cause for this “in/out” setup is that the attachment of the membrane to the supporting layer is very weak. Because of large diameter, plugging of tubular membranes during the filtration process is not likely to occur. However, a disadvantage of tubular membranes is that the packing density is very low, which results in high price per module.

Figure 2.1.5 Tubular membrane system from Koch®

The design of the capillary membrane system is similar to that of the tubular membrane system which consists of outer support tube and inner membranes. Compared with the tubular membrane system, the capillary membrane system has smaller diameter and the membrane itself is sufficiently strong to resist filtration pressure. Therefore, the flow through capillary membranes can be both “in/out” and “out/in”. The flow type of the capillaries membranes applied in the T-rack system in this project is “in/out”.

Diameters of capillary membranes range from 0.5 to 5 mm (0.9 mm in this work). Because of the smaller diameter, the possibility of sticking is much higher with capillary membranes than with tubular membranes. A benefit is that the packing density is much higher.

Diameters of hollow fiber membranes are smaller than 0.5 mm. The hollow fiber membrane system is operated in out/in way. These membranes can only be used to treat the water with low suspended solids content. The packing density of a hollow fiber membrane system is very high.

2.2 Computational Fluid Dynamics

Computational fluid dynamics has been developed in recent years in both research and industry organizations. With ongoing development of computer hardware, mathematical–physical models and numerical solution algorithms, the simulation results of complex fluid-dynamic problems with CFD become more reliable [3, 7, 8, 10, 30]. The research work in the process engineering and chemical industry, which contains a lot of work with fluid mechanics, could be speeded up with the help of CFD methods.

Mass, momentum and energy balances are the basic laws in the fluid flow and the transport process, which have been described with a series of governing laws in different situations. CFD involves the numerical solution of these governing laws of fluid dynamics. The complex sets of partial differential equations are solved in geometrical domain divided into small segments/volumes, commonly known as mesh (or grid).

CFD is based on the mathematical equation systems of fluid dynamics. The basic general equation to solve the fluid problem is named Boltzmann equation derived by Ludwig Boltzmann. It shows the statistical description of one particle. This equation can be considered as the super equation which was derived from kinetic considerations of molecular dynamics and is valid for rarefied flows and continuum flows [7]. The Navier–Stokes equations are the most general equations for continuum flow problems, which are employed in simulation work of membrane filtration processes. The Euler equations are the conservation equations for the inviscid fluid problem, derived from the Navier–Stokes equations by neglecting the stress and heat flux terms. The potential equation is a further simplification of the Euler equation under the assumption of irrotational flow. The boundary layer equations are simplified equations based on the Navier–Stokes equations. The essential assumption is that with high Reynolds numbers, the viscous effects take place on a surface only in a thin layer which is called boundary layer.

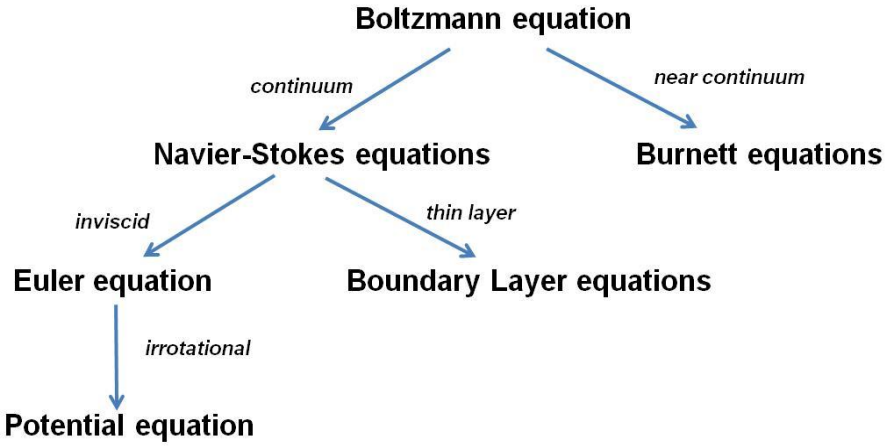

Figure 2.2.1 Main structures of governing laws in fluid dynamics [7]

The integral form of conservation equations for mass, momentum and energy of fluids follows directly from the principle of conservation in the classic theory of physics (mechanics). The conservation principle is applied for a finite control volume with volume V and surface A in a coordinate system (Eulerian frame). The direction of a surface element dA of V is determined by the normal unit vector $\vec{n}$, directed outwards of the volume by definition. (see Figure 2.2.2)

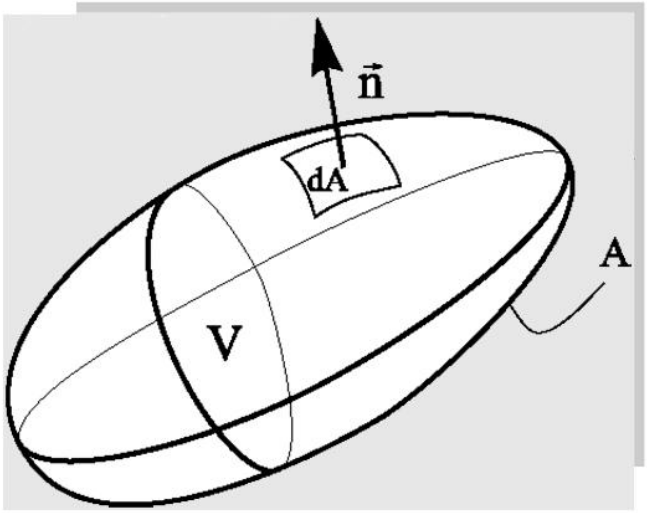

Figure 2.2.2 Control volume with surface area A in the fluid domain

The mathematical formulation results in the integral form of the conservation equation:

$$\int_v \frac{\partial \vec{U}}{\partial t} dV + \oint_A \vec{H} \cdot \vec{n} dA = \int_V \vec{S} dV \qquad \textbf{Equation 2.2.1}$$

where $\vec{U}$ is conservation parameter like specific mass, $\vec{H}$ is the flux on the surface like mass flux and $\vec{S}$ is the source of the conservation parameter i.e. chemical reaction, gravity and so on.

The integral form is widely used as basic equation for the two main different discretization methods in CFD which are called finite element method (FEM) and finite volume method (FVM). The main differences between FEM and FVM are: FEM use simple piecewise functions (e.g. linear or quadratic) to describe the local variations of unknown variables; while FVM uses a formal integration of Navier–Stokes equations over all the control volumes of the solution domain [10]. Both methods involve subdividing the fluid domain into a large number of finite elements (with FEM) or finite control volumes (with FVM) and then solving the governing equations of fluid flow such as Navier-Stokes or Euler equations in the conservation forms. In this process, the governing equations are formed and solved by iterative methods. These methods differ in their derivation and definition of these equations.

The initial and boundary conditions define the special flow problem and the geometry. The initial conditions define all variables at the beginning of the calculations. In most cases they are defined by assuming uniform flow state, if no other values are known. The boundary conditions are in general much more complicated to prescribe. From the mathematical point of view there are different types of possible boundary conditions, such as Dirichlet boundary conditions, Gradient conditions (Neumann boundary condition), Linear combination of Dirichlet and Gradient condition and Periodical boundary conditions. Dirichlet boundary condition is the boundary condition with a given value of a variable, e.g. no-slip condition (tangential velocity is equal to a known value) on a wall or symmetric condition (the velocity in the normal direction is equal to 0). Gradient condition is the condition that the gradient of a variable normal to boundary is prescribed, e.g. adiabatic wall. Linear combination condition is that linear combination

of value and gradient is prescribed, e.g. slip flow on a wall under rarefied conditions. Periodical boundary condition is the boundaries for repeating sequences of integration domains, e.g. for simulating turbine grids.

Main steps of simulation with CFD tools are:

- Defining the physical flow problems for geometry of integration domain, governing equations, initial and boundary conditions;
- Discretizing the integration domain in time and space (geometry);
- Discretizing the differentials or integrals of governing equations by using finite volume or finite element methods;
- Formulating an integration method in time and space for the resulting algebraic system of equation for all grid points;
- Evaluating and validate the numerical results.

Coupling with other equations such as convection-diffusion equations or Darcy's Law, CFD can be used to predict what will happen, quantitatively for fluid flows, often with the complications of:

- Simultaneous flow of heat, mass transfer (i.e. perspiration, dissolution), phase change (i.e. melting, freezing, boiling);
- Chemical reaction (i.e. combustion, rusting), mechanical movement (i.e. pistons, fans, rudders), stresses in and displacement of immersed or surrounding solids;
- Multiphase problem like bubble flows in water.

The performance of a membrane filtration system is strongly influenced by pressure, velocity, and temperature of the fluid, all of which can be simulated with CFD tools. Of course different processes have their own simulation solutions. Some of them can be solved just with the normal traditional method, while some of them need additional special methods. However the CFD offers a possibility to optimize the design of a

membrane filtration system in a simple, easy, flexible and economical way.

3. Theoretical Consideration and Modeling

3.1 Membrane Surface

The main driving force for membrane filtration process in water technology is a pressure difference that affects the water transport through a membrane. The transport of the solute may be controlled by concentration gradient, thermal gradient, electrical potential gradient or convection. Thus, in general the transport of solute is controlled by the gradient of electro-chemical potential.

The transport of different compounds through a membrane depends on following mechanisms:

- Diffusion: concentration gradient between feed and permeate sides;
- Convection: dragging along compounds in the water due to the flux of water through the membrane;
- Sieving effects: larger or similar size of compounds in water than of membrane pores;
- Electrostatic interaction: affinity or repulsion between charged particles themselves and between particles and the membrane surface.

The driving force induces a flux of water from feed side to permeate side. The flux which flows through the membrane surface is referred to as "J" in unit [l/(m²·h)].

Proportionality between the flux and the driving force can be described by a phenomenological equation:

$$J = -A_p \cdot \frac{dX}{dx} \qquad \textbf{Equation 3.1.1}$$

The flux J is proportional to the driving force, which is expressed as the gradient of X

(pressure, concentration, electrical voltage or temperature) in the direction x perpendicular to the membrane surface. The proportionality constant A_p is called phenomenological coefficient. Because the gradient $\frac{dX}{dx}$ is negative in the direction of flux, a minus sign is necessary in the equation.

From the pore size, membranes can be classified into NF, UF and MF (see Chapter 2.1.2). In this work, employed membrane is MF membrane from Microdyn-Nadir and UF membrane from inge. Hence, in the Equation 3.1.1, for water flux (J_w), the term dX can be replaced by pressure difference between feed side and permeate side which is called Trans Membrane Pressure (TMP), and $-A_p \cdot \frac{1}{dx}$ is considered as the permeability coefficient of membrane and be shortened as Pb. Inserting this in Equation 3.1.1 yields an expression called Darcy's Law:

$$J_w = Pb * TMP \qquad \textbf{Equation 3.1.2}$$

The permeability coefficient also depends on the dynamic viscosity of the fluid which is transported through the membrane and the resistance towards mass transport: [12]

$$Pb = 1/(\eta \cdot R_m) \qquad \textbf{Equation 3.1.3}$$

R_m is membrane resistance, η is the dynamic viscosity of the fluid. In this work, pure water is employed in both simulation and experiment. It means that there is no fouling or concentration polarization during the filtration. Equation 3.1.2 and 3.1.3 are enough to calculate the flux through membrane surface.

If fouling and concentration polarization are considered, the letter "R_{tot}" represents the total resistance will be applied in Equation 3.1.3 instead of membrane resistance R_m. The permeability coefficient includes influence of membrane, fouling and concentration polarization.

$$R_{tot} = R_m + R_{cp} + R_f$$ **Equation 3.1.4**

Where R_{cp} and R_f are concentration polarization layers and membrane fouling resistance.

3.2 Pressure Loss in a Pipe or a Capillary Membrane with a Smooth Wall

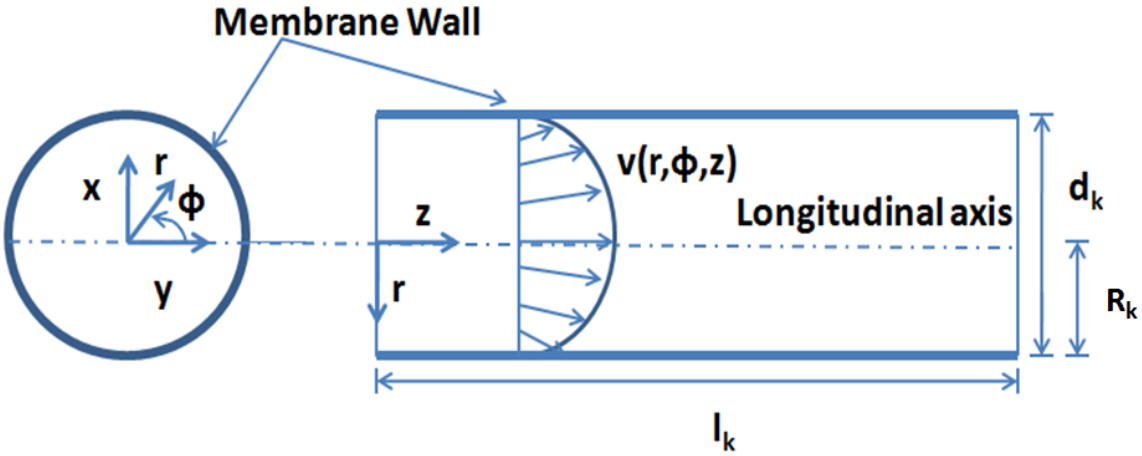

Figure 3.2.1 The capillary membrane in cylindrical coordinates [9]

The so called Hagen-Poiseuille equation is considered as the basic law of the fluid flow inside pipes and capillaries. [9]

$$\frac{dp}{dz} = \frac{\Delta p}{l_k} = -\frac{8\eta}{{R_k}^2}\bar{v_z}$$ **Equation 3.2.1**

In the laminar flow case due to the smooth wall setup, pipe friction factor λ [9][14] is defined as

$$\lambda = \frac{64}{Re_d}$$ **Equation 3.2.2**

Here Reynold's number of the capillary Re_d will be induced which is defined as

$$Re_d = \frac{\rho \bar{v_z} \mathrm{D}}{\eta} = \frac{\rho \bar{v_z} 2R_k}{\eta}$$ **Equation 3.2.3**

Here D is the hydraulic diameter of pipe or capillary and η is the viscosity of fluid ρ is the density of fluid, $\bar{v}_z$ is the mean flow velocity along the capillary direction, z is longitudinal axis of the pipes, R_k is the radius of capillary. Derive from Equation 3.2.2 and Equation 3.2.3, the pipe friction factor λ can be expressed as:

$$\lambda = \frac{32\eta}{\rho \bar{v_z} R_k} \qquad \textbf{Equation 3.2.4}$$

Then the Equation 3.2.1 can be also written in other form like:

$$\frac{\Delta p}{l_k} = -\lambda \frac{\rho}{4R_k} \bar{v}_z{}^2 \qquad \textbf{Equation 3.2.5}$$

In 2001, Stefan Panglisch has developed the flow distribution equations in the capillary membrane in his PhD dissertation [9], with the known boundary condition $p(0) = p_{in}$ and $\frac{dp}{dx}|_{z=0} = -\frac{8\eta \dot{V}_{in}}{\pi {R_k}^4}$, the pressure at position z can be calculated [18]:

$$p(z) = p_p + A_k cosh(az) + B_k sinh(az) \qquad \textbf{Equation 3.2.6}$$

when

$$A_k = p_{in} - p_p \qquad \textbf{Equation 3.2.7}$$

$$B_k = -\frac{8\eta \dot{V}_{in}}{\pi {R_k}^4} \frac{1}{a} \qquad \textbf{Equation 3.2.8}$$

$$a = \sqrt{\frac{16}{R_k^3 R_m}} \qquad \textbf{Equation 3.2.9}$$

where p_{in} is the pressure at the inlet of capillary, $\dot{V}_{in}$ is the volume flow at the inlet and p_p is the pressure at the permeate side of membrane.

The average axial velocity in the capillary at position z can be calculated with equation:

$$\bar{v}_z(z) = -\frac{{R_k}^2}{8\eta}[A_k asinh(az) + B_k acosh(az)] \qquad \textbf{Equation 3.2.10}$$

and the permeation flux at position z ($v_p(z)$) can be also calculated with equation:

$$v_p(z) = \frac{1}{R_m \eta}[A_k cosh(az) + B_k sinh(az)] \qquad \textbf{Equation 3.2.11}$$

In a dead-end capillary membrane filtration process, there is an additional boundary condition $\bar{v}_z(l_k) = 0$: the velocity at the end of capillary is zero. With this additional boundary condition, the relationship between inlet volume flow and inlet pressure can be expressed as:

$$\dot{V}_{in} = (p_{in} - p_p) tanh(al_k) a \frac{\pi {R_k}^4}{8\eta} \qquad \textbf{Equation 3.2.12}$$

With this equation, the permeation performance is easy to be calculated with different inlet pressure and permeate pressure in the dead-end situation, when the geometry of capillary and fluid viscosity are known.

3.3 Friction Loss in a Pipe with a Rough Wall

3.3.1 Moody Friction Loss

The calculation of pressure loss caused by viscosity of fluid in a pipe with ideal wall was introduced in Chapter 3.2. However, in reality, there are no ideal smooth walls, but rough walls everywhere. The roughness of a wall has an effect on friction resistance which is introduced by Coulomb [20] in 1800. This effect is negligible for the laminar pipe flow, so all the laminar formulas derived in Chapter 3.2 are valid for rough wall. However the roughness height ε has great influence on turbulent flow. Different values for ε are summarized in Table 3.3.1.

Table 3.3.1 Recommended Roughness Height Values ε of Commercial Ducts [1]:

Material	Condition	Roughness[mm]	Uncertainty, %
Steel	Sheet metal, new	0.05	± 60
	Stainless, new	0.002	± 50
	Commercial, new	0.046	± 30
	Riveted	3.0	± 70
	Rusted	2.0	± 50
Iron	Cast, new	0.26	± 50
	Wrought, new	0.046	± 20
	Galvanized, new	0.15	± 40
	Asphalted cast	0.12	± 50
Brass	Drawn, new	0.002	± 50
Plastic	Drawn tubing	0.0015	± 60
Glass	---	Smooth	
Concrete	Smoothed	0.04	± 60
	Rough	2.0	± 50
Rubber	Smoothed	0.01	± 60
Wood	Stave	0.5	± 40

In 1972, Prandtl developed one series equations to calculate the friction factor under the turbulent flow conditions [21]. His student Nikuradse developed the turbulent flow model by experiments and drew a diagram to show the relationship between roughness height ε and Reynolds number.

In the experiment, Nikuradse simulated the roughness by gluing uniform sand grains onto the inner wall of the pipes. He then measured the flow velocity, corresponding pressure drops and flow rates, and correlated friction factor versus Reynolds number as shown in Figure 3.3.2. At high Reynolds number the friction factor becomes constant which means for wholly turbulent flow, the friction factor is independent on Reynolds number for any given roughness ratio ε/d. d is the diameter of the pipe here.

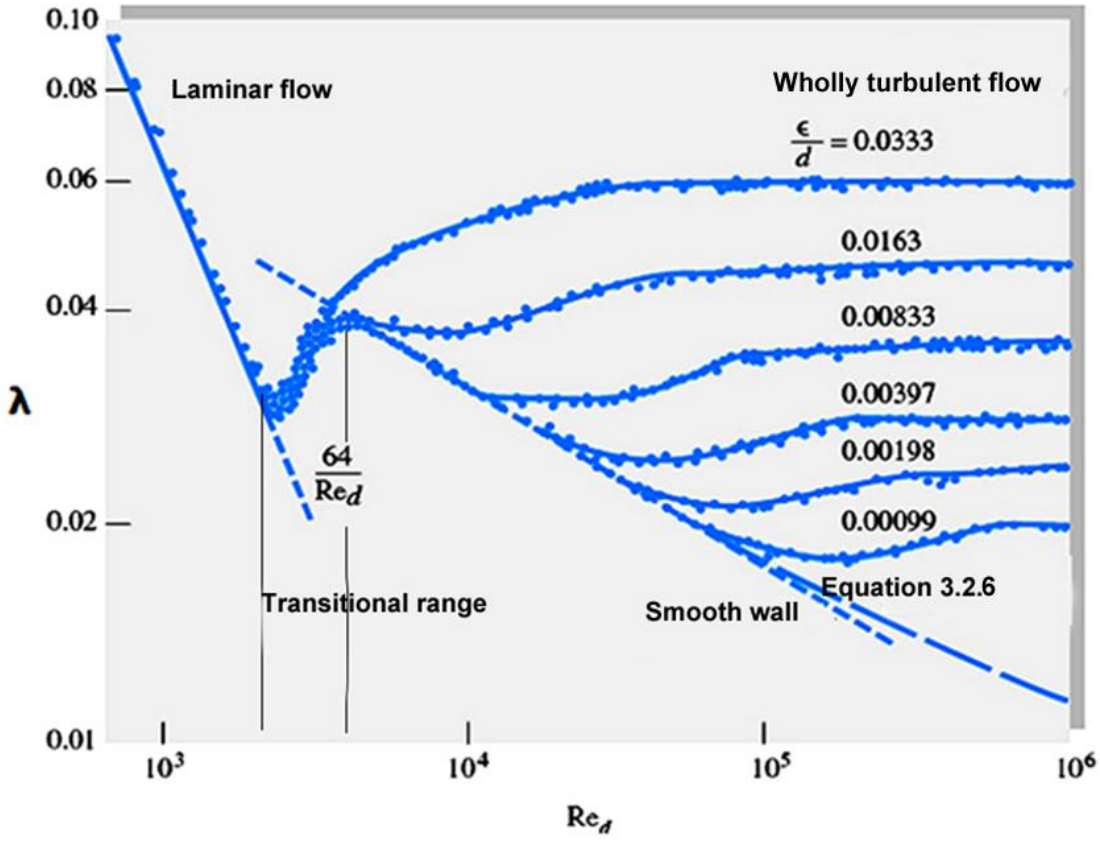

Figure 3.3.2 Experiments with sand grain roughness by Nikuradse [21] show a systematic increase of turbulent friction factor with the roughness ratio.

The laminar friction $\lambda = \frac{64}{Re_d}$ is unaffected by the roughness ratio ε/d. The turbulent friction also is unaffected before an onset point (transitional range), but after the onset point (wholly turbulent flow), λ increases with the roughness ratio ε/d.

If one derives the equation for the wholly turbulent flow, the Reynolds number vanishes and the equation is shown as:

$$\frac{1}{\lambda^{1/2}} = -2.0 log \frac{\varepsilon/d}{3.7} \qquad \textbf{Equation 3.3.1}$$

The pressure loss varies exactly as the square of the velocity in the wholly turbulent case. Some values of friction factor for Wholly turbulent cases are listed in the following table:

Table 3.3.2 Numerical Value of Friction Factor:

ϵ/d	*0.00001*	*0.0001*	*0.001*	*0.01*	*0.05*
λ	0.00806	0.0120	0.0196	0.0379	0.0716

This table shows that the friction factor increases by 9 times when the roughness increases by 5000 times.

The sand grains behavior works well in the wholly turbulent case, but in the transitional region, it behaves somewhat differently from the normal rough pipes, so the Moody Chart [22] (See Figure 3.3.3) was employed recently instead of Nikuradse Diagram in Figure 3.3.2.

In 1939, Colebrook [19] combined the smooth wall equation and wholly turbulent equations into an interpolation equation to solve the turbulent problem:

$$\frac{1}{\lambda^{1/2}} = -2.0\log\left(\frac{\epsilon/d}{3.7} + \frac{2.51}{Re_d\lambda^{1/2}}\right) \qquad \textbf{Equation 3.3.2}$$

This is the accepted design formula for the turbulent friction. It was plotted in 1944 by Moody [22] into Moody Chart for pipe friction. The Moody chart is probably the most famous and useful figure in fluid mechanics. It is accurate to $\pm$ 15 percent for the design calculations over the full range. It can be also used for open channel flows. [1]

In 1980's, with the development of computer technique, Moody equation was developed to be able to calculate λ in numerical calculations. Haaland [23] derived an alternate explicit equation based on Equation 3.3.2 which varies less than 2 percent from Moody chart.

$$\frac{1}{\lambda^{1/2}} \approx -1.8\log\left[\frac{6.9}{Re_d} + \left(\frac{\epsilon/d}{3.7}\right)^{1.11}\right] \qquad \textbf{Equation 3.3.3}$$

In this work, Equation 3.3.3 is used to calculate the pressure loss in the pipes for turbulent situations in order to simplify the simulation.

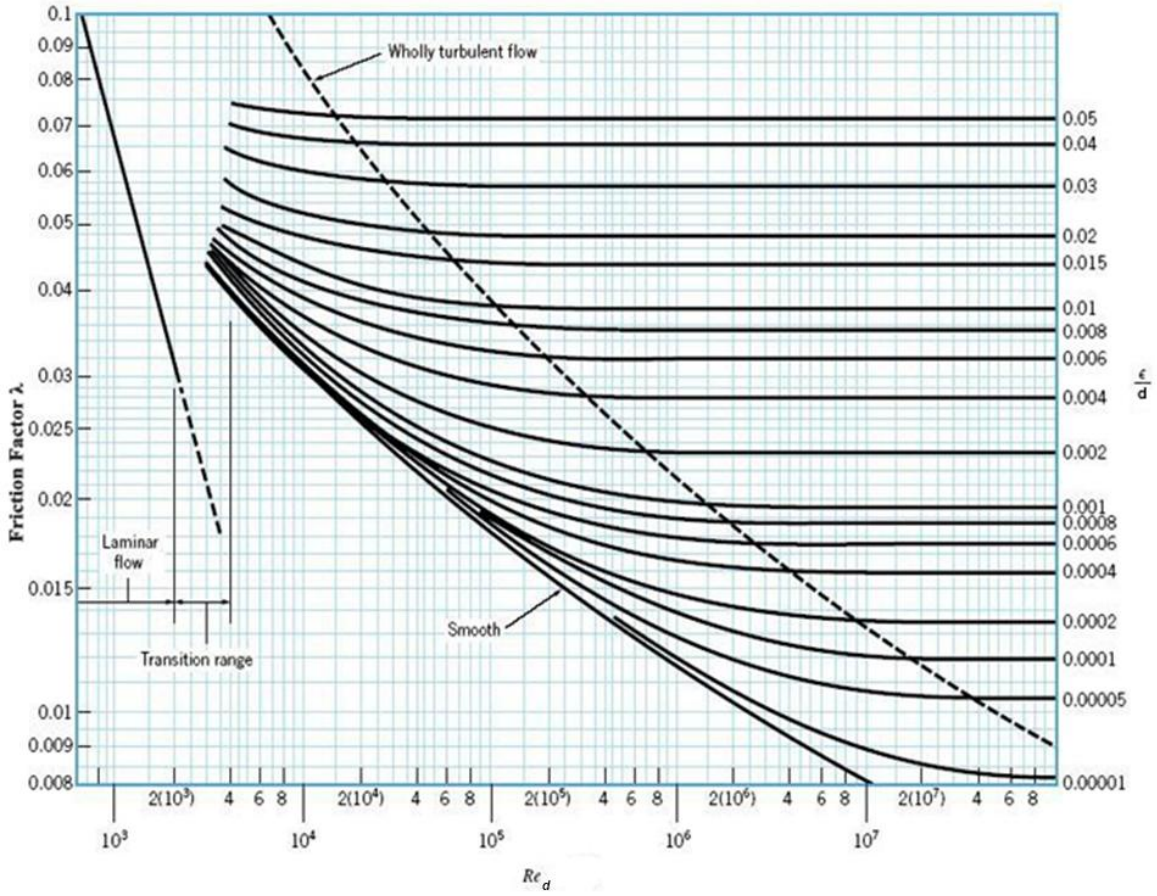

Figure 3.3.3 Moody chart with smooth and rough walls [22] (detail see Appendix B)

3.3.2 Minor Friction Loss and Pressure Loss Coefficient K

In a piping system, the Moody friction loss is called major friction loss, resulting from the roughness of the pipe, there is also minor friction loss due to

- Pipe entrance or exit;
- Sudden expansion or contraction;
- Bends, elbows, tees, and other fittings;
- Valves, on-off applications;
- Gradual expansions or contractions.

However the name “minor friction loss” does not mean that it’s smaller in quantity, for example, a partially closed valve can have greater pressure loss than a long pipe. Since the flow pattern in fittings and valves is quite complex, the theoretical description becomes more difficult. The losses are commonly measured experimentally and correlated with the pipe geometry. The data, especially for valves or other connectors with complex geometry, is somewhat dependent on the particular manufacture’s design, so that the values listed here must be taken as average design estimates [23, 24, 25, 26, 27].

The minor friction loss is usually shown as a ratio of the head loss through the device (Δh_m) to the velocity head of the associated piping system ($\frac{v^2}{2g}$) which is expressed as the Pressure Loss Coefficient K.

$$K = \frac{\Delta h_m}{v^2/_{2g}} = \frac{\Delta p}{\frac{1}{2}\rho v^2} \qquad \textbf{Equation 3.3.4}$$

The Pressure Loss Coefficient K is dimensionless, and correlated not with the Reynolds number and roughness ratio but rather only with the geometry of the piping system.

In Table 1.1.1, the Pressure Loss Coefficient correlated to different type of commercial valves is shown. A single piping system may have many kinds of minor losses. Since all of them are correlated with $\frac{v^2}{2g}$, they can be summed into a single total system loss if the pipe has constant diameter: [1]

$$\Delta h_{tot} = \Delta h_\lambda + \sum \Delta h_m = \frac{v^2}{2g}\left(\frac{\lambda L}{d} + K_{tot}\right) \qquad \textbf{Equation 3.3.5}$$

where λ is the friction factor of pipe, L is the total length of the pipe axis, including any bends, d is the diameter and K_{tot} consists of different terms of Pressure Loss Coefficient K.

Besides the valve system, a bend or curve in a pipe, as in Figure 3.3.4, sudden contraction (SC), and sudden expansion (SE) between two sizes of pipe can also lead to large Pressure Loss Coefficient.

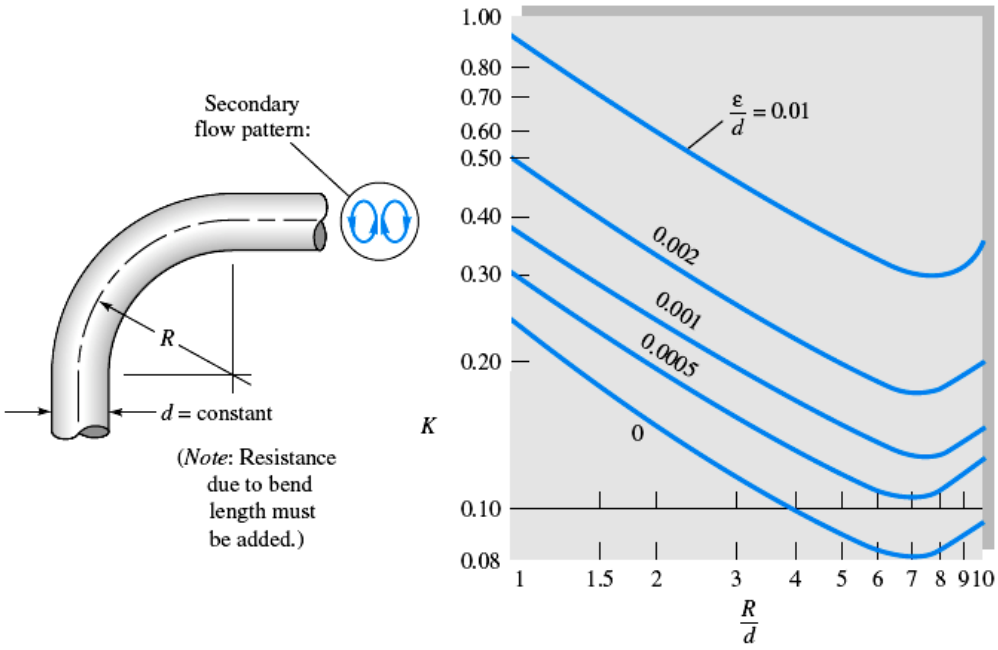

Figure 3.3.4 Pressure Loss Coefficient K for 90° bends [1]

For the sudden expansion (SE), the shear stress in a corner, or dead-end region, is negligible. The analysis between the expansion section and the end of the separation zone gives a theoretical Pressure Loss Coefficient:

$$K_{SE} = (1 - \frac{d^2}{D^2})^2 = \frac{\Delta h_m}{v^2/(2g)} \qquad \textbf{Equation 3.3.6}$$

Here K_{SE} is based on the velocity head in the small pipe, and d is the diameter of the small pipe, D is the diameter of the big pipe. (see Figure 3.3.5)

For the sudden contraction (SC), flow separation in the downstream pipe causes the stream to contract through a minimum diameter d, called the *vena contracta*. Because the theory of the *vena contracta* is not well developed, the Pressure Loss Coefficient for sudden contraction is collected from experiments. It shows as:

$$K_{SC} \approx 0.42\left(1 - \frac{d^2}{D^2}\right)$$ **Equation 3.3.7**

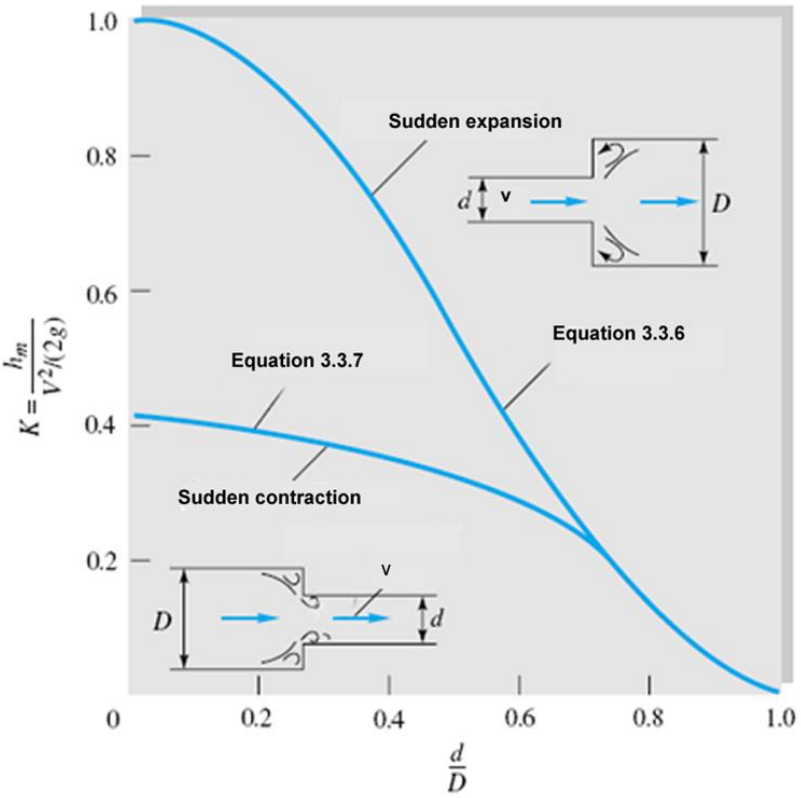

Figure 3.3.5 Sudden expansion and contraction Pressure Loss Coefficient (v is the velocity in the small pipe.) [1]

3.4 Pressure Distribution in Multi–Piping Systems

The membrane filtration systems consist of membrane modules and connecting pipes. Same as valves, membrane modules need high pressure to overcome the resistant. If the membrane modules are taken place by valves, then the filtration system can be simplified to a piping system consists of several pips and valves. The investigation of piping system has been already done and some rules have been already concluded.

Some certain basic multi-pipe rules can be used to analyze the multi-piping system. In Figure 3.4.1, there are three examples of multi-piping systems which include three main multi-pipe rules. Of course these rules can be applied to the piping system with more than three pipes.

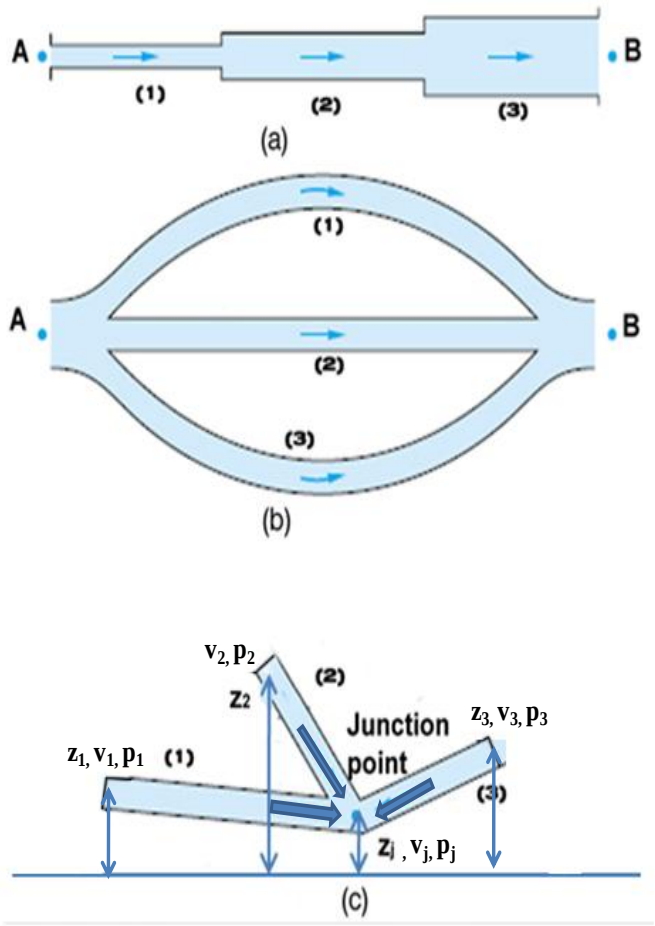

Figure 3.4.1 Examples of multi piping systems: a) pipes in series; b) pipes in parallel; c) the three reservoir junction problem [1]

Figure 3.4.1 (a) is a set of pipes with different diameters in series. In this setup, rule 1 is that the flow rate $\dot{V}$ is constant in all pipes.

$$\dot{V}_1 = \dot{V}_2 = \dot{V}_3 = \dot{V}_i \qquad \textbf{Equation 3.4.1}$$

or

$$v_1 {d_1}^2 = v_2 {d_2}^2 = v_3 {d_3}^2 = v_i {d_i}^2 \qquad \textbf{Equation 3.4.2}$$

Figure 3.4.1 (b) shows three pipes in parallel, and rule 2 is that the head loss through the system is equal in each pipe.

$$\Delta h_1 = \Delta h_2 = \Delta h_3 = \Delta h_i \qquad \textbf{Equation 3.4.3}$$

In terms of the Moody friction loss and minor friciton losses in each pipe, we could rewrite this as

$$\Delta h_i = \frac{{v_1}^2}{2g}\left(\frac{\lambda_1 L_1}{d_1} + K_{tot1}\right) = \frac{{v_2}^2}{2g}\left(\frac{\lambda_2 L_2}{d_2} + K_{tot2}\right) = \frac{{v_3}^2}{2g}\left(\frac{\lambda_3 L_3}{d_3} + K_{tot3}\right)$$

$$= \frac{{v_i}^2}{2g}\left(\frac{\lambda_i L_i}{d_i} + K_{toti}\right) \qquad \textbf{Equation 3.4.4}$$

Figure 3.4.1 (c) is called a reservoir pipe junction. If all of these flows are considered as positive toward the junction, then it can be derived based on mass conservation:

$$\sum \dot{V}_{1,2,3} = 0 \qquad \textbf{Equation 3.4.5}$$

The Equation 3.4.5 obviously implies that at least one flow must be outlet of the junction.

The water head must change through each pipe to get the same water head h_j at the junction point. The water head at the inlet of each pipes and junction point (See Figure 3.4.1 (c)) can be expressed with following equation:

$$h_i = z_i + \frac{p_i}{\rho g} + \frac{{v_i}^2}{2g} \ (i = 1,2,3,j) \qquad \textbf{Equation 3.4.6}$$

where z_i is the height of water head at inlet of pipe i which it needs a referent level, v_i is the flow velocity and p_i is the static pressure at inlet of each pipes and junction point. Here height stands for potential energy, velocity stands for kinetic energy, and pressure stands for work.

The head loss through each pipe can be expressed as:

$$\Delta h_1 = \pm\frac{{v_1}^2}{2g}\frac{\lambda_1 L_1}{d_1} = h_1 - h_j = z_1 + \frac{p_1}{\rho g} + \frac{{v_1}^2}{2g} - \left(z_j + \frac{p_j}{\rho g} + \frac{{v_j}^2}{2g}\right) \qquad \textbf{Equation 3.4.7}$$

$$\Delta h_2 = \pm\frac{{v_2}^2}{2g}\frac{\lambda_2 L_2}{d_2} = h_2 - h_j = z_2 + \frac{p_2}{\rho g} + \frac{{v_2}^2}{2g} - \left(z_j + \frac{p_j}{\rho g} + \frac{{v_j}^2}{2g}\right) \qquad \textbf{Equation 3.4.8}$$

$$\Delta h_3 = \pm \frac{{v_3}^2}{2g}\frac{\lambda_3 L_3}{d_3} = h_3 - h_j = z_3 + \frac{p_3}{\rho g} + \frac{{v_3}^2}{2g} - \left(z_j + \frac{p_j}{\rho g} + \frac{{v_j}^2}{2g}\right) \qquad \textbf{Equation 3.4.9}$$

"±" shown in the equations is decided by the flow direction. For example, if the flow is from pipe 1 to junction point, then the head loss is positive. If the flow is from junction point to pipe 1, then the head loss is negative. Here during the water head loss calculation, the velocities' differences are neglected practically [2]. Then the pressure must change through each pipe to give the same static pressure p_j at the junction point. So the Equation 3.4.7, 3.4.8 and 3.4.9 can be expressed as:

$$\Delta h_1 = \pm \frac{{v_1}^2}{2g}\frac{\lambda_1 L_1}{d_1} = (z_1 + \frac{p_1}{\rho g}) - (z_j + \frac{p_j}{\rho g}) \qquad \textbf{Equation 3.4.10}$$

$$\Delta h_2 = \pm \frac{{v_2}^2}{2g}\frac{\lambda_2 L_2}{d_2} = \left(z_2 + \frac{p_2}{\rho g}\right) - (z_j + \frac{p_j}{\rho g}) \qquad \textbf{Equation 3.4.11}$$

$$\Delta h_3 = \pm \frac{{v_3}^2}{2g}\frac{\lambda_3 L_3}{d_3} = (z_3 + \frac{p_3}{\rho g}) - (z_j + \frac{p_j}{\rho g}) \qquad \textbf{Equation 3.4.12}$$

In Equation 3.4.10, 3.4.11, 3.4.12, $p_1, p_2, p_3, z_1, z_2, z_3, z_j$, friction factors λ and geometries of different pipes L_i, d_i are known, v_1, v_2, v_3 and p_j are unknown. The calculation process based on three reservoir rule is an iteration loop. We guess the static pressure p_j and solve the Equation 3.4.10, 3.4.11 and 3.4.12 for v_1, v_2, v_3 and hence $\dot{V}_1, \dot{V}_2, \dot{V}_3$, iterating until the flow rates balance at the junction point according to Equation 3.4.5. If p_j is guessed too high, the sum of $\dot{V}_1, \dot{V}_2, \dot{V}_3$ will be negative and the remedy is to reduce p_j. If p_j is guessed too low, the sum of $\dot{V}_1, \dot{V}_2, \dot{V}_3$ will be positive and the remedy is to increase p_j.

In this work, this three reservoir rules will be applied in calculation of the piping system simplified from the membrane system. The details of the calculation iterations will be introduced later (see Chapter 3.8.1.1).

3.5 Porous Media Approximation and Modified Navier-Stokes Equation

In the pillow-shaped membrane system, the spacer is used to prevent sticking of two membrane sheets and maintain the constant channel height between the membrane sheets (see Figure 3.5.1). The spacer can be considered as a porous media. The spacer has a very complex geometry which is difficult to simulate with CFD tools in the traditional way.

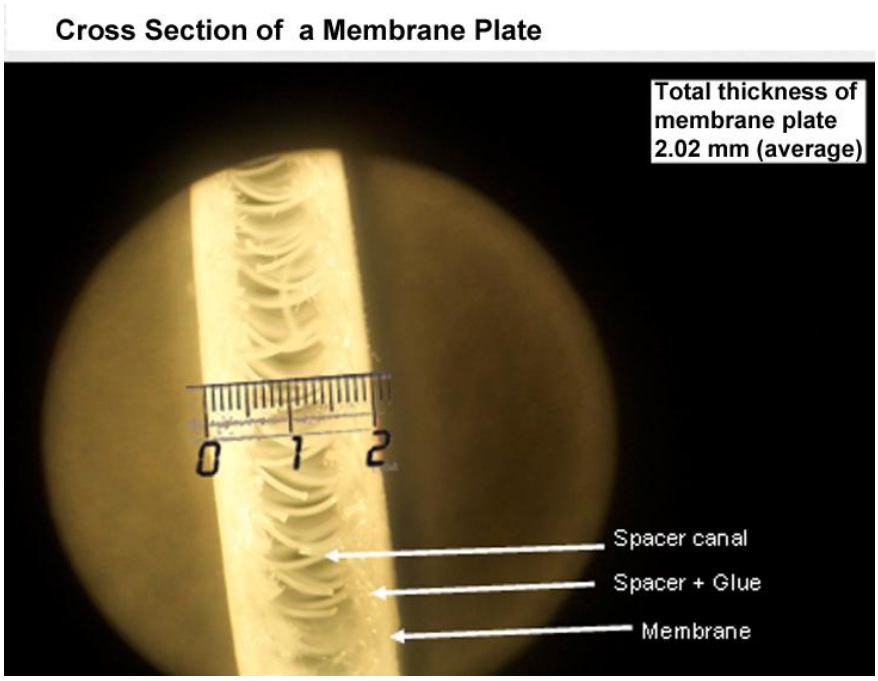

Figure 3.5.1 Membrane spacer in BioCel® membrane filtration system from Microdyn-Nadir GmbH

In the traditional complex geometry simulation, there are two phases present in the porous media domain: fibers and fluid. In order to simplify the CFD model, a porous media approximation method is employed in this work instead of complex geometry simulation. With the porous media approximation method, it is considered that the fluid is the only phase presents in the porous media domain.

As is known, Darcy's Law is the governing equation that describes the flow through porous media which is introduced by Henry Darcy based on the results of experiments

on flow of water through sand [29]. It can be written in one direction format as:

$$\frac{\partial p}{\partial x} = -\frac{\eta}{K_{porous}} v_x \qquad \textbf{Equation 3.5.1}$$

Where $\frac{\partial p}{\partial x}$ is pressure gradient across the porous media in *x* direction, K_{porous} is the permeability of the porous media, v_x is the average velocity calculated as if the fluid is the only phase present in the porous media called the superficial velocity of fluid, and η is the dynamic viscosity.

Darcy's Law works well when there is only body force caused by the grains in the porous media or in the ideal wall situation where the influence of the viscous force is negligible. When there is an additional solid wall, an extra viscous term is needed. Brinkman introduced a correction to Darcy's Law to account for viscous shear effects and the changes in viscosity that arises due to the introduction of the solid wall [31]. This equation is named Brinkman's Equation.

$$\frac{\partial p}{\partial x} = \eta_\varepsilon \nabla^2 v_x - \frac{\eta}{K_{porous}} v_x \qquad \textbf{Equation 3.5.2}$$

where η_ε is the effective viscosity which is related to the porosity of the porous media and dynamic viscosity of fluid. The effective viscosity should not be thought as the viscosity of the fluid but only a parameter for matching the shear stress boundary condition from the porous media (two phases) to the free-fluid (one phase). Clearly the Equation 3.5.2 is reduced to Darcy's Law (Equation 3.5.1) when $\eta_\varepsilon = 0$. While Brinkman may have preferred $\eta = \eta_\varepsilon$ (it works only when the porosity of porous media $\epsilon > 0.975$ [44]), a number of authors have stressed that the two viscosity coefficients could be different depending on the pore geometry of the porous media [44, 46]. For example, when the porosity of porous media ϵ = 50%, it was found that η_ε/η = 4 for an overlapping sphere model of porous media [45]. In order to simplify the calculation, the fibers are assumed to have a homogeneous distribution in the x-y plane (see Figure

3.5.2). Compared with other complex porous media problems [44, 45, 46, 47, 48], the calculation of our porous media is relatively simple.

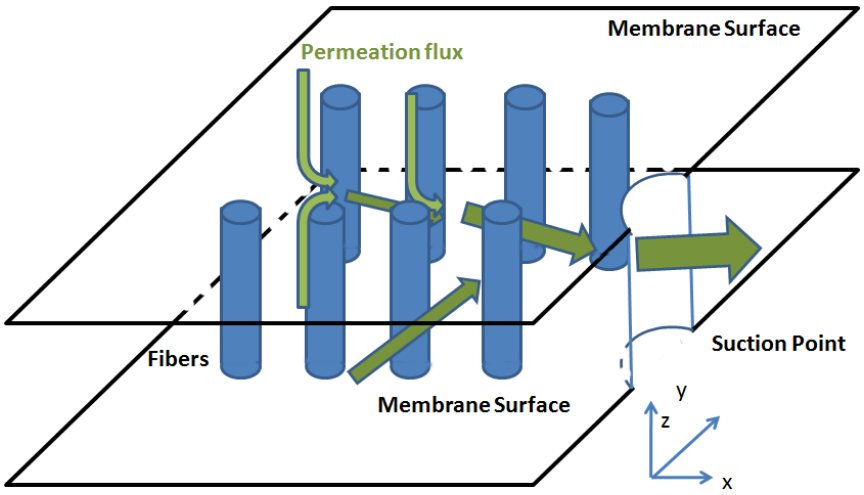

Figure 3.5.2 Structure of porous media inside the membrane plate built by Microdyn-Nadir GmbH.

In the z axis direction, the thickness of the plate is only 2 mm while the length and the width of the plate are 2 m and 1m. If there is a flow from one membrane surface to the other surface, the path length of the flow is only 2 mm while the distance between the solid walls which effects the velocity profile is 2 or 1 m (distance between two parallel walls). As is introduced in last section, the friction is proportional to the flow path length and inversely proportional to the height of the flow channel (distance between two parallel walls). It means the influence of the viscous walls to the velocity profile in z direction is very small, so the Darcy's Law is enough for the calculation where $\eta_\varepsilon = 0$. In the x and y axis directions, the distance between solid walls is 2 mm while path length of flow can be 1 m (suction pipe is in the center of plate) which means the influence of the solid walls here can't be neglected. The relationship between the superficial velocity v_x and the average velocity inside the porous media when there are two phases (fluid and fibers) $v_x{}^*$ is: $v_x{}^* = \frac{1}{(1-\sqrt[2]{1-\epsilon})} v_x$. The flow inside the porous media is always considered as laminar flow. The friction factor is $64/\mathrm{Re_d}$ shown in the Moody Chart (See Figure 3.3.3). With the porous media approximation method, the water head loss caused

by the friction of the solid walls (the membrane surfaces) is

$$\Delta h = \frac{L}{H}\frac{1}{2}\rho {v_x}^2 \frac{64}{Re_d} = \frac{L}{H}\frac{1}{2}\rho {v_x}^2 \frac{\eta_\varepsilon 64}{\rho v_x D} = \frac{L}{H} v_x \frac{\eta_\varepsilon 32}{D} \qquad \textbf{Equation 3.5.3}$$

when there is only fluid phase in the porous media. Here L is length of flow path and H is the distance between solid walls, D is the hydraulic diameter. With the complex geometry simulation when both fluid and fibers are considered, the Δh^* becomes $\frac{L}{H} {v_x}^* \frac{\eta 32}{D}$. In order to use the porous media approximation method instead of complex geometry simulation, Δh should be equal to Δh^*, so $\eta_\varepsilon/\eta = {v_x}^*/v_x$; hence $\eta_\varepsilon/\eta = \frac{1}{\left(1-\sqrt[2]{1-\epsilon}\right)}$ in x and y directions. This calculation is only valid for the situation shown in Figure 3.5.2 because of the special fiber distribution inside membrane plate.

The Brinkman's Equation is a practical method to describe coupled flow problems in plain and porous media [37]. As shown in Figure 3.5.2, the permeation flow changes its direction from z axis direction to x and y directions. In the Brinkman's Equation there is no term to describe this effect, so the convective acceleration term is needed here. The convective acceleration term $\rho \cdot \left(v_x \frac{\partial v_x}{\partial x} + v_y \frac{\partial v_x}{\partial y} + v_z \frac{\partial v_x}{\partial z}\right)$ can describe the effect of a fluid with respect to space. Hence Modified Navier-Stokes equations (x direction) is used:

$$\rho \cdot \left(v_x \frac{\partial v_x}{\partial x} + v_y \frac{\partial v_x}{\partial y} + v_z \frac{\partial v_x}{\partial z}\right) + \frac{\partial p}{\partial x} - g_x$$

$$= \eta_\varepsilon \nabla^2 v_x - \frac{\eta}{K_{porous}} v_x \qquad \textbf{Equation 3.5.4}$$

In the work with BioCel® system, only porous media approximation method is not enough to simulate the complex compression of the membrane spacer during the operation. The characterization of the permeability of the spacer is necessary and introduced in the Appendix A.

3.6 CLI Method

As is introduced in Chapter 1.1, the membrane filtration system consists of pipes, modules and connectors. For example, a basic T-rack unit is constructed with four feed (inflow) pipes, one permeate pipe and eight capillary modules. The standard diameter of feed pipes is 142 mm, and the standard diameter of permeate pipe is 235 mm, while the capillaries inside the modules are only 0.9 mm in diameter. The membrane filtration system normally is built by several basic T-rack units. The CFD model of a membrane filtration system consists of large amount of boundary condition setups. The discretization of space also becomes very complex because both large scale geometry as hundreds mm diameter pipes and small scale geometry as 0.9 mm diameter capillaries exist in one membrane filtration system. This complexity decides hardware' strength and time consumption of CFD simulation [7, 8, 10]. To precisely simulate such complex systems like an integrated membrane filtration system needs high capacity computers working in parallel with the traditional simulation method. In order to avoid this, an additional method named **Calibration-Library-Interpolation (CLI) Method** was employed. As shown in Chapter 1, BioCel® and T-racks membrane filtration systems are built by several equal uniform structure units. In the simulation, each unit was considered as a separated model. For different flow velocity setups, the associated pressure loss was simulated for a unit, and the simulation results were saved in a library which was then applied for further simulation steps. This is called here the **calibration-library method**. As different module geometries cause a variety of pressure losses, several libraries had to be generated. While simulating the integrated system, the pressure losses in different modules caused by different flow velocities were interpolated with the libraries which are the calibration results. This is called **interpolation method**.

3.7 Scale Method

Normally the thickness of a membrane plate is in millimeter range, while the length and

width of the membrane is in meter range. The CFD model is based on the segment grids (meshes) which represent the discretized fluid domain. The equilateral segment grid is the best quality grid which means the highest accuracy and the best performance of simulation are provided [7]. If equilateral segment grids are used, the number of grids will be huge. This huge number of grids means high capacity hardware demand and long time consumption. In order to avoid this, the **scale method** was used as shown by the following equations. Scale method is the method adjusting the dimensions with scale factors in order to keep the dimensions of fluid domain in the same range which can be easily discretized with high quality meshes. Taking the momentum equation of Navier-Stokes equations as example, the original format in x direction is shown as follows:

$$u\frac{\partial u}{\partial x}+v\frac{\partial u}{\partial y}+w\frac{\partial u}{\partial z}=-\frac{\partial p}{\partial x}+\frac{\partial}{\partial x}\left(-\frac{2}{3}\mu\left(\frac{\partial u}{\partial x}+\frac{\partial v}{\partial y}+\frac{\partial w}{\partial z}\right)+2\mu\frac{\partial u}{\partial x}\right)+\frac{\partial}{\partial y}\left(\mu\left(\frac{\partial v}{\partial x}+\frac{\partial u}{\partial y}\right)\right)+\frac{\partial}{\partial z}\left(\mu\left(\frac{\partial u}{\partial z}+\frac{\partial w}{\partial x}\right)\right)$$ **Equation 3.7.1**

With the scale mode, the ratio $\frac{\partial Z}{\partial z}$ is set to λ_s which is named scale factor, where z is the real size, and Z is the geometry size in the simulation model. Then the equation can be transferred to a new format.

$$u\frac{\partial u}{\partial x}+v\frac{\partial u}{\partial y}+w\frac{\partial u}{\partial Z}\lambda_s=-\frac{\partial p}{\partial x}+\frac{\partial}{\partial x}\left(-\frac{2}{3}\mu\left(\frac{\partial u}{\partial x}+\frac{\partial v}{\partial y}+\frac{\partial w}{\partial Z}\lambda_s\right)+2\mu\frac{\partial u}{\partial x}\right)+\frac{\partial}{\partial y}\left(\mu\left(\frac{\partial v}{\partial x}+\right.\right.$$
$$\partial u\partial y+\partial\partial Z\lambda s\mu\partial u\partial Z\lambda s+\partial w\partial x$$ **Equation 3.7.2**

The thickness of the membrane plate model can be transferred from millimeter to decimeter range with λ_s = 100, which can strongly improve the quality of simulation grids and reduce simulation time and hardware requirement.

In order to simplify the model, the compression of the membrane plate spacer is considered as an average value of the whole spacer. That is the change of thickness of the

plate and the porous media permeability caused by compression is the same at different positions of the plate. This compression can be calculated from the thickness - TMP equation shown in Appendix A (see Equation A.2.1) with the known trans-membrane pressure.

3.8 CFD Modeling

As is already mentioned, the CFD technique is well developed and applied in research and industry. However CFD is just an analytic technique based on the theoritical analysis and experimental analysis. Compared with a pure mathematical calculation, the CFD technique involves the creation of a set of numbers that constitutes a realistic approximation of a real physical system. The errors still exist and lead to the difference between CFD simulation and real system. These errors are iteration error, numerical error, discretization error and some other parameter errors [8, 34, 35]. The numerical error of the CFD model is based on the calculation with the software COMSOL Multiphysics 3.3 ® and FLUENT 6.0 ®. The tolerance of iterations in the simulation of membrane system is allowed to be 1 ~ 2% in order to have fast convergence, maximal it will not exceed 5% in this work.

COMSOL Multiphysics is an advanced software environment to model and simulate of physical processes for scientific and engineering problems based on partial differential equations. It is developed and distributed by the company COMSOL AB (Sweden). The software can be used for linear and nonlinear stationary, transient, time dependent and eigenvalue analyses of arbitrary models. The software package can handle systems of first and second order partial differential equations in one, two and three space dimensions (1D, 2D and 3D). For example, the membrane plates of BioCel® were modeled by using the application modes ‘incompressible Navier-Stokes’ and 3D user defined PDE system. The simulation results were used to build the libraries of CLI method.

FLUENT is the general name for the collection of computational fluid dynamics (CFD) programs sold by FLUENT, Inc.. It contains the broad physical modeling capabilities to model flow, turbulence, heat transfer, and reactions for industrial applications ranging from air flow over an aircraft wing to combustion in a furnace, from bubble columns to oil platforms, from blood flow to semiconductor manufacturing, and from clean room design to wastewater treatment plants. The T-connectors of T-rack system and pipe-connectors of BioCel® system were modeled by using FLUENT.

Additionally, a software package is built with Visual C++ to apply the CLI method. The software package can read the libraries built by FLUENT and COMSOL Multiphysics, and do the further simulation with them. The capillaries inside the module of T-rack system is also modeled with this software package based on the Equations shown in Chapter 3.2.

In this work the simulation can be separated into three steps: model building, model solving and model validation. The validation is to check whether the accuracy of the CFD model is high enough to apply for further simulation. The difference between the simulation and the experimental results is checked under the same operation conditions. The experimental results are strongly influenced by a lot of factors e.g. the feed water quality, the inhomogeneous membrane surface area (capacity) in different modules, the inhomogeneous permeability at different position of membrane, and even the measuring devices. Hence absolutely identical working conditions setup between experiment and simulation is impossible. If the difference between experimental and simulation results is less than 15%, the model is accepted as a correct model and could be used for further simulations. Parameters and their interaction mechanism in filtration systems can be satisfied by this accuracy.

In the simulation, some parameters are unnecessary to be included in the model like gravity, some parameters are impossible to be included in the model like the pressure at

the outlet of permeate pipe in the filtration process and the pressure at the inlet of the feed pipes in the backwash process because there are unknown. The gravity has the same influence to both feed side and permeate side. It cannot influence the performance of the system. So in the simulation, the gravity was considered as 0. The pressure at the outlet of permeate pipe or at the inlet of the feed pipes is strongly dependent on the external piping system which is impossible to be included in the model as a parameter. The performance of membrane is influenced by the pressure gradient across the membrane and pressure loss inside the piping systems which is not influenced by the absolute pressure at the outlet. Hence in the simulation, these two pressures at outlet of system in filtration and back wash were possible to be set as 0. In order to make the results of simulation and experiments comparable, the post process is necessary. In the post process, the pressure at the outlet of permeate pipe in the filtration process and the process at the inlet of the feed pipes in the back wash process from experimental results will be adapted to the simulation results. For example, in the simulation of T-rack model, the measured pressure at the outlet of the permeate pipe in the experiment was added to the simulated pressure profile of the system. With the same method, the influence of the gravity to the system was also added in the post process.

3.8.1 T-rack Simulation

The main structure and possible flow distribution of inge T-rack system should be introduced firstly. As shown in Figure 3.8.1, the T-rack membrane filtration system consists of four feed pipes, one permeate pipe, and several *Dizzer 5000 plus* modules which are linked to the feed pipes with T-connectors and linked to the permeate pipe with module to permeate pipe connectors.

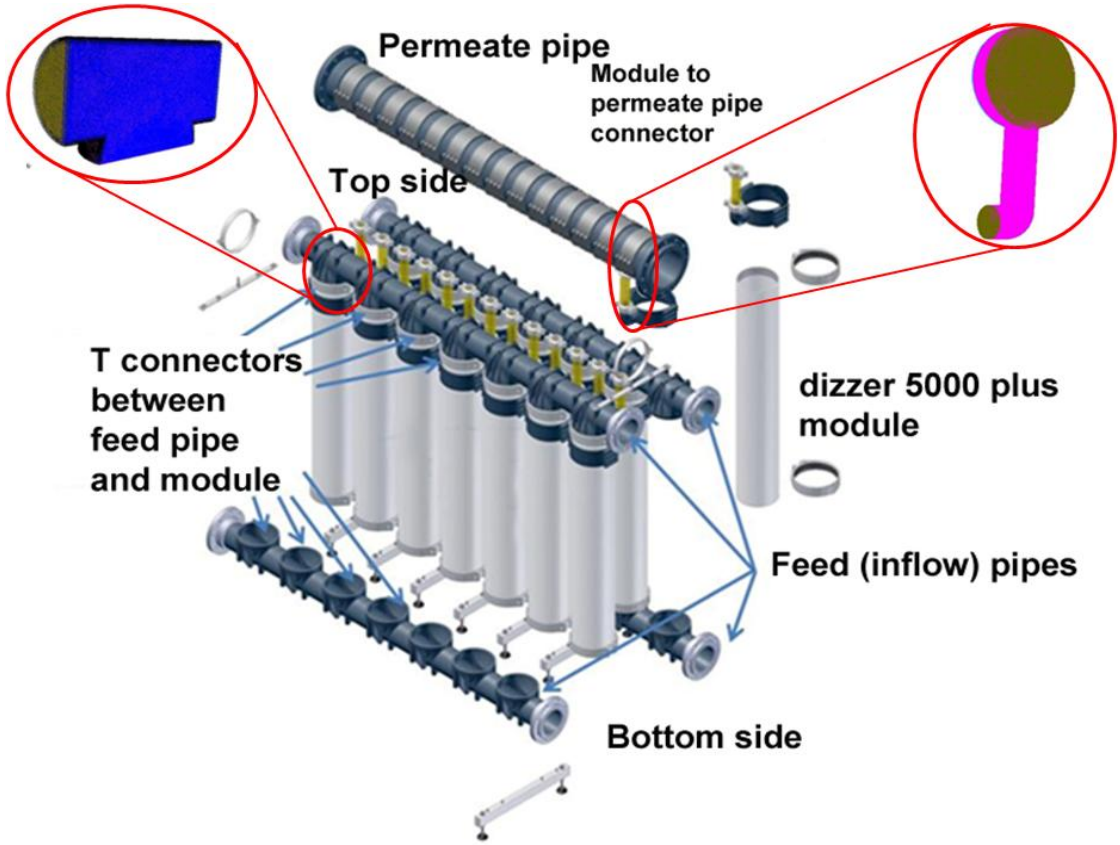

Figure 3.8.1 Structure of T-rack system and details of T-connectors and permeate pipe connectors

During the operation of filtration process, a pump drives the fluid into the two feed pipes on the top right side. Normally the fluid flows into the modules and is permeated through the capillary membranes and collected in the permeate pipe. This is called co-current flow set. For T-rack system, due to the additional bottom pipes, there is another flow distribution as shown in Figure 3.8.2. Part of the fluid flows from the feed pipes on the top side to the feed pipes on the bottom side through the modules instead of complete permeation process.

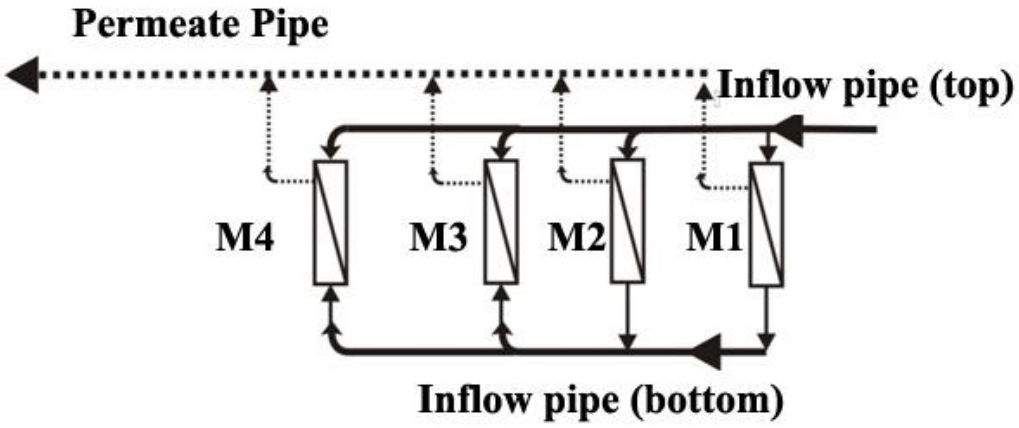

Figure 3.8.2 Possible flow distribution in a T-rack system (Filtration process)

In the first two *Dizzer 5000 plus* modules near the inlet, part of the fluid flows through the membrane into the permeate pipe and the other part directly flows through the capillaries from top feed pipes to the bottom feed pipes. Then in the modules which are a little far away from the inlet, the fluid flows into the modules from both top and bottom feed pipes and permeates into the permeate pipe. This kind of flow distribution is determined by the pressure of the top side feed pipe, bottom side feed pipe and of the permeate pipe. The pressures calculation here can be done with the multi-pipe rules, coupled with the pressure loss in the pipes caused by friction, the pressure loss in the capillaries caused by permeation flow, and the pressure change in the pipes caused by the change of velocity in value and direction. (see Chapter 3.2 – 3.4). In the backwash process, the fluid flows into the system from the left side of the permeate pipe and flows out from the right side of feed pipes.

As already introduced, the T-rack system is a complex system which consists of several different parts. In order to simulate this complex system, a procedure with eight steps is designed as following:

- Building a 3D CFD model to get the library which contains the information of pressure loss of T-connectors and pipes with corresponding velocity for the CLI

method (see chapter 3.6);

- Building the capillary model to analyze the pressure drops along the capillary (assume all capillaries in the *Dizzer 5000 plus* has same performance);
- Simulating the pressure and flow distribution of the integrated system include membrane modules, connectors and pipes, with momentum equilibrium, mass conservation and interpolation of libraries (built in step 1) with CLI method;
- Analyzing the pressure on both feed (top and bottom) and permeate sides of modules and calculate the individual permeation with help of the capillary model (built in step 2) for each module of the system;
- Validating the filtration simulation model with experiments. (See Chapter 4.1)
- Predicting the performance of the system with influencing parameters i.e. different number of modules, different diameters of inflow and permeate pipes and different permeability of membranes.
- Simulating the backwash process in the same way as the filtration process shown in step 1~4.
- Validating the backwash simulation and do the prediction with influencing parameters i.e. different number of modules, different diameters of inflow and permeate pipes and different permeability of membranes.

From these steps, the simulation can be separated into three main models: the CFD model to show pressure losses in the feed (inflow) and permeate pipes, the model to calculate the flow distribution of one capillary in a *Dizzer 5000 plus* module, and the model to simulate the pressure and flow distribution of the whole integrated system.

3.8.1.1 Friction Loss Model of the Feed (Inflow) and Permeate Pipes

As shown in Chapter 3.3, major friction loss has enough theory and mathematical support which is validated by former researchers for both laminar and turbulent flow, while the minor friction loss has only partially mathematical support. But the minor

friction loss can be got from experimental results (see Chapter 3.3.2) or CFD simulation. In recent decades, CFD is popular and widely used to simulate the pressure loss of piping systems, because it can simulate both major friction loss and minor friction loss quantitatively and efficiently. There are two kinds of connectors employed in the T-rack system to connect the pipes in the feed and permeate sides (see Figure 3.8.1). One is called T- connector in the feed side and the other is called module to permeate pipe connector in the permeate side. The CFD model setup for T-connector and “module to permeate pipe connector” is shown in the Figure 3.8.3.

The outer surfaces of the connectors are set to no slip wall boundary condition (see Figure 3.8.3 a) and b)). The no slip wall boundary condition is one of Dirichlet boundary conditions where both tangential and normal velocities on the surface of a rigid wall are defined as 0. The inflow, outflow (Pipe) and outflow (Module) cross sections are set to the boundary conditions which are constant in velocity or pressure. The symmetric surface of the T-connector (see Figure 3.8.3 b)) is set to the symmetric boundary condition which means that the gradient of density, pressure, temperature and tangential velocity in the normal direction of the boundary is 0. The symmetric surface boundary condition also means no mass transfer in the normal direction, so the velocity in the normal direction is defined as 0 too.

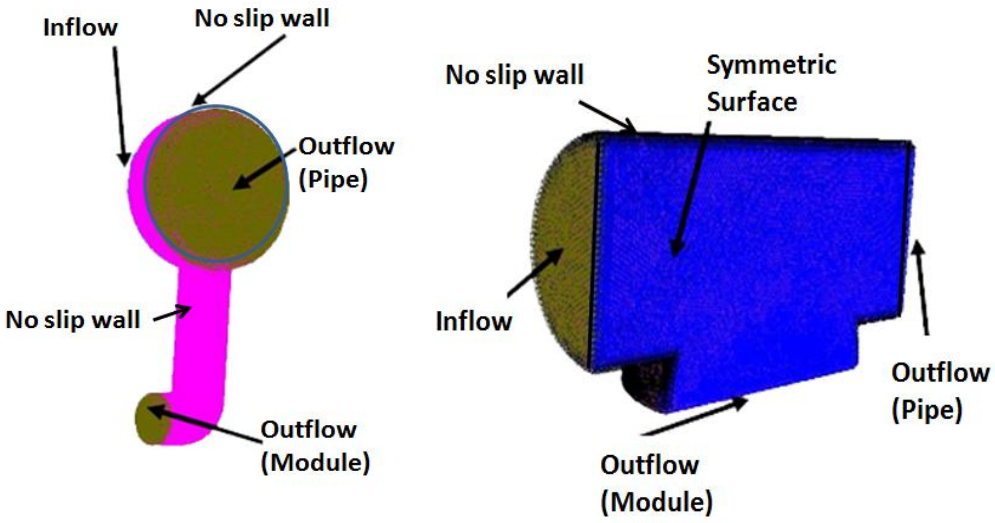

a) b)

Figure 3.8.3 CFD model setup of a) "module to permeate pipe connector" and b) T-connector

In order to explain how the CFD model works, the flow situation inside the T-connector is taken as example. Figure 3.8.4 shows the typical flow distribution inside the T-connector. The flow field inside the T-connector can be divided into three main parts which are connected by a junction point. Then the T-connector can be transferred to a three reservoir junction piping system. The feed flow of T-connector can be separated into 2 parts at the junction point:

- One part of fluid flows out with velocity v_{outp} from the "outflow (Pipe)";
- The other part of fluid flows out with velocity v_{outm} from the "outflow (Module)" side.

v_{in} is the feed velocity, L_i is the length the fluid flows through in different parts, d_i is the diameter in different parts, K_{toti} is the Pressure Loss Coefficient of minor friction loss, λ_i is the friction factor where i = 1,2,3 for different parts of T-connector and Δp_1, Δp_2 and Δp_3 are the pressure loss in three parts of T-connector (can be considered as three pipes as shown in the reservoir junction rules) respectively.

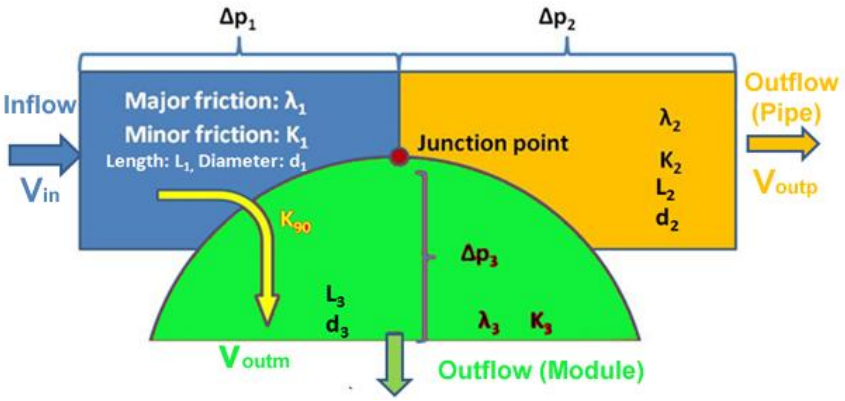

Figure 3.8.4 The flow distribution inside the T-connector

As already mentioned, in order to reduce the simulation time and hardware cost, the **Calibration-Library-Interpolation (CLI) method** was applied in this work (see Chapter 3.6). The Libraries of the pressure loss due to different parts of T-connector are generated based on the simulation model of the flow situation shown in Figure 3.8.4. The setup of simulation model is shown in Figure 3.8.5 a) and b). As is shown in Figure 3.8.5 a), in the simulation model of fluid in the pipe, the outflow (Module) is considered as a no slip condition which means no fluid flowing through this boundary. In Figure 3.8.5 b), in the simulation model of fluid from pipe to module, the outflow (Pipe) is set to no slip condition.

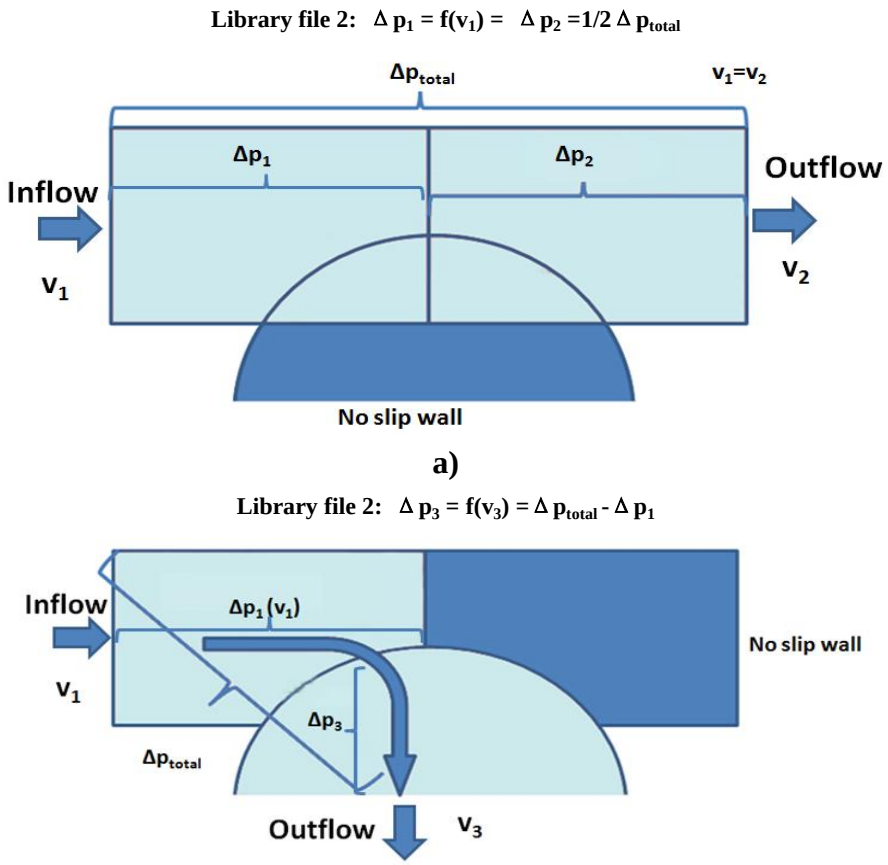

Figure 3.8.5 Simulation model setup for the generation of libraries a) pressure loss inside the pipe b) pressure loss from pipe to module.

In the simulation model, the pressure difference at different parts of T-connector can be considered as a function of responsible velocity, e.g. $\Delta p_1 = f(v_1)$, $\Delta p_2 = f(v_2)$ and $\Delta p_3 = f(v_3)$. The library of $\Delta p_1 = f(v_1)$ and that of $\Delta p_2 = f(v_2)$ which are considered in Figure 3.8.5 a) are the same because both are based on the same pipe geometry. So here only two libraries are necessary to be generated: one is the library of pressure loss in the pipe ($\Delta p_1 = f(v_1)$ or $\Delta p_2 = f(v_2)$) and the other is the library of the pressure loss in the "pipe to module" part ($\Delta p_3 = f(v_3)$). Take Δp_1 as example, it can be expressed as $\Delta p_1 = f(v_1) = \frac{{v_1}^2}{2g}\left(\frac{\lambda_1 L_1}{d_1} + K_{tot1}\right)$ which includes the influence of both the major friction and the minor friction loss.

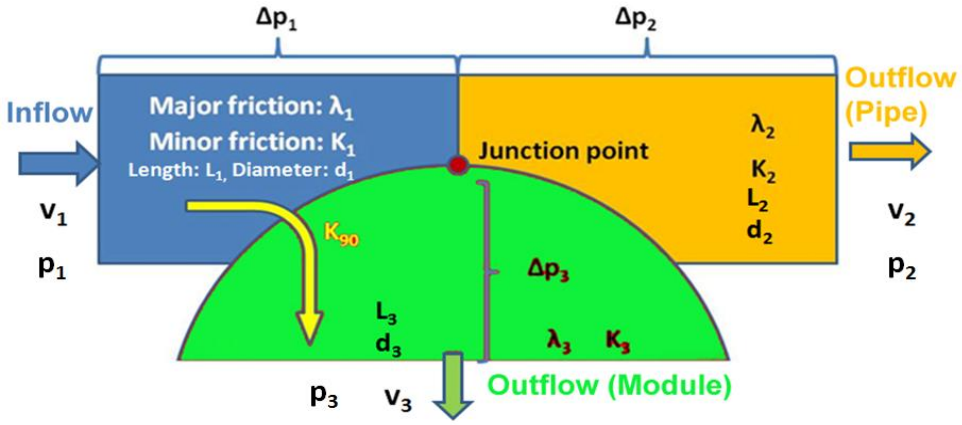

Figure 3.8.6 The typical flow situation in the T-connector with the analysis of three reservoir junction

Compared to the conventional three reservoir junction problem in multi pipes analysis (see Chapter 3.4), the three reservoir junction problem in T-connector (see Figure 3.8.6) has following differences.

- the pressures at inflow (p_1) and outflow (Module) (p_3) are unknown;
- the velocities' difference can't be negligible;
- the gravity can be negligible which means z_1, z_2, z_3 and z_j are 0;
- the pressure and velocity at outflow (Module) p_2 and v_2 are known already.

But the rules of three reservoir junction can be also applied here. The mass conservation shown in Equation 3.4.5 is still valid. The water head must change through each pipe to give the same water head h_j at the junction point.

With the Minor friction loss is also considered and flow direction shown in Figure 3.8.6, the Equations 3.4.10, 3.4.11, 3.4.12 become:

$$\Delta h_1 = \frac{v_1^2}{2g}\left(\frac{\lambda_1 L_1}{d_1} + K_{tot1}\right) = h_1 - h_j = \frac{v_1^2}{2g} - \frac{v_j^2}{2g} + (p_1 - p_j)/\rho g \qquad \textbf{Equation 3.8.1}$$

$$\Delta h_2 = -\frac{v_2^2}{2g}\left(\frac{\lambda_2 L_2}{d_2} + K_{tot2}\right) = h_2 - h_j = \frac{v_2^2}{2g} - \frac{v_j^2}{2g} + (p_2 - p_j)/\rho g \qquad \textbf{Equation 3.8.2}$$

$$\Delta h_3 = -\frac{v_3^2}{2g}\left(\frac{\lambda_3 L_3}{d_3} + K_{tot3}\right) = h_3 - h_j = \frac{v_3^2}{2g} - \frac{v_j^2}{2g} + (p_3 - p_j)/\rho g \quad \textbf{Equation 3.8.3}$$

and

$$h_j = h_i - \Delta h_1 = h_2 - \Delta h_2 = h_3 - \Delta h_3 \quad \textbf{Equation 3.8.4}$$

Take the Equation 3.8.1, Equation 3.8.2 and Equation 3.8.4 as example,

$$\Delta p_p = p_2 - p_1 = \frac{\rho v_1^2}{2} - \frac{\rho v_2^2}{2} - \frac{\rho v_1^2}{2}\left(\frac{\lambda_1 L_1}{d_1} + K_{tot1}\right) - \frac{\rho v_2^2}{2}\left(\frac{\lambda_2 L_2}{d_2} + K_{tot2}\right)$$

Equation 3.8.5

Δp_p is the pressure difference between inlet and outlet of the pipe. The right side terms of this Equation 3.8.5 will be simulated and calculated by the software FLUENT (Term $\frac{v_1^2}{2g}\left(\frac{\lambda_1 L_1}{d_1} + K_{tot1}\right)$ and $\frac{\rho v_2^2}{2}\left(\frac{\lambda_2 L_2}{d_2} + K_{tot2}\right)$) and C++ software package (Term $-\frac{\rho v_1^2}{2} + \frac{\rho v_2^2}{2}$).

Based on the same rule, the pressure difference between inflow (Pipe) and outflow (Module) Δp_m can be expressed as:

$$\Delta p_m = p_3 - p_1 = \frac{\rho v_1^2}{2} - \frac{\rho v_3^2}{2} - \frac{\rho v_1^2}{2}\left(\frac{\lambda_1 L_1}{d_1} + K_{tot1}\right) - \frac{\rho v_3^2}{2}\left(\frac{\lambda_3 L_3}{d_3} + K_{tot3}\right)$$

Equation 3.8.6

As is introduced, the T-connector can be considered as a three reservoir junction problem. The iterations are needed to calculate the velocity and pressure distribution inside the T-connector. Similar to the conventional three reservoir junction problem, the iteration can start with an estimated parameter. However due to some different known parameters, the estimated parameter where the iteration starts is different. For T-connector, the iteration starts from the v_3 instead of p_j. Firstly an estimate is made by v_3 using mass conservation, the v_1 can be calculated when v_2 is known already. The volume flow $\dot{V}_3$

and $\dot{V}_1$ can be calculated based on velocities. With the known p_2, v_2 and v_1, based on Equation 3.8.5, Equation 3.8.6 and the libraries generated by CLI method, the pressure at outflow (Module) p_3 can be calculated. p_3 is also the pressure which drives the fluid permeating through the membrane module. With known pressure at permeate side p_3 decides the velocity at the outlet to the module named v_3' and volume flow $\dot{V}_3'$. Then the sum of volume flow at the junction point can be expressed as:

$$\sum \dot{V}_{1,2,3} = \dot{V}_1 + \dot{V}_2 + \dot{V}_3' \qquad \textbf{Equation 3.8.7}$$

This iteration is running until the mass is balanced at the junction point according to Equation 3.4.5. If v_3 is estimated too high, the sum of $\dot{V}_1, \dot{V}_2, \dot{V}_3'$ will be positive and the remedy is to reduce v_3. If v_3 is estimated too low, the sum of $\dot{V}_1, \dot{V}_2, \dot{V}_3'$ will be negative and the remedy is to increase v_3..

In the practical experiments, the pressure along the pipe sometimes was found to increase though the friction existed (this problem was mentioned and discussed during the team meeting in the customer company). This situation can be explained by Equation 3.8.5. There are two causes for pressure difference: kinetic energy (velocity) between inflow pipe and outflow pipe which is expressed as $\frac{\rho {v_1}^2}{2} - \frac{\rho {v_2}^2}{2}$ and friction which is expressed as $\frac{\rho {v_1}^2}{2}\left(\frac{\lambda_1 L_1}{d_1} + K_{tot1}\right) + \frac{\rho {v_2}^2}{2}\left(\frac{\lambda_2 L_2}{d_2} + K_{tot2}\right)$. If the influence of kinetic energy difference is larger than friction, the pressure increases along the pipe. If the influence of kinetic energy difference is smaller than friction, the pressure decreases.

The "module to permeate pipe connector" is calculated based on the same law, while the iteration starts from the pressure at the permeation side of membrane because the known parameter is different (See Chapter 3.8.1.3).

3.8.1.2 Pressure and Flow Distribution Model in the Capillary

In Chapter 3.2, the pressure distribution in a smooth wall pipe or capillary is introduced. In this work, in order to simplify the simulation model, the surface of the capillary membranes is assumed to be smooth and all the capillaries in one module have the same flow and pressure distribution. From the numerical iterations shown in chapter 3.8.1.1, the pressure at the outflow (Module) can be calculated from the known pressure and velocity at the outflow (Pipe). The pressure at the outflow (Module) is equal to the pressure at top and bottom sides of modules (the modules are connected to the pipes from both top and bottom sides, see also Figure 3.8.7). Then with the equations shown in Chapter 3.2, the pressure distribution, the velocity distribution in the capillaries and the permeation volume flow for both top and bottom sides can be calculated. This permeation volume flow will change the velocity at the top and bottom sides of the module which is also the velocity at the outflow (Module). As is introduced in Chapter 3.8.1.1, the pressure and velocity at the outflow (Module) can be calculated by the iterations. In the T-rack system, the calculation is even more complex, because there are two T-connectors at the top and bottom sides of membrane module. The velocity at the outflow (Module) of T-connector is not only determined by the pressure at outflow (Module) of T-connector at its side, but also by the pressure at outflow (Module) of T-connector at the other side. With different pressures at the top and bottom sides of a module, the permeation volume flow distribution can be classified into two different types: dead-end and cross flow (see Figure 3.8.7). The total permeation volume flow of a module is expressed with $\dot{V}_{total}$ which is equal to the sum of the volume flow permeation from top side $\dot{V}_{top}$ (positive when fluid flows in and negative when fluid flows out) and from bottom side $\dot{V}_{bot}$ (positive when fluid flows in and negative when fluid flows out). The length of capillaries is divided into two parts: permeation length from top and permeation length from bottom. The permeation length is defined as the length of module where the feed fluid comes from the same direction (top or bottom).

For example the permeation length from top is defined as the length of the part of the module which has permeation from the top feed pipe. To distinguish the different flow situations in a module, an important parameter should be known: $\Delta p_{critical}$, which is defined as the pressure difference between top and bottom side of the module, when the permeation length from top is just equal to the total length of capillary (see Figure 3.8.7 c)). In this situation, there is no fluid entering into bottom pipes. In the other word, $\Delta p_{critical}$ occurs only when the flow situation just changes from the dead-end flow to cross flow. Because cross flow and dead-end flow have different calculation rules and equations, the $\Delta p_{critical}$ should be calculated firstly with the known inflow pressure (top) and permeability of membrane of module with Equation 3.2.6.

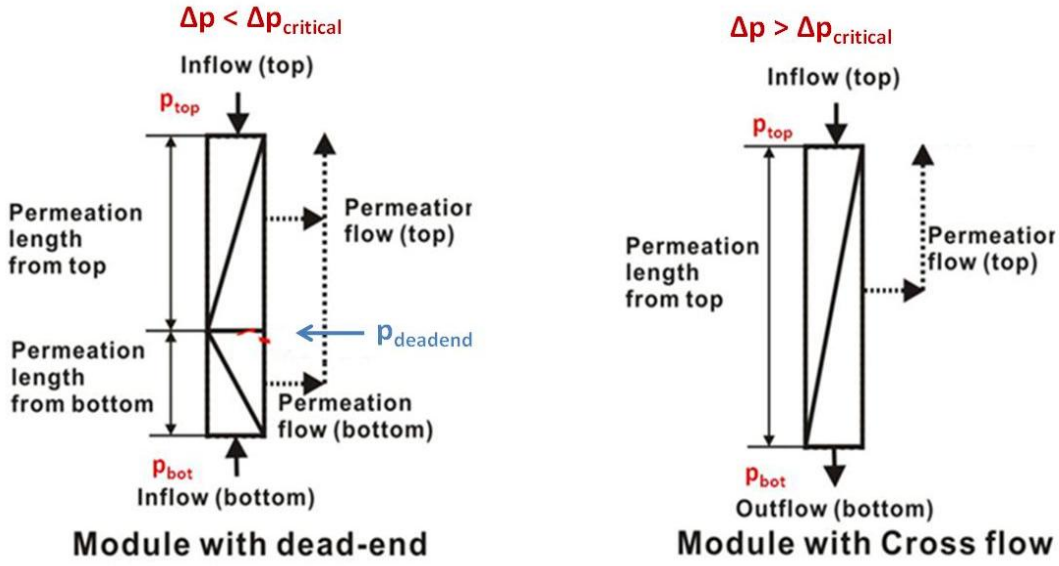

a) **b)**

Figure 3.8.7 a) b) Volume flow distribution and permeation length from both the top and the bottom side in the capillary module depending on $\Delta p = p_{top} - p_{bot}$: a) dead-end, b) cross flow.

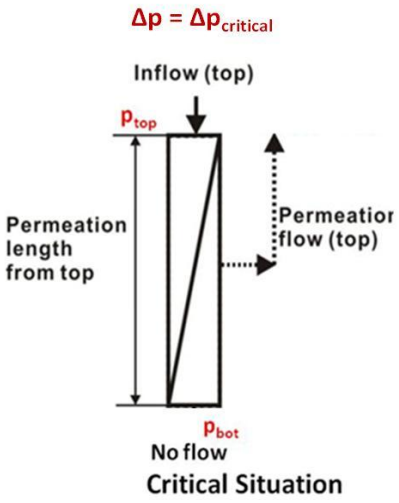

c)

Figure 3.8.7 c) Volume flow distribution and permeation length from both the top and the bottom side in the capillary module depending on $\Delta p = p_{top} - p_{bot}$: c) critical situation

If $\Delta p_{critical} < \Delta p$, it is the cross flow situation (see Figure 3.8.7 b)). The permeation length from top side is equal to the length of capillary. In this situation, part of fluid will flow into the bottom side pipe. From Equation 3.2.6, the relationship between inlet volume flow and pressure on the top and bottom side can be derived as:

$$B_k = (p(l_k) - p_p - A_k cosh(a \cdot l_k))/\sinh(a \cdot l_k) \qquad \textbf{Equation 3.8.8}$$

When

$$A_k = p_{in} - p_p \qquad \textbf{Equation 3.8.9}$$

$$B_k = -\frac{8\eta \dot{V}_{in}}{\pi R_k^4}\frac{1}{a} \qquad \textbf{Equation 3.8.10}$$

$$a = \sqrt{\frac{16}{R_k^3 R_m}} \qquad \textbf{Equation 3.8.11}$$

So the volume flow

$$\dot{V}_{in} = -\frac{\pi R_k^4}{8\eta a} \cdot (p(l_k) - p_p - A_k cosh(a \cdot l_k))/sinh(a \cdot l_k) \qquad \textbf{Equation 3.8.12}$$

l_k is the length of capillary. The $\dot{V}_{in}$ is the inlet volume flow of the capillary from the top side. Then the volume flow through the capillaries entering into the bottom side pipes can be calculated (see Equation 3.2.10).

If $\Delta p_{critical}$ > Δp, it is the dead-end flow mode inside capillary (see Figure 3.8.7 a)). In this mode, the flow will enter into capillary from both top and bottom sides and meet at one point in the capillary named dead-end point here. The volume flow at both top side and bottom side can be calculated by Equation 3.2.11 with an estimated permeation length of the top or bottom side. Then these calculated volume flows will be used to calculate the pressure at the dead-end point from both sides. According to the pressure definition of fluid dynamics, the pressure at the dead-end point from both sides should be equal. With this condition, the estimated permeation length will be adapted and multi-steps iterations will be run until the calculated pressures at dead-end point from both sides are the same. The logical diagram for the pressure and flow distribution in the capillary is shown in the Figure 3.8.8.

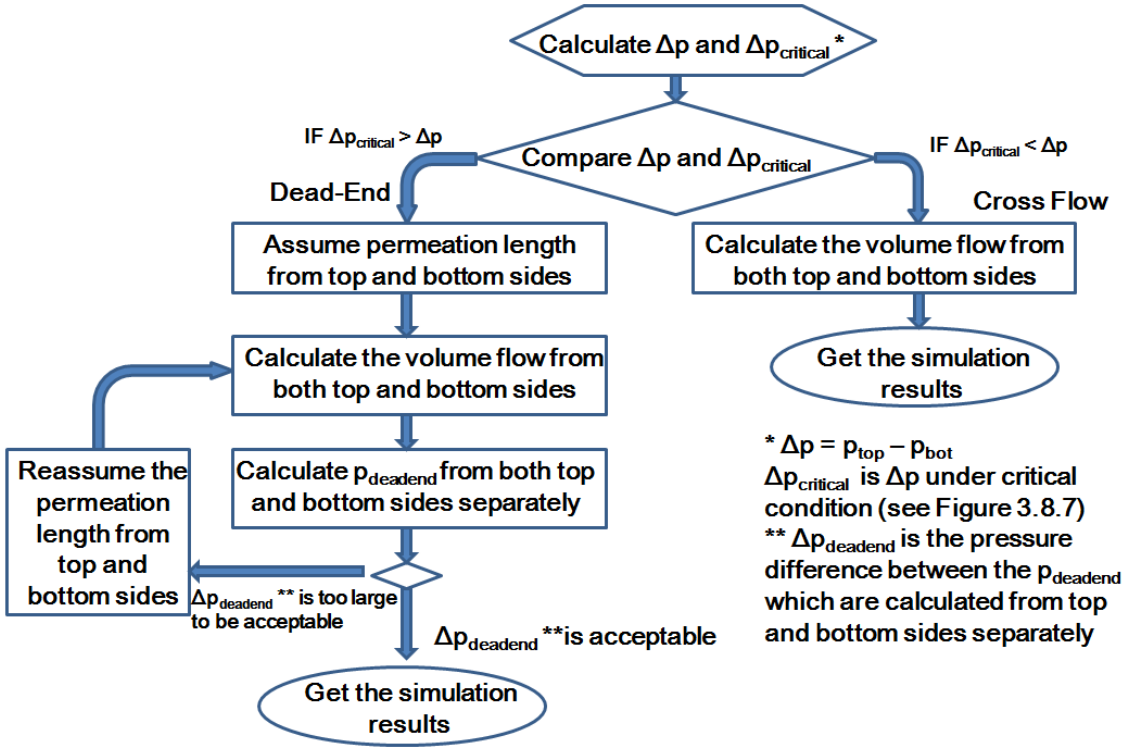

Figure 3.8.8 Logical diagram for the pressure and volume flow calculation in one capillary

3.8.1.3 General Logical Model of Filtration and Backwash Process

From last two sections, the calculation of pressure and velocity in the pipes and capillaries is introduced. In this section, the principle to combine the simulation models of pipes and capillaries to build the model of the complete system will be introduced.

In the filtration simulation, the known parameters are the required total volume flow, the pressure at the outlet of the permeate pipe, the pure water permeability of the membranes and the geometry of the system. A filtration system with eight modules including two rows (four modules in one row respectively) is taken as an example to show the simulation iteration principle and the logical diagram here.

As is introduced in last chapter, the permeation in the modules can be classified as dead-end and cross flow. If in one system, the permeation in some modules is in cross flow situation, there must be some other modules are in dead-end situation. The reason is that the flow which enters into bottom side feed pipes from top side feed pipes should be permeated in some modules where must be in dead-end situation. In other words, in the system, there must be minimal one module working in dead-end situation. The pressure difference between top and bottom sides of modules in dead-end situation must be smaller than that in cross flow situation as shown in last section. When one module has the smallest pressure difference between two sides, it is sure that the flow condition is dead-end. In all simulations, the iteration always started from the module which has smallest pressure difference between the top and bottom side. In order to show the simulation process in a simple way, the smallest pressure difference between the top and bottom side feed pipes is assumed in the 4^{th} module of one row (M4a shown in Figure 3.8.9).

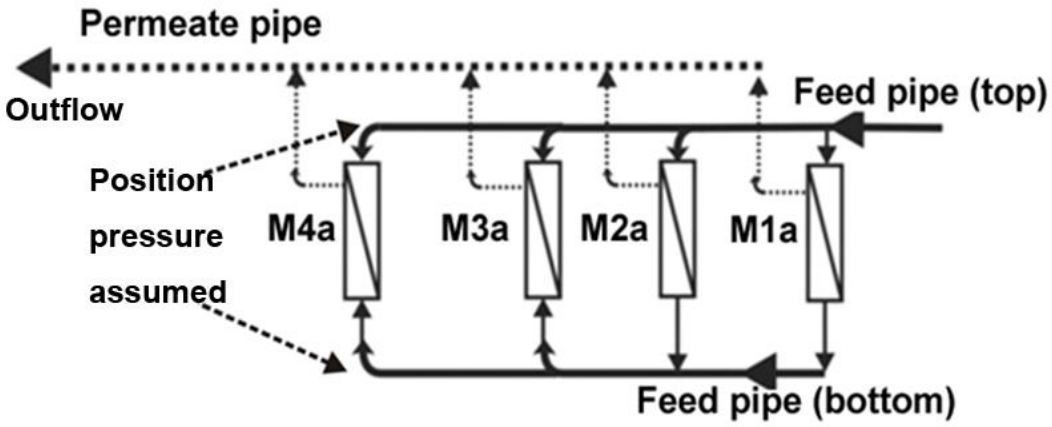

Figure 3.8.9 Flow distribution in one row of T-rack system. (The volume flow and the pressure of pipe at outlet of permeate pipe are known. The iterations start with the pressure assumption from the M4a.)

As shown in Figure 3.8.9, the simulation starts from the assumption of pressure at the end of the feed pipe. The detailed steps are shown as follows (see Figure 3.8.10):

- Assuming the pressures in the top and bottom sides feed pipes at the position of module M4a;
- Calculating the permeation flow of the corresponding module (firstly the fourth module M4a) with the logical diagram shown in Figure 3.8.8;
- Calculating the volume flows and the pressure loss, in the feed pipes (top and bottom sides) and the permeate pipe based on T-connector simulation model shown in Chapter 3.8.1.1, at the position of corresponding module respectively (e.g. the inflow volume flows of the pipes at position M4a are equal to the outflow volume flows of the pipes at position M3a);
- Calculating the pressure on both top feed, bottom feed and permeate sides of the connected module (e.g. M3a to M4a) based on the pressure loss calculated in step 3;
- Calculating the permeation flows in all modules following step 2 to 4;
- Checking the mass conservation of the bottom feed pipe and permeate pipe, if it is not balanced then reassume the bottom side feed pipe pressure at the module M4a

and calculating from steps 1 to 6 again.

- Checking the mass conservation of the whole system, if it is not balanced then reassume the top and bottom sides feed pipe pressures at the M4a and calculating from step 1 to 7 again.

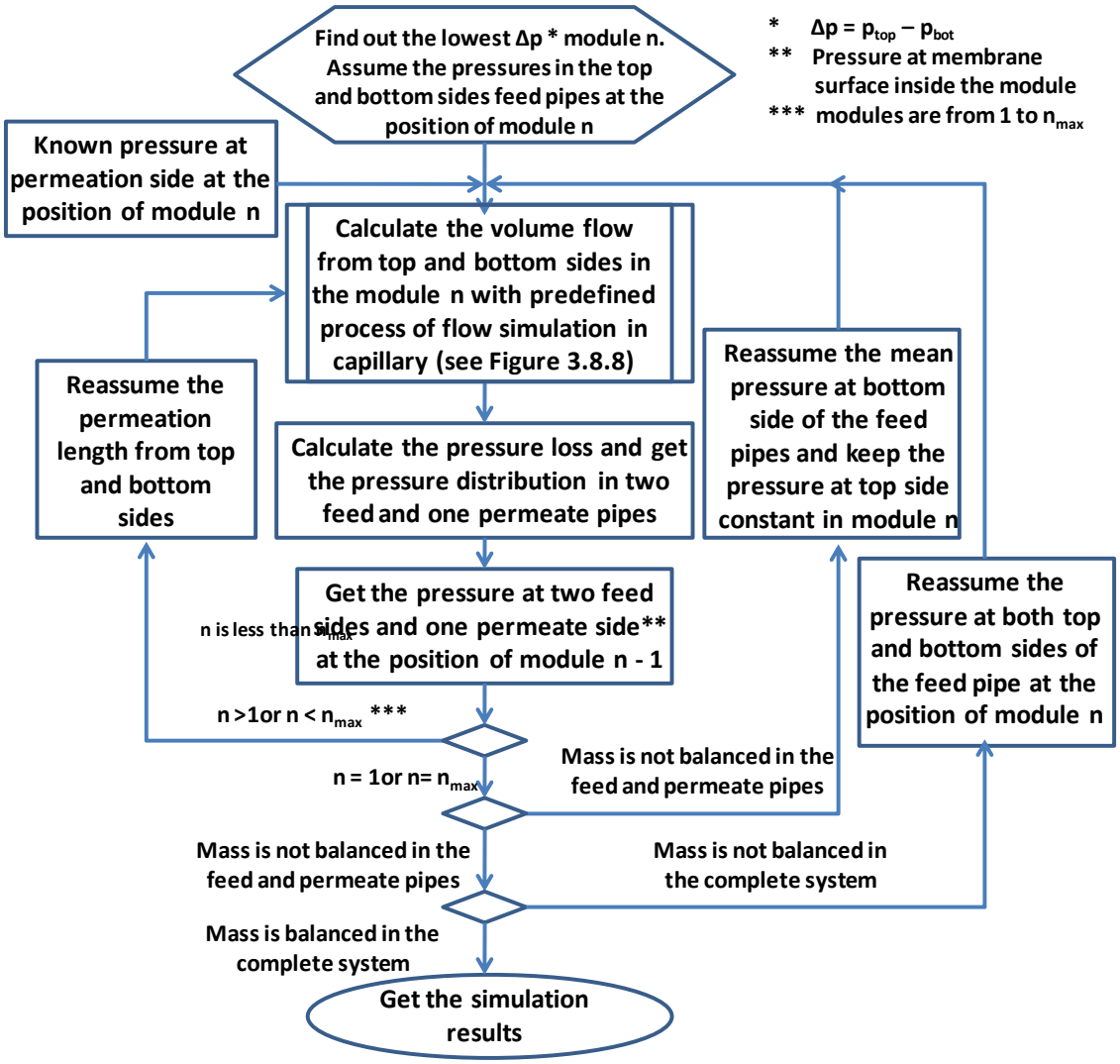

Figure 3.8.10 Logical diagram of the pressure and volume flow calculation for the filtration process of the T-rack filtration system

For the calculation of the permeation flow of modules, an additional iteration is needed for the "module to permeate pipe connector". This additional iteration is also based on the three reservoir rule (mass conservation and same water head at junction position) and starts with the pressure at the permeation side of the module. The pressure at the

permeation side of the module is assumed to be equal to the pressure inside the permeate pipe at the corresponding position firstly. For example, for the module M4a shown in Figure 3.8.9, the pressure at the permeation side of the module is assumed to be equal to the pressure at the outlet of permeate pipe. Based on the iterations and the three reservoir rule shown in Chapter 3.8.1.1, the pressure and velocity at the permeation side of the module M4a can be calculated with the known pressure and volume flow at the outlet of the permeate pipe.

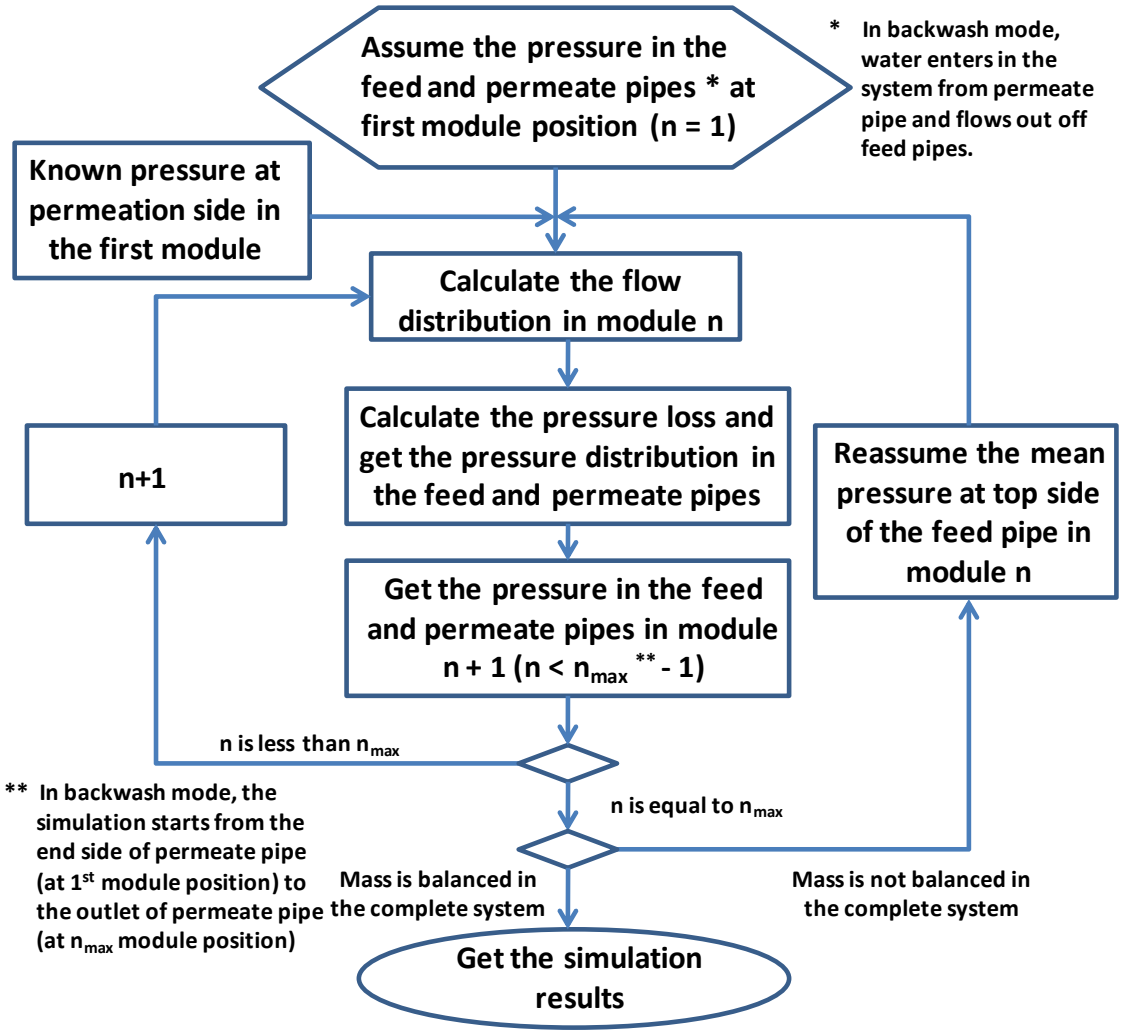

Figure 3.8.11 Logical diagram of the pressure and volume flow calculation for the backwash process of the T-rack system

Compared to the filtration situation, the simulation model of the backwash process can be considered as a simplified model. In this model, bottom side feed pipes are not

employed anymore, which means the flow simulation in the capillary as shown in Chapter 3.8.1.2 is unnecessary.

So the logical diagram can be simplified as following (see Figure 3.8.11):

- Assuming the pressure in the feed and permeate pipes at the position of module 1;
- Calculating the flow in both feed pipes and permeate pipe at the position of the corresponding module;
- Calculating the pressure loss in both feed and permeate pipes at the position of corresponding module;
- Calculating the pressure at both the feed and permeate sides of the connected module (e.g. module n to module n+1) based on the pressure loss calculated in step 3;
- Calculating the permeation flows all modules following step 2 to 4;
- Checking the mass conservation of whole system, if it is not balanced then reassuming the pressure in the feed and permeate pipes at the position of module 1 and calculating from step 1 to 6 again.

4. Simulation and Optimization Results

4.1 Validation of Simulation Model

The simulation model was validated with experiments in order to make sure the simulation results are reliable. Series of experiments were done with a 48 modules T-rack system. The diameter of feed pipes is 142 mm, the diameter of permeate pipe is 235 mm, the diameter of module inner cylinder is 225 mm and the height of the module is 1680 mm. This geometry is considered as the standard geometry. With these data, the accuracy of simulation model was tested and certified. After that, the model was applied to predict, analyze and further optimize the influencing parameters. In the simulation and experiments, the trans-membrane pressure (TMP) is the pressure difference between the pressures in the feed and permeate pipe at different modules, because it is easy to be measured in the experiments.

4.1.1 Validation of T-rack System

The denotation of the filtration system is necessary to be introduced firstly. From the denotation, the parameters at the surface of the membrane or in the pipes, at the permeate side or retentate side and in different rows of feed pipes can be easily defined and recognized. In Figure 4.1.1, the denotation of the parameters is shown. The definition of denotation is explained in Appendix C.

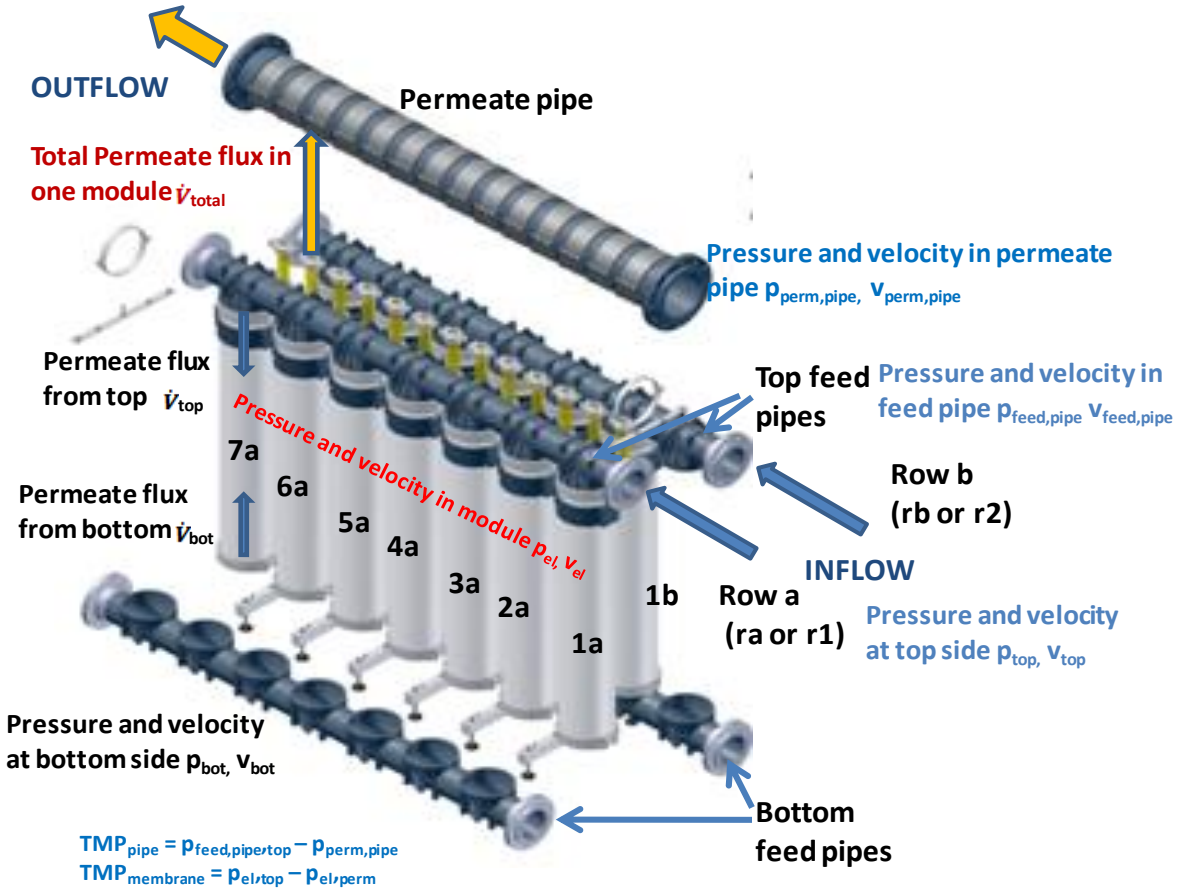

Figure 4.1.1 The denotation for the parameters at different position

The validation of the model was done under three different experimental setups: the first is the filtration process with a required volume flow of Q = 240 m³/h for 48 modules (2 rows with 24 modules each see Figure 4.1.1), the second is the filtration process with a volume flow of Q = 550 m^3/h for 48 modules, and the third is the backwash process with a volume flow of Q = 550 m³/h for 48 modules. In order to have a fast simulation, the calculation iteration tolerance is set to be less than 2% normally, maximal 5%. In the simulation, the permeability of the membrane was set to 380 l/ (m²hbar) which should be homogenously distributed in all modules, while in the experiment the permeability of each module is not perfectly identical.

4.1.1.1 Filtration process with 48 Modules

In the experiments, the fluid flowed into the system from the right side of both top side

feed pipes, and flowed out from the left side of the permeate pipe. In the simulation, the pressure at the outlet of permeate pipe is assumed to be 0, while in the experiments it has an unsure value which is strongly dependent on the external piping system. In order to make the results of simulation and experiments comparable, the post process is needed. (see Chapter 3.8)

In Figure 4.1.2 the experimental results show, that along the flow direction the pressure in the permeate pipe obviously decreases while in the top feed pipe slightly increases. The pressure in the top feed pipe increases from 420 mbar to 430 mbar. The pressure in the bottom feed pipe is nearly constant about 570 mbar. The pressure in the permeate pipe decreases from 152 mbar to 121 mbar. The TMP, which was calculated by the pressure difference between the top side feed pipe and permeate pipe at different module positions, increases along the flow direction and the corresponding permeation flux also increases.

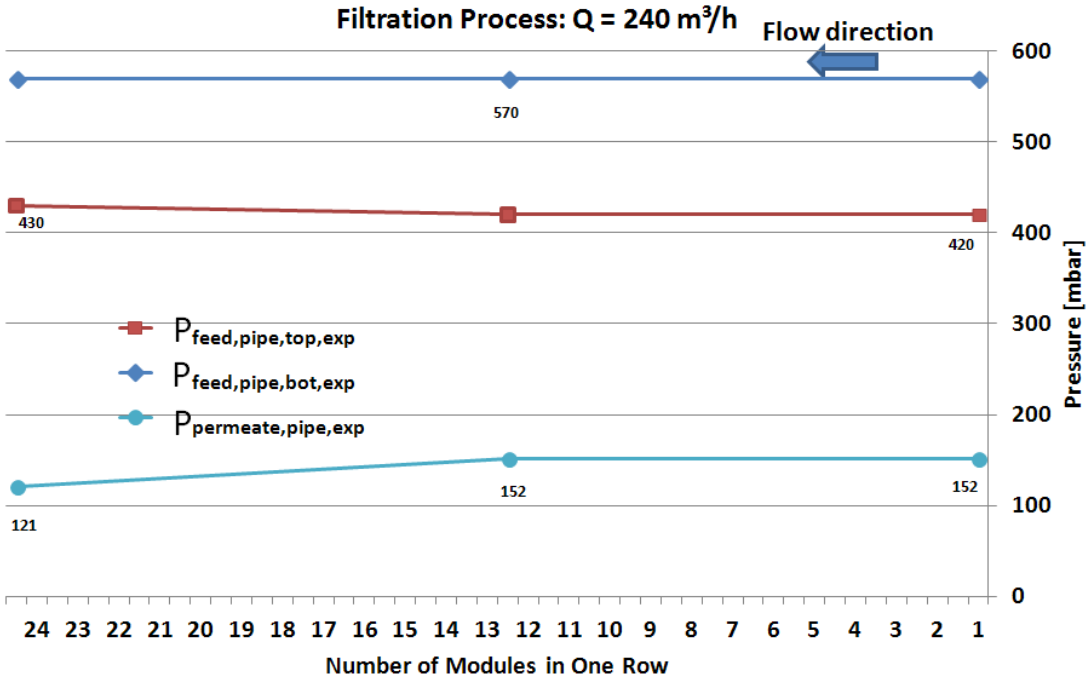

Figure 4.1.2 Experimental results: the pressure distribution in the pipes in a 48-modules filtration system with a required volume flow of 240 m³/h.

In the simulation, the flow direction is the same as in the experiment. After the gravity

and pressure at the outlet of the permeate pipe are adjusted, the simulation results are shown in the Figure 4.1.3. In the simulation the pressure in the permeate pipe decreases from 163 to 121 mbar along the flow direction. The difference between the pressure at the dead-end side (right side in Figure 4.1.3) of the permeate pipe in the simulation and that in the experiments is 11 mbar which is 7.2% of the experimental value. The pressure in the top side feed pipes decreases from 440 mbar to 437 mbar and then increases to 439 mbar along the flow direction. The minimum pressure of 437 mbar arises at module 8. The difference of the pressure in the top side feed pipe between simulation and experiment is about 15 mbar, or 3.5% of the experimental value in average. The pressure in the bottom pipe is nearly constant about 544 mbar which is -26 mbar or 5.3% less than that in the experiment in average. From the comparison, the largest difference of the pressure in the pipes between experiment and simulation is less than 7.2%.

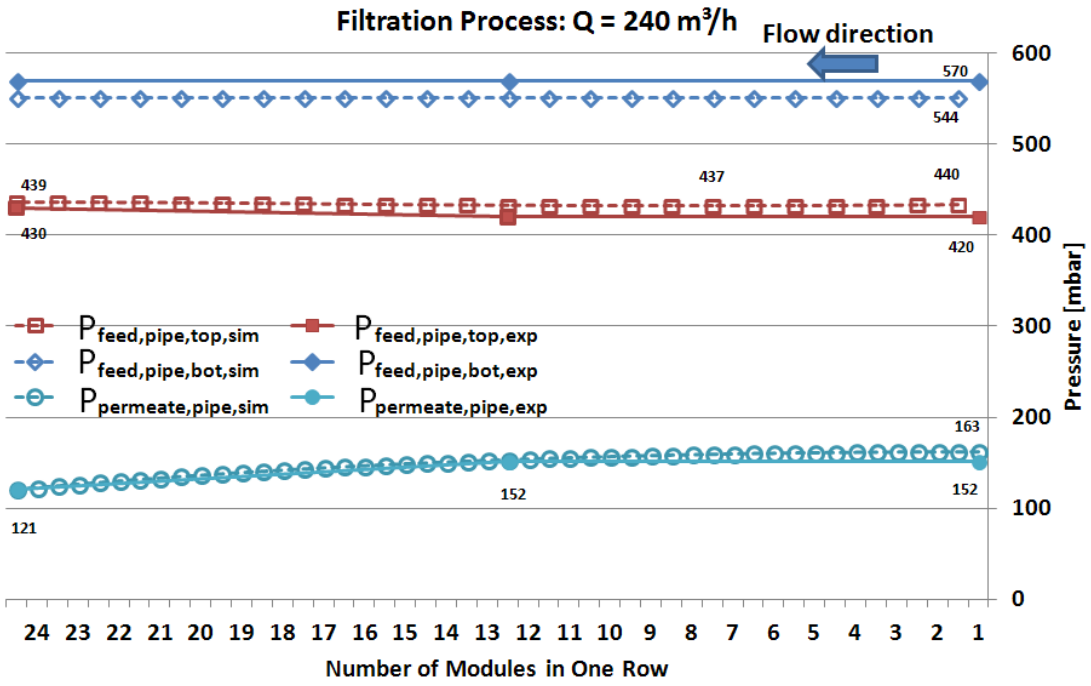

Figure 4.1.3 Experimental and Simulation results: the pressure distribution in the pipes in a 48-modules filtration system with a required volume flow of 240 m³/h.

The experimental results of the permeation volume flow distribution of modules in the system are shown in Figure 4.1.4. From the experimental results, the total permeation

volume flow of each module is around 7.5 m³/h. On this basis the complete system volume flow is calculated to be 360 m³/h which is higher than the predefined value of 240 m³/h. The permeation volume flow of modules should be dependent on the TMP respectively. Based on the Darcy's Law and permeability of membranes, the TMP should be around 395 mbar if the permeation flow is about 7.5 m³/h. The possibility is the inhomogeneous permeability of membrane in different modules. The measured modules are with high permeability and others are low. The measured permeation flow is much higher than what it should be, while the TMP is the more or less to what it should be for the required permeation volume flow 240 m³/h of 48-modules system, which theatrically be around 263 mbar.

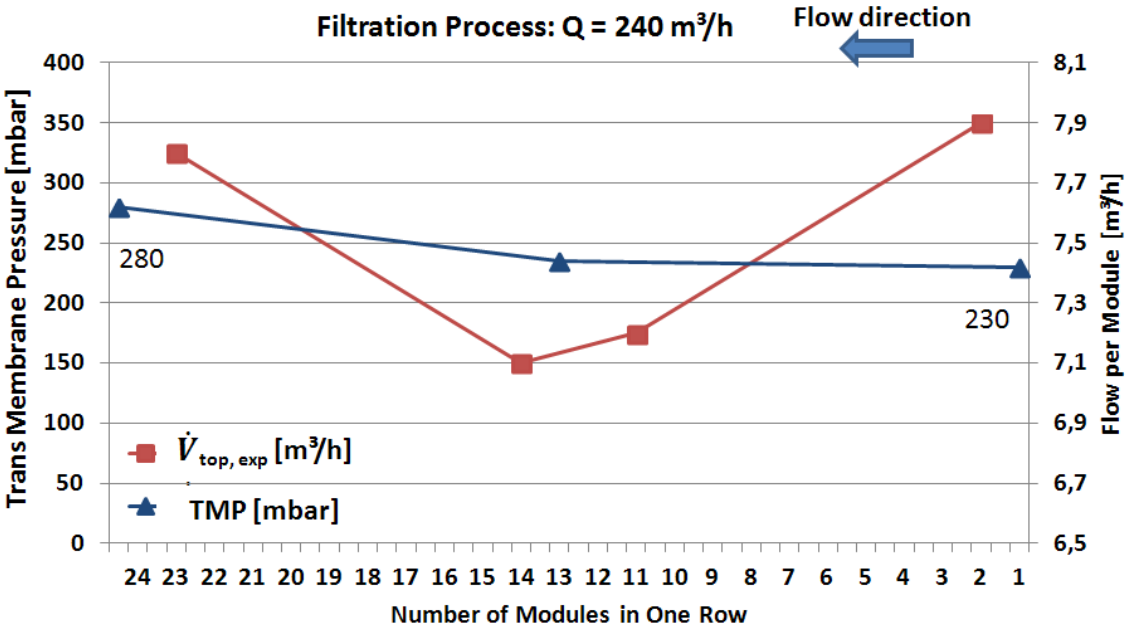

Figure 4.1.4 Experimental results: the permeation volume flow and TMP distribution of modules in a 48-modules filtration system with a required volume flow of 240 m³/h

Compared to the experimental results, the simulation results shown in Figure 4.1.5 are more reliable. As is introduced in Chapter 3.8.1.2, $\dot{V}_{total}$ is defined to be the total permeation flow of one module and $\dot{V}_{top}$ is the volume flow entering into the module from the top side pipe. The total permeation flow per module $\dot{V}_{total}$ (red curve or dark

color) increases from 4.8 to 5.2 m³/h along the flow direction shown in Figure 4.1.5. The reason for the difference between $\dot{V}_{total}$ and $\dot{V}_{top}$ is the effect of the bottom pipe. The sum of the volume flows shown by two curves in Figure 4.1.5 will be same due to the mass conservation.

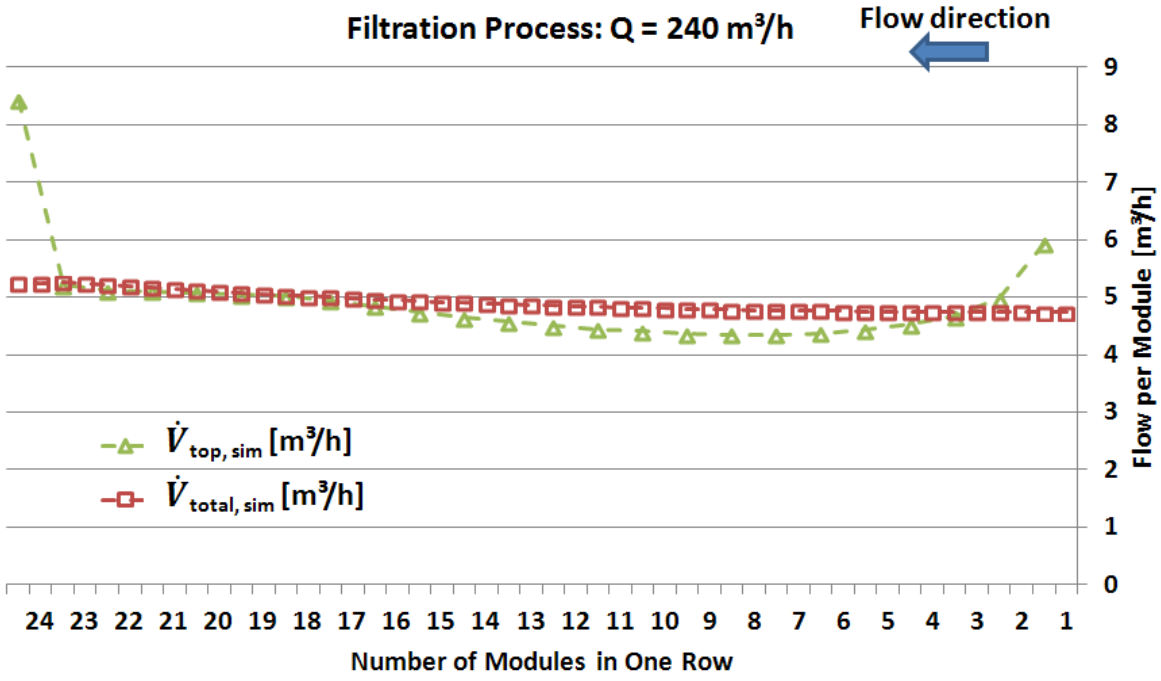

Figure 4.1.5 Simulation results: the total permeation volume flow and the permeation volume flow from top side of modules in a 48-modules filtration system with a required volume flow of 240 m³/h

In the experiment, the TMP in each module increases from 230 mbar to 280 mbar along the flow direction (see Figure 4.1.4). In the simulation results, the TMP increases from 256 mbar to 290 mbar as shown in Figure 4.1.6. The largest difference between experimental and simulation results is 26 mbar which is 11.3% of the experimental value and the smallest difference is 10 mbar, or 3.6%.

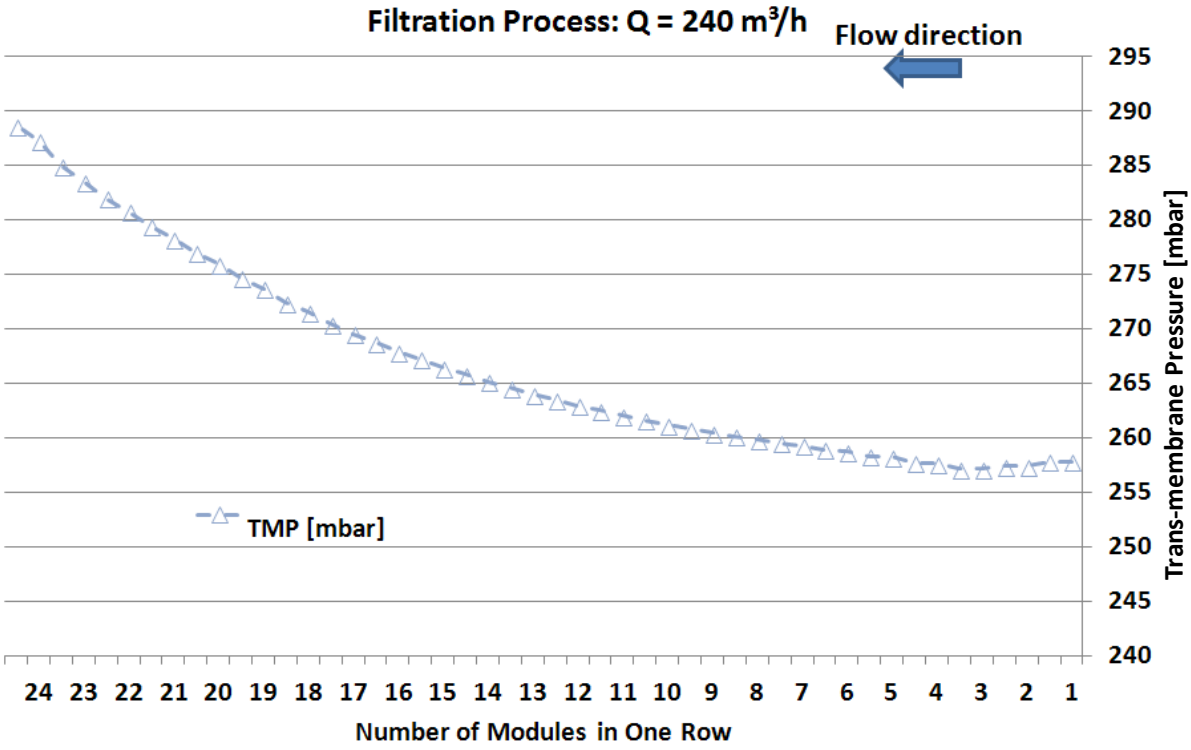

Figure 4.1.6 Simulation results: the TMP of modules in a 48-modules filtration system with a required volume flow of 240 m³/h

In order to make the simulation model more reliable, besides the process with a required volume flow of 240 m³/h, the process with a volume flow of 550 m³/h was also tested for the same structure system. The required volume flow set to 550 m³/h can be used to check the flexibility and stability of the model in different velocities.

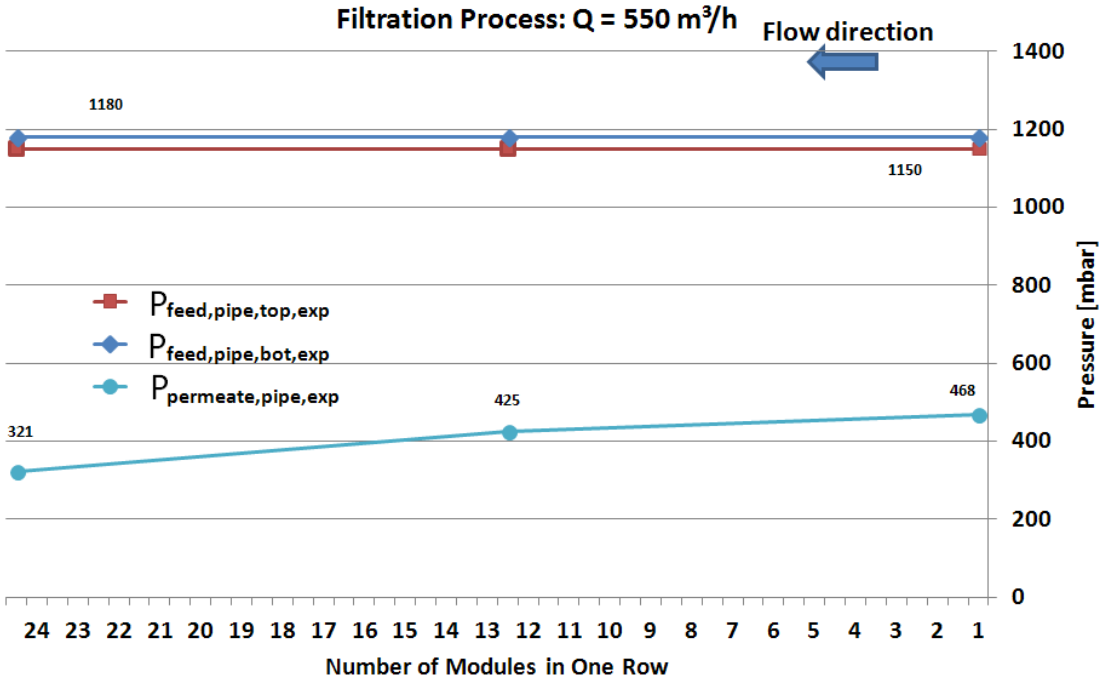

Figure 4.1.7 Experimental results: the pressure distribution inside pipes in a 48-modules filtration system with a required volume flow of 550 m³/h

In the experimental results (see Figure 4.1.7), along the flow direction, the pressure in the permeate pipe decreases from 468 mbar to 321 mbar. This 321 mbar is due to the outer piping system and will be applied as adjusted value in the post process for the simulation. The pressures in the top feed pipes and bottom pipes are nearly constant which are about 1150 mbar and 1180 mbar.

In the simulation results, along the flow direction, the pressure in the permeate pipe decreases from 495 to 321 mbar as shown in Figure 4.1.8. The pressure in the top side feed pipes at first decreases from 1102 to 1086 mbar and then increases to 1100 mbar. The minimum value occurs at module 13. The pressure in the bottom feed pipes is nearly constant 1183 mbar.

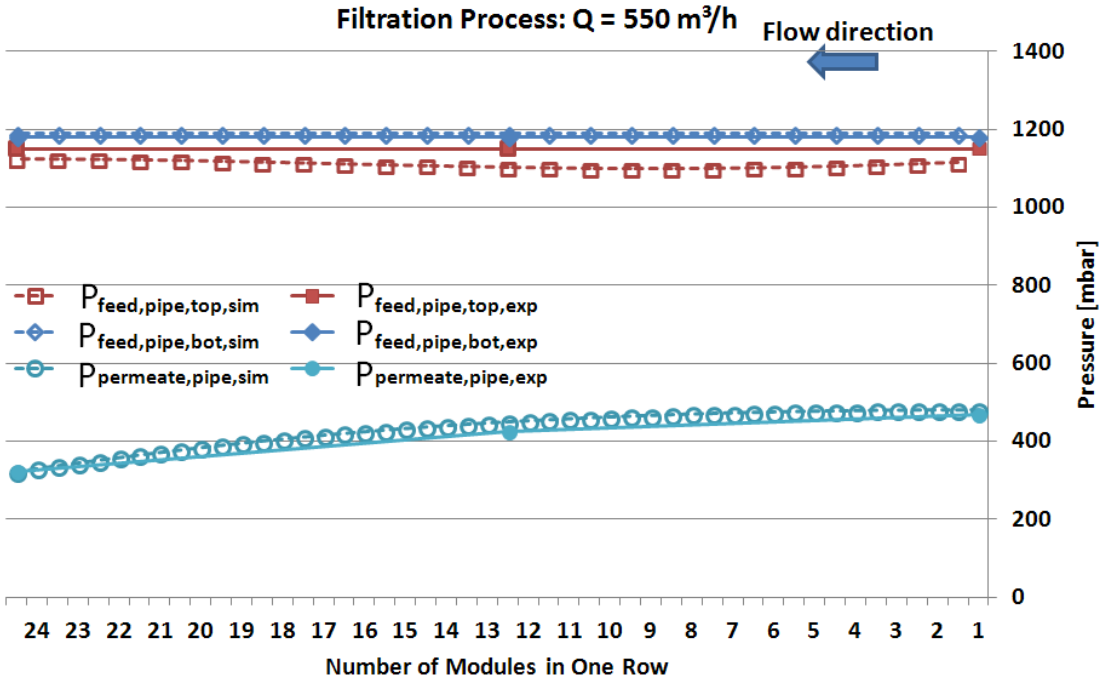

Figure 4.1.8 Simulation results: the pressure distribution inside pipes in a 48-modules filtration system with a required volume flow of 550 m³/h

From comparison between the simulation and experimental results, the difference between the pressures at the right side of the permeate pipe is 27 mbar which is 5.6% of the experimental value. The largest difference of the pressures in the top feed pipe between the simulation and experiment is -64 mbar or -5.8%, and the smallest difference is -48 mbar or -4.3% of the experimental value. Compared to the required flow of 240 m³/h situation, the pressure decrease and increase trend is more obvious in required flow of 550 m³/h.

Besides the comparison of the pressure distribution, the permeation volume flow distribution of modules in the system was compared too. From the experimental results shown in Figure 4.1.9, along the flow direction, the volume flow per module firstly decreases from 12 m³/h to 11 m³/h and then increases to 13.4 m³/h, while the TMP here keep increasing from 580 to 700 mbar.

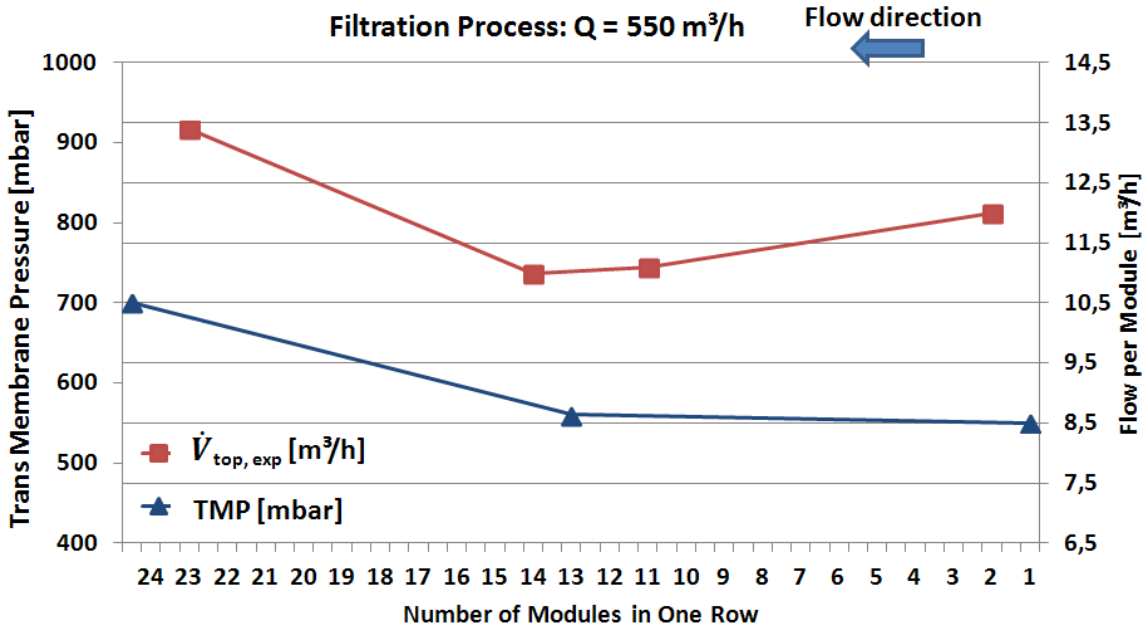

Figure 4.1.9 Experimental results: the permeation volume flow and TMP of modules in a 48-modules filtration system with a volume flow of 550 m³/h

In the simulation results shown in Figure 4.1.10, the total permeation flow per module $\dot{V}_{total}$ slightly decreases from 11.3 m³/h to 11.1 m³/h and then increases to 13.2 m³/h and the lowest permeation occurs at module 7. The volume flow of water entering the modules from the top side pipes $\dot{V}_{top}$ is also shown in the figure. In one module, $\dot{V}_{top}$ is larger than $\dot{V}_{total}$ means that water not only permeates through membranes but also enters into bottom side pipes from top side pipes. The Figure 4.1.10 shows that one part of the fluid will enter into the bottom pips from top pipes from first and last modules and permeate from the middle modules.

Compared to the curves shown in Figure 4.1.5, the difference between $\dot{V}_{total}$ and $\dot{V}_{top}$ is larger here, which means the influence of bottom pipe is stronger when the volume flow is 550 m³/h.

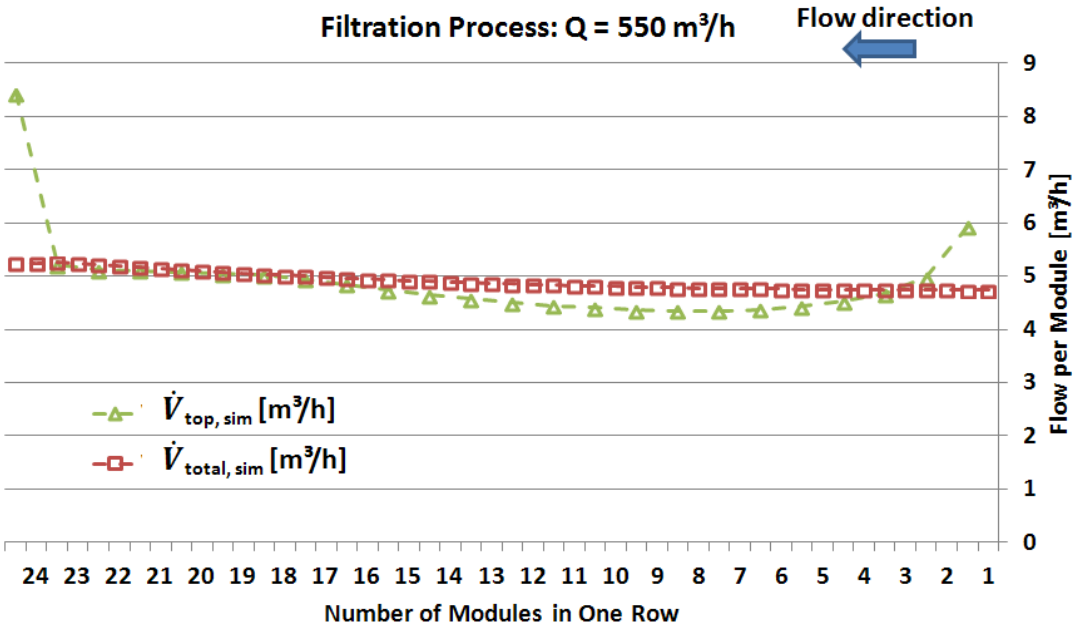

Figure 4.1.10 Simulation results: the total permeation volume flow and the permeation volume flow from top side of modules in a 48-modules filtration system with a required volume flow of 550 m³/h

In the simulation results, the corresponding TMP also decreases firstly from 612 mbar to 598 mbar at module 7 and then increases to 715 mbar as shown in Figure 4.1.11.

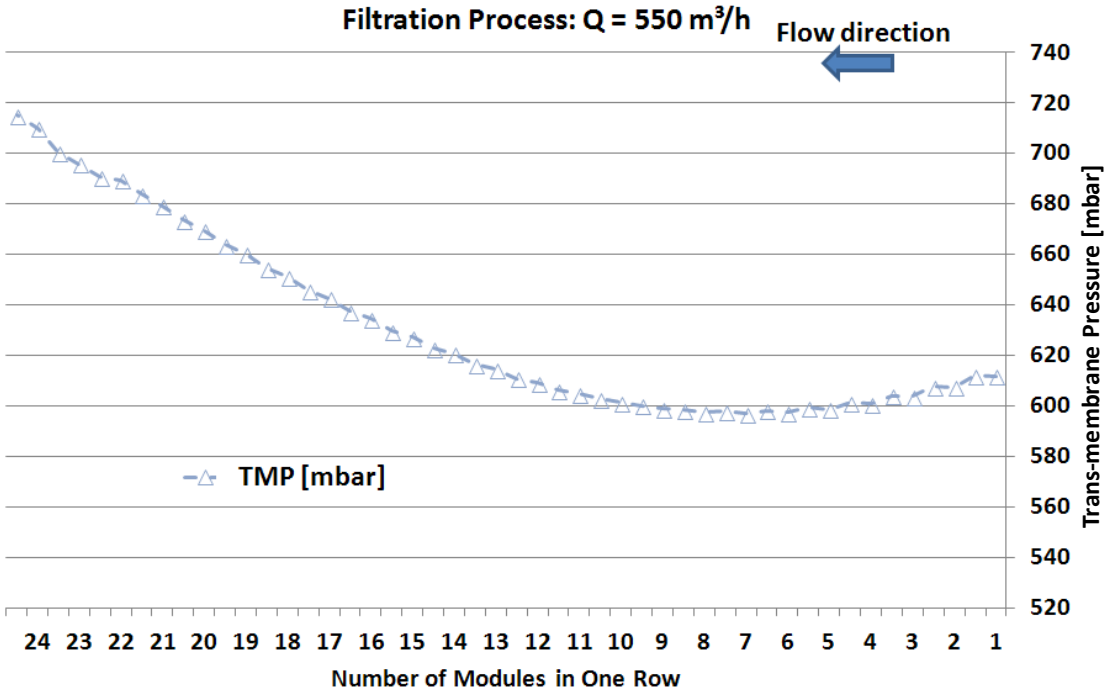

Figure 4.1.11 Simulation results: the TMP of a 48-modules filtration system with a required volume flow of 550 m³/h

Comparing Figure 4.1.9, Figure 4.1.10 and Figure 4.1.11, the difference of the permeation volume flow and TMP of modules between the simulation and experimental results is not so large than that shown in the 240 m³/h situation. The difference of permeation volume flow of modules between the simulation and experiment is about 0.5 m³/h which is 3.8% of the experimental value in average. The maximum difference of TMP between the simulation and experiment is 30 mbar which occurs at the inlet position of feed pipe (right side shown in the Figures) or 5.2% of the experimental value. At the end of feed pipe (left side shown in the Figures), the difference of TMP between the simulation and experiment is only 18 mbar or 2.6% of the experimental value. Although the module which has lowest permeation flux in the experimental and simulation results is different, whatever, the firstly increase and then decrease trend of the permeation fluxes in different modules along the flow direction is confirmed.

4.1.1.2 Validation of Backwash process with 48 Modules

The validation of backwash process was also done based on the comparison of the pressure and volume flow. In the backwash process, the fluid flows from the left side permeate pipe to the right side feed pipes, through the capillary modules. As shown in Figure 4.1.12, the pressure increases from 1230 mbar at inlet of permeate pipe to 1272 mbar in the middle of the module and finally to 1280 mbar at the dead-end side (right side shown in the Figure 4.1.12) along the flow direction. The pressure in the top feed pipe decreases from 709 mbar to 450 mbar. The pressure in the bottom feed pipe decreases from 1000 mbar to 990 mbar. While in theory it should be constant because of the unemployment of bottom feed pipes in the backwash process. But the decline of the pipe along the bottom feed pipe is very small which satisfies the theoretical calculation. As in the filtration process, the pressure at outlet of top side feed pipe and gravity was used to adjust the simulated results in the post process.

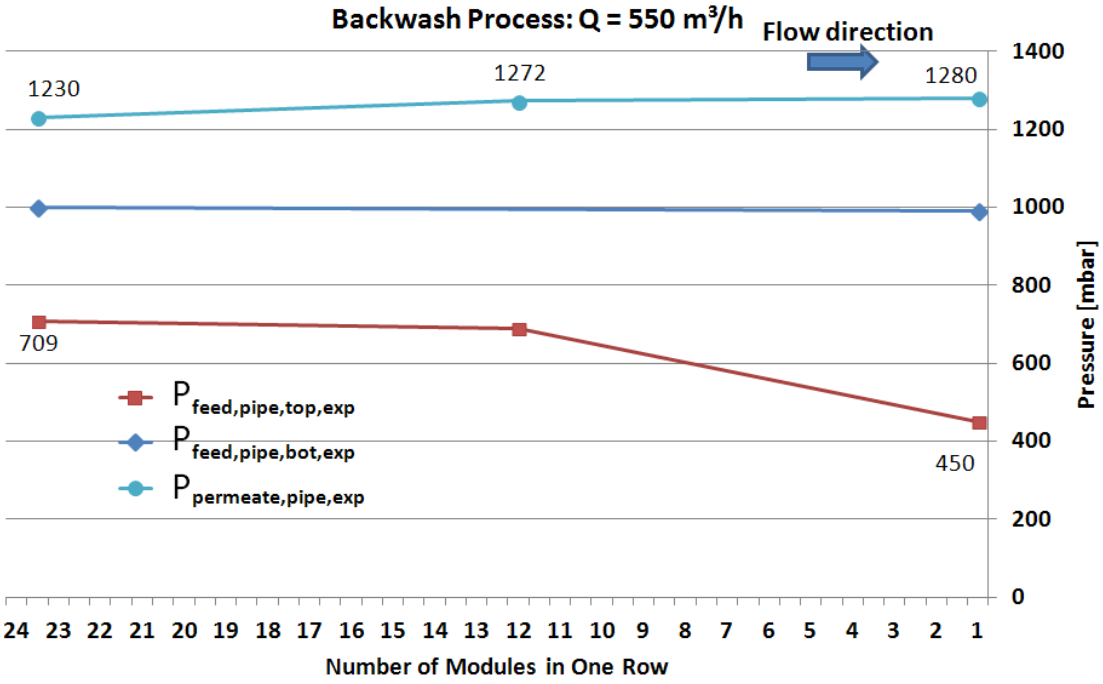

Figure 4.1.12 Experimental results: the pressure distribution inside pipes in a 48-modules filtration system with a required backwash volume flow of 550 m³/h

In the simulation results shown in Figure 4.1.13, the pressure in the permeate pipe increases from 1287 mbar to 1348 mbar along the flow direction. The difference of the pressure in the permeate pipe at the inflow side (in Module 24 shown in Figure 4.1.13) between the simulation and experiment is 57 mbar. The simulation value is 5% higher than the experimental value. The difference of the pressure in the permeate pipe at the dead-end side (in Module 1 shown in Figure 4.1.13) between the simulation and experiment is 68 mbar. The simulation value is 5.3% higher than the experimental value. In the simulation, the pressure in the top side feed pipes decreases from 654 to 450 mbar. The difference of the pressure in the top feed pipe at the inflow position between the simulation and experimental results is 55 mbar. The simulation value is 7.8% less than the experimental value. The pressure in the bottom feed pipe is constant 1000 mbar in the simulation, which is 10 mbar or 1% more than that of experiment.

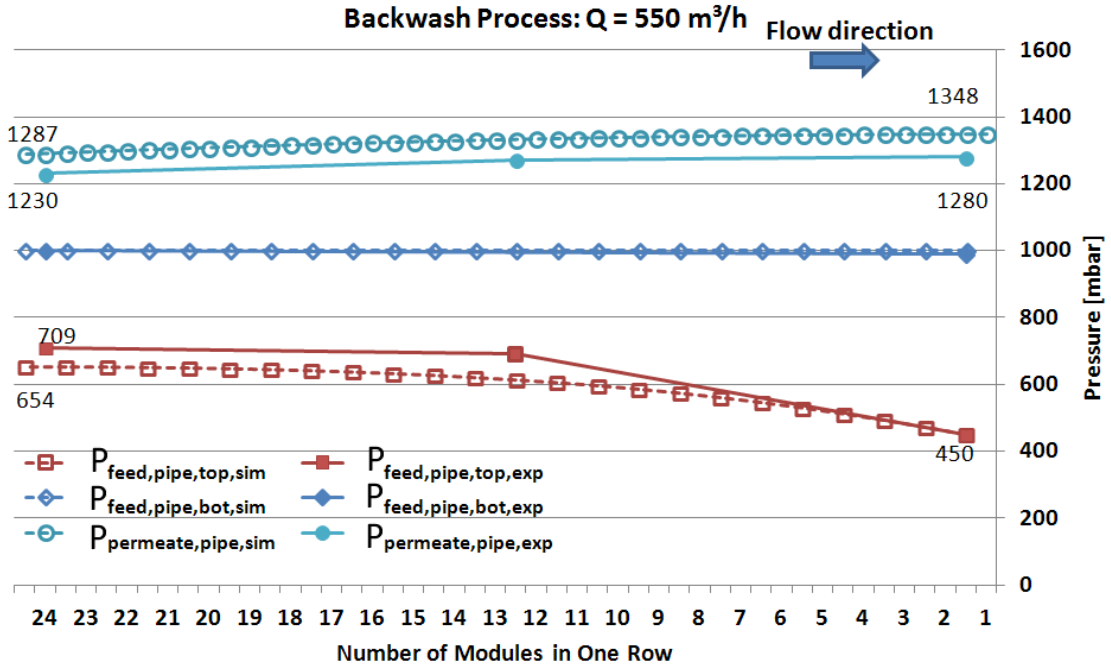

Figure 4.1.13 Simulation results: the pressure distribution inside pipes of a 48-modules filtration system with a required backwash volume flow of 550 m³/h

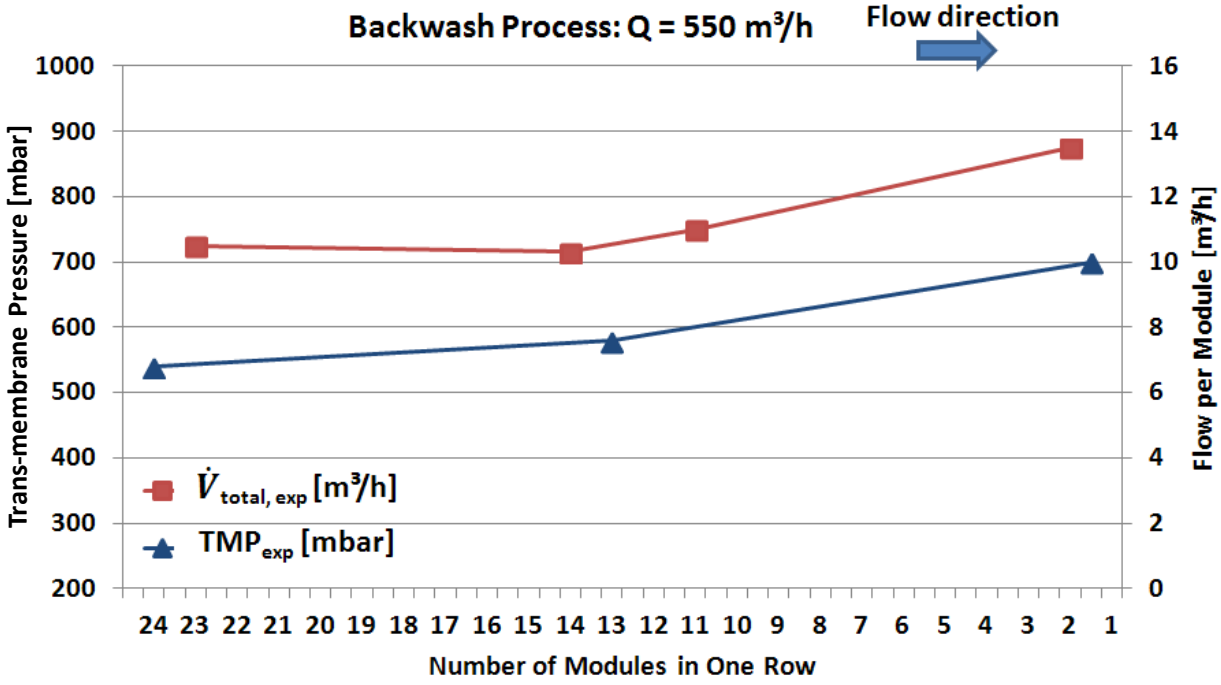

Figure 4.1.14 Experimental results: the permeation volume flow and TMP distribution of modules in a 48-modules filtration system with a required backwash volume flow of 550 m³/h.

In the experimental results shown in Figure 4.1.14, the volume flow per module

increases from 10.5 m³/h at the inflow of the permeate pipe to 13.5 m³/h at the right side outflow of the feed pipe. The TMP increases from 500 mbar to 700 mbar along the flow direction.

In the simulation results shown in Figure 4.1.15, the permeation volume flow of modules increases from 10.8 m³/h to 13.4 m³/h. The difference of the permeation volume flow of the module 23 between the simulation and experimental results is about 0.3 m³/h, 1% of the experimental value which is also the maximum difference of the permeation volume flow between the simulation and experimental results. The difference of the permeation volume flow of the module 2 between the simulation and experimental results is 0.1 m³/h or 0.7% of the experimental value which is the minimum difference.

In the simulation, the TMP increases from 645 mbar to 740 mbar. The maximum difference of TMP between the simulation and experimental results occurs in Module 1 where water leaves the system from the feed pipes, which is 100 mbar, 18.5% higher than the experimental value. The minimum difference of TMP between the simulation and experimental results occurs in Module 24 where the flow enters into the system from the permeate pipes, which is 40 mbar, 1% higher than the experimental value.

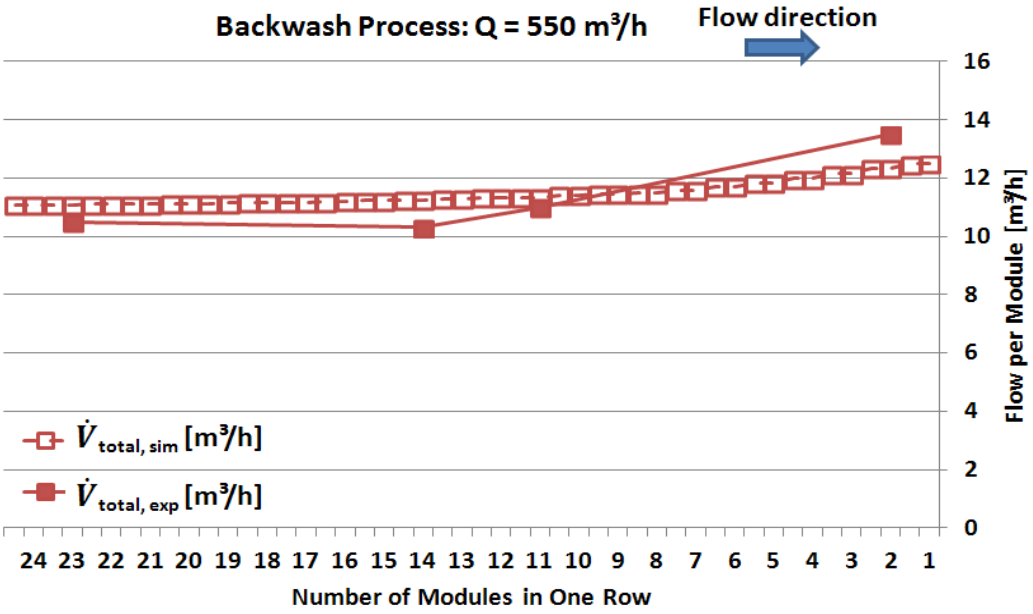

a)

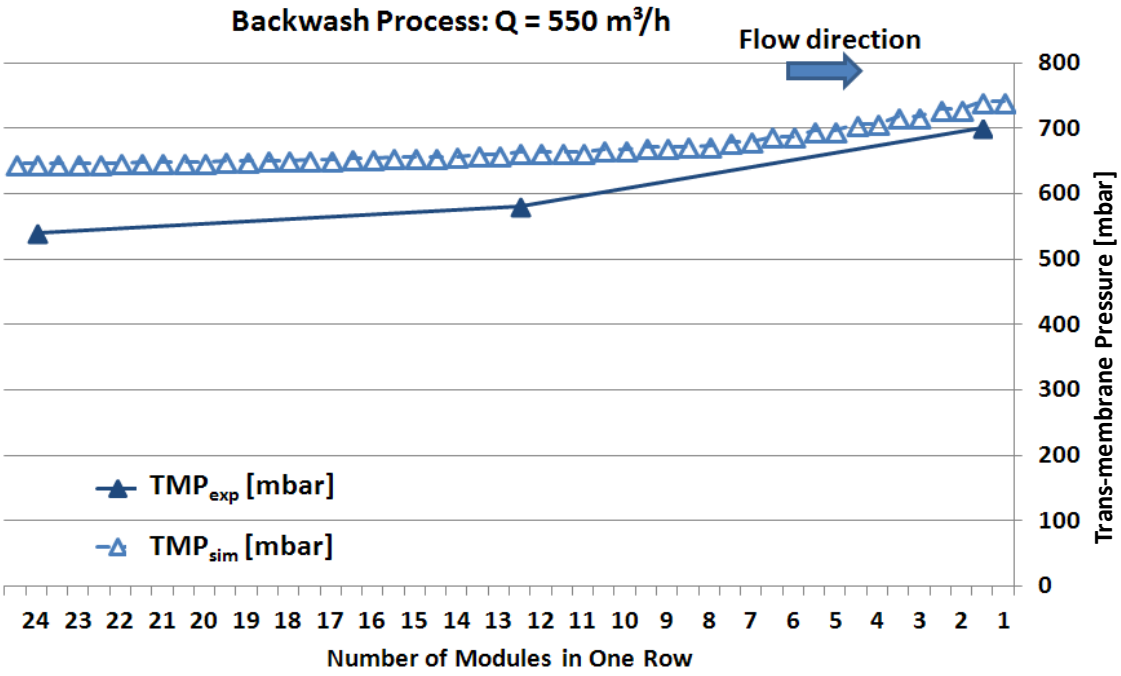

b)

Figure 4.1.15 Simulation results: a) the permeation volume flow and b) TMP distribution of modules in the 48-modules filtration system with a required backwash volume flow of 550 m³/h

From comparison of the simulation and experimental results of the backwash process, it shows that the maximum difference of TMP between simulation and experimental results

happens in the Module 1 where water leaves the system from the feed pipe which is 16.6% of experimental value. From the view of permeation volume flow per module, the pressure in feed and permeate pipes, and the TMP in the modules, the simulation results are acceptable; hence the model of backwash process was employed for the further topic: analysis of system influencing parameters.

4.2 Analysis of System Influencing Parameters of the T-rack System

The parameters such as the required volume flow (velocity), membrane permeability, number of modules, bottom pipe design, geometry (diameter) of inflow and permeate pipes and an optimal inflow design are required to be checked and analyzed in both filtration and backwash process with an influencing parameter analysis.

The criteria of the influencing parameter analysis are the performance homogeneity, the energy consumption and productivity of the system. The performance homogeneity is a key parameter to show the stability of the system operation. A stable system usually means long life cycle, easy and safe operation As is mentioned in Chapter 1.1, the performance homogeneity shows whether the different modules in one system have similar permeability, productivity etc. In order to check the performance homogeneity, the complete system was divided into two half parts: Rack 1 and Rack 2. The sum of permeation flows of modules in Rack 1 and Rack 2 are expressed with Q_{rack1} and Q_{rack2}. For example in a 24-modules system, Rack 1 consists of 1 to 12 which is from inlet to middle of the system and Rack 2 consists of modules 13 to 24 where $Q_{rack1}=\sum_{1}^{12}\dot{V}_{total}$ and $Q_{rack2}=\sum_{13}^{24}\dot{V}_{total}$. If the difference between Q_{rack1} and Q_{rack2} is smaller, the permeation homogeneity is higher. If the difference between them is larger, then permeation homogeneity is lower. The energy consumption can be expressed by the required driving pressure of the system and the productivity is the ratio of the volume of permeation flow to the required energy. Other consumption parameters like chemical substances are not considered here.

4.2.1 Influencing Parameters in the Filtration Process

4.2.1.1 Volume Flow

As is described in Chapter 4.1, the TMP in the T-rack system is strongly correlated to the pressure drops in the permeate pipe. From the theory, higher flow velocity will lead to a higher pressure loss. Higher pressure loss in the permeate pipe leads to larger differences of TMP between different modules in one filtration system. Then the permeation flow driven by the TMP in different modules surely has higher difference and the system performance homogeneity becomes worse. The influence of different volume flows to the system homogeneity is shown in Figure 4.2.1 by the sum of permeation volume flow of modules in Rack 1 and Rack 2: Q_{rack1} and Q_{rack2}.

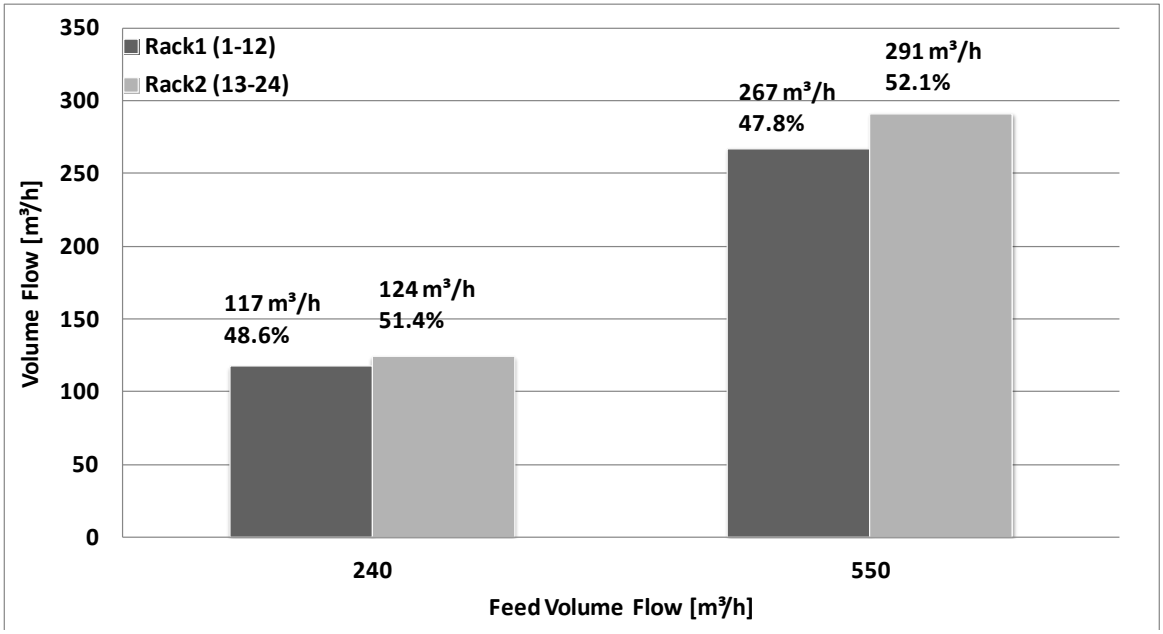

Figure 4.2.1 Simulation results: the sum of permeation volume flow of the modules belong to Rack 1 and Tack 2 in a 48-modules filtration system with different required volume flows in the filtration process

In Figure 4.2.1, the difference between Q_{rack1} and Q_{rack2} is very small in the filtration system with required volume flow Q = 240 m³/h which is only 7 m³/h, 2.8% of the required 240 m³/h volume flow. When the required permeation flow of the system

increases to 550 m³/h, the difference between Q_{rack1} and Q_{rack2} increases to 24 m³/h, 4.3% of the required permeation flow of the system which is still a quite good performance homogeneity. However, with an increase of the volume flow by a factor of 2.3 (Q = 240 m³/h to Q = 550 m³/h), the difference between Q_{rack1} and Q_{rack2} increases by a factor of 3.4 (7 m³/h to 24 m³/h).

As shown in Figure 4.1.3 and 4.1.8, the pressure at the inlet of the top side feed pipe can be considered as the required driving pressure. With the influence of gravity and external piping system, the required driving pressures of the systems with 240 m³/h and 550 m³/h are 440 and 1102 mbar respectively. In another word, the required driving pressure increases 2.5 times while the volume flow increases 2.5 times. As is introduced in Chapter 3.8, the influence of the external piping system is calculated from experimental results and added in the post process of simulation. All the required driving pressure in the simulation results shown in the next chapters will not have the influence of external piping system and gravity.

4.2.1.2 Permeability of Membranes

From the governing law of membrane permeation, the permeation flux is proportional to TMP. The proportionality factor is the permeability of the membrane. The permeability of the membrane is an important parameter which can change the performance homogeneity and the required driving pressure of a filtration system.

From the view of permeation volume flow of a rack (see Figure 4.2.2), it turns out that the performance homogeneity of a system becomes better with lower permeability. The respective differences between Q_{rack1} and Q_{rack2} for assumed membrane permeability of 500, 400, 300 l/(m²hbar) are 6%, 5% and 4% of the required permeation flow of the system.

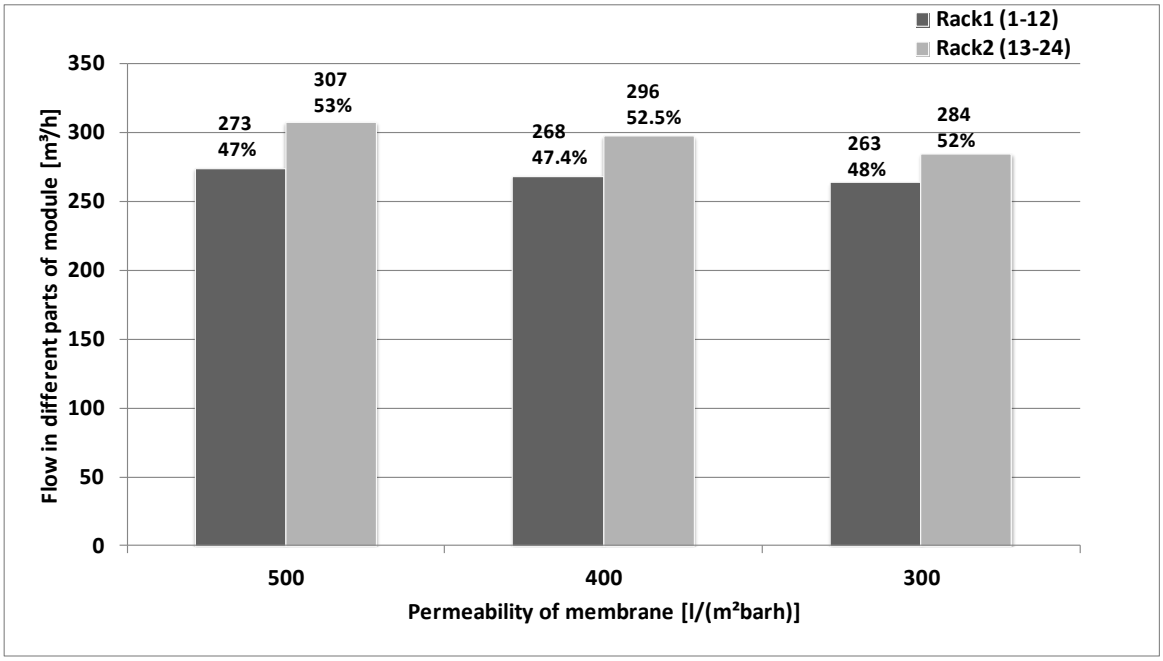

Figure 4.2.2 Simulation results: comparison of the volume flow of Rack 1 and Rack 2 in a system for different membrane permeability (Pb_{mem}): Q = 550 m³/h, a 48-modules system

The permeability of the membranes has a strong influence to the required driving pressure. When the permeability decreases from 500 l/(m²hbar) to 400 and 300 l/(m²hbar), the required driving pressure increases from 651 to 754 and 927 mbar which is 1.2 times and 1.4 times respectively (see Figure 4.2.3). In order to compare the performance difference of the whole system caused by different membrane permeability, the system permeability is applied here.

$$Pb_{sys} = {Q}/{(A_{sys} \cdot p_{required})} \qquad \textbf{Equation 4.3.1}$$

Pb_{sys} is the system permeability [l/(m²hbar)], Q is the required volume flow of the system, A_{sys} is the total membrane surface in the system and $p_{required}$ is required driving pressure of the system. The difference of the system permeability and membrane permeability is caused by the pressure loss in the pipes. With different membranes, the system permeability decreases with the decrease of the membrane permeability. As shown in Figure 4.2.3, the system permeability are 350, 300 and 248 l/(m²hbar) for 500,

400 and 300 l/(m²hbar) membrane respectively. The system permeability are 70.4%, 76% and 83.4% of corresponding membrane permeability, which means that less driving pressure is used to overcome the friction loss in the system with decrease of membrane permeability. But due to the decrease of membrane permeability, the required pressure becomes higher to keep the constant permeation flux.

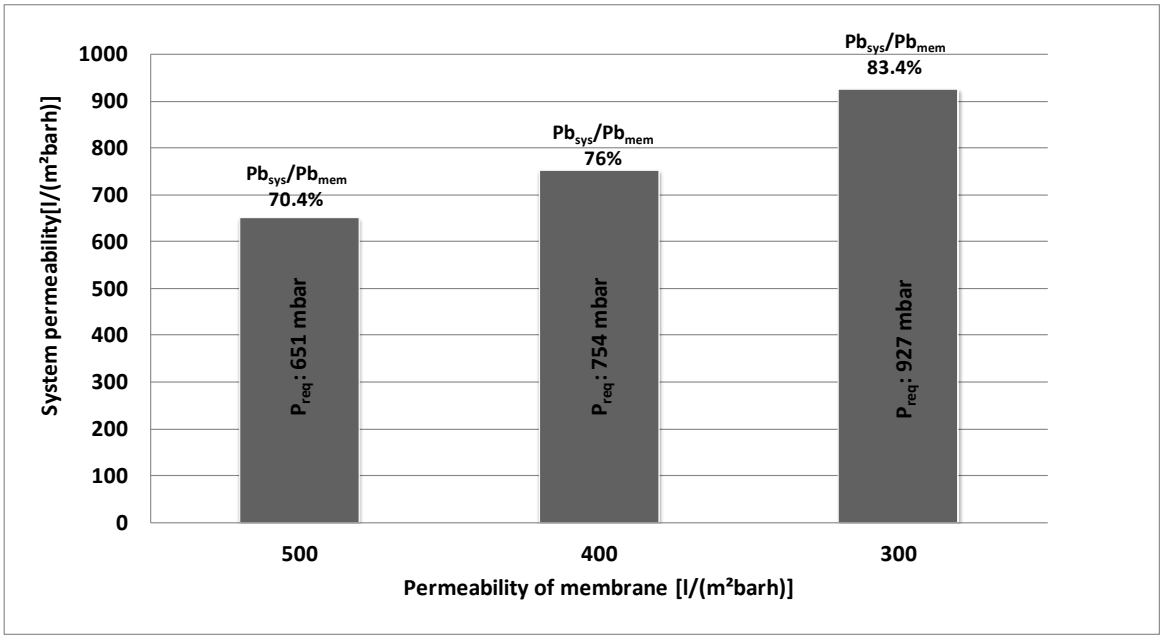

Figure 4.2.3 Simulation results: system permeability and required driving pressure of the 48-modules filtration system with different permeability membrane in the filtration process

In the practical use of a filtration system, the fouling layer always occurs and decreases the permeability of the system. Fast permeation leads to fast fouling layer formation. As it was shown, lower membrane permeability leads to better performance homogeneity. It means, due to the fouling, the membrane filtration system will have better performance homogeneity but higher energy consumption after an operation period.

4.2.1.3 Number of Modules

The number of modules in the filtration system is a very important parameter. Constructed with the same type of module, a system with larger number of modules has

a higher filtration capacity. However, more modules need longer pipe, which leads to larger pressure drop. Larger pressure drop leads to larger difference of TMP between modules (See Figure 4.2.4 a) and b)).

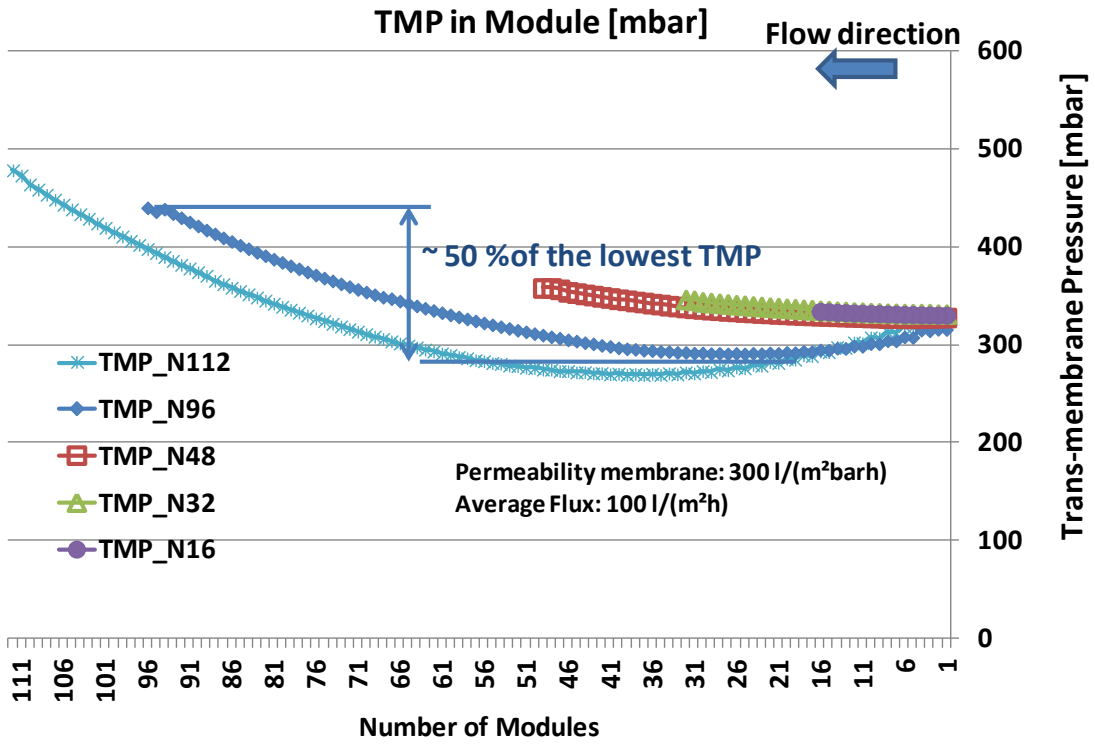

a)

Figure 4.2.4 Simulation results: TMP distribution of modules of the system with different number modules in the filtration process when the permeability of the membrane is a) 300 l/(m²hbar)

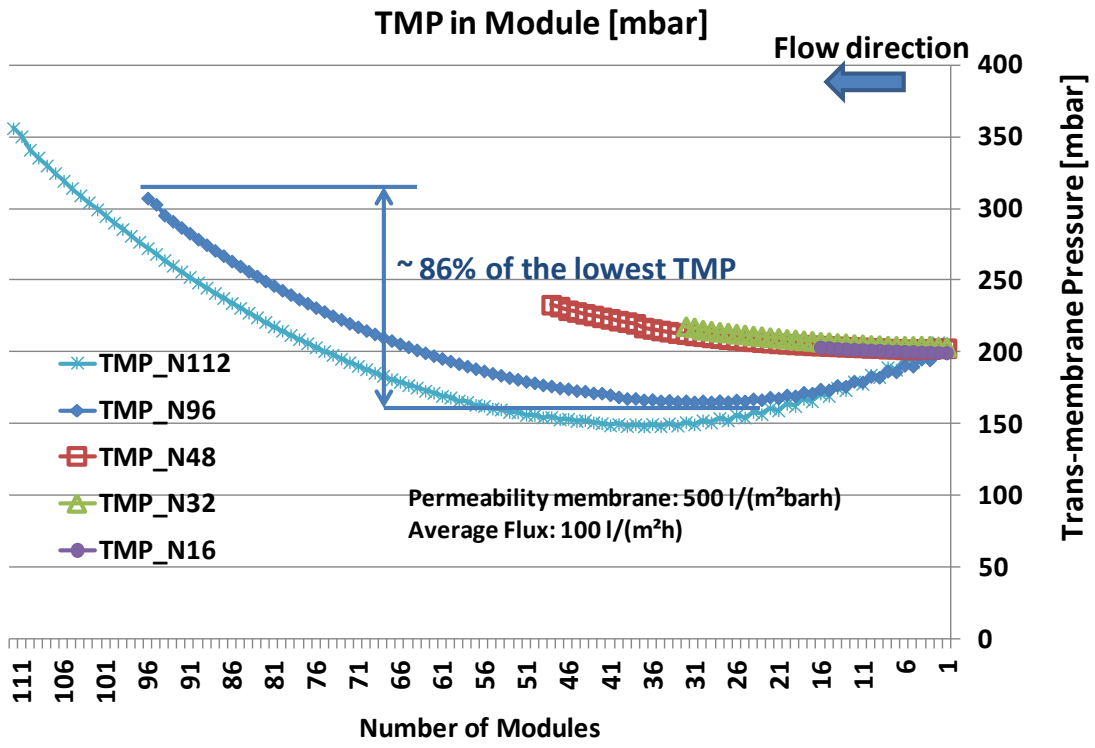

b)

Figure 4.2.4 Simulation results: TMP distribution of modules of the system with different number modules in the filtration process when the permeability of the membrane is b) 500 l/(m²hbar)

Except the TMP distribution of modules, the number of modules can also influence the required driving pressure (see Figure 4.2.5). For example, in the system with a membrane permeability of 300 l/(m²hbar), the required driving pressure of the system with 16, 32 and 48 modules increases from 348 bar to 353 and 381 mbar, by 5% and 10% respectively while the amount of modules increases 2 and 3 times. When the number of modules increases from 16 to 96 and 112, the required driving pressure increases from 348 mbar to 527 mbar and 627 mbar, by 50% and 80% respectively.

Looking on the system permeability, with increasing module number, the ratio of system permeability and membrane permeability decreases which means that the system needs more energy to overcome the friction loss in the system. For example in Figure 4.2.5, in the system with a membrane permeability of 300 l/(m²hbar), the ratio of system

permeability and membrane permeability decreases from 96% to 92%, 88%, 63% and 53% when the number of modules increases from 16 to 32, 48, 96 and 112. It means more energy is consumed to overcome the friction in the piping system with increase of modules. High permeability system needs more energy to overcome the friction of the piping system compare to low permeability system.

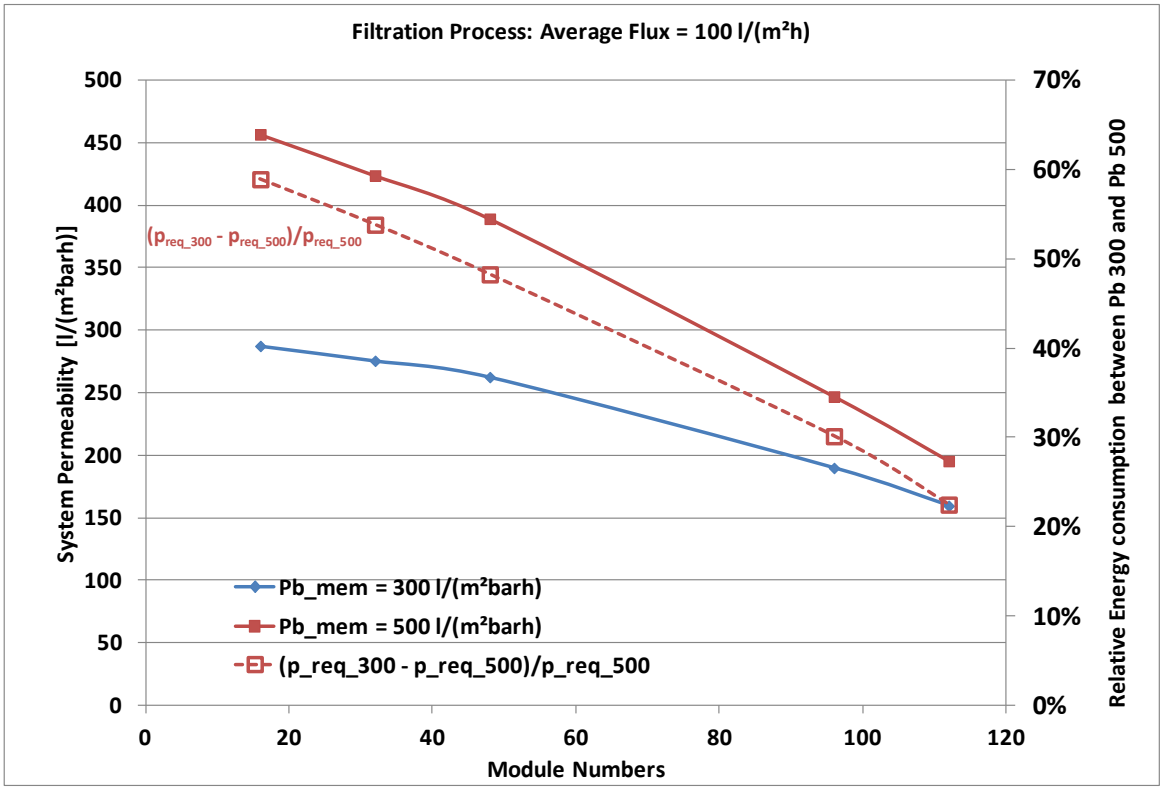

Figure 4.2.5 Simulation results: system permeability and required driving pressure of the T-rack system with the membrane of 300 l/(m²hbar) and 500 l/(m²hbar)

Here one conclusion can be made regarding the influence of modules number in the filtration system. A larger number of modules in one system leads to lower performance homogeneity, more energy consumption and lower productivity: the ratio of permeation flow to the cost of energy.

The conclusion of the influence of permeability (See Chapter 4.2.1.2) is also certified by Figure 4.2.5. Comparing the systems with 300 l/(m²hbar) and 500 l/(m²hbar) membrane,

The difference of energy requirement between lower permeability and high permeability system becomes smaller with increase of module numbers. This is means that high permeability system is influenced more by the pressure loss in the piping system. For example, in the 48 modules system, the ratio of system permeability and membrane permeability decreases from 88% to 78% when membrane permeability increases from 300 l/(m²hbar) to 500 l/(m²hbar). And the required pressure is 381 mbar with 300 l/(m²hbar) permeability membrane while it decreases to 257 mbar with 500 l/(m²hbar) permeability membrane.

4.2.1.4 Bottom Pipe

The bottom pipe can change the flow distribution in the filtration system. In Figure 4.1.5 and Figure 4.1.10, the difference between the volume flow entering into the module from the top side pipe $\dot{V}_{top}$ and total permeation flow of the module $\dot{V}_{total}$, and the permeation length distribution are shown. These Figures show that the bottom pipe can improve the performance homogeneity when the number of module is small. Take the 48-module filtration system as an example, the volume flow and permeation length distribution are shown in Figure 4.2.6. The arrows show the flow direction in the pipes and capillaries. The flow distribution is controlled by the pressure distribution in the 4 feed pipes and 1 permeate pipe.

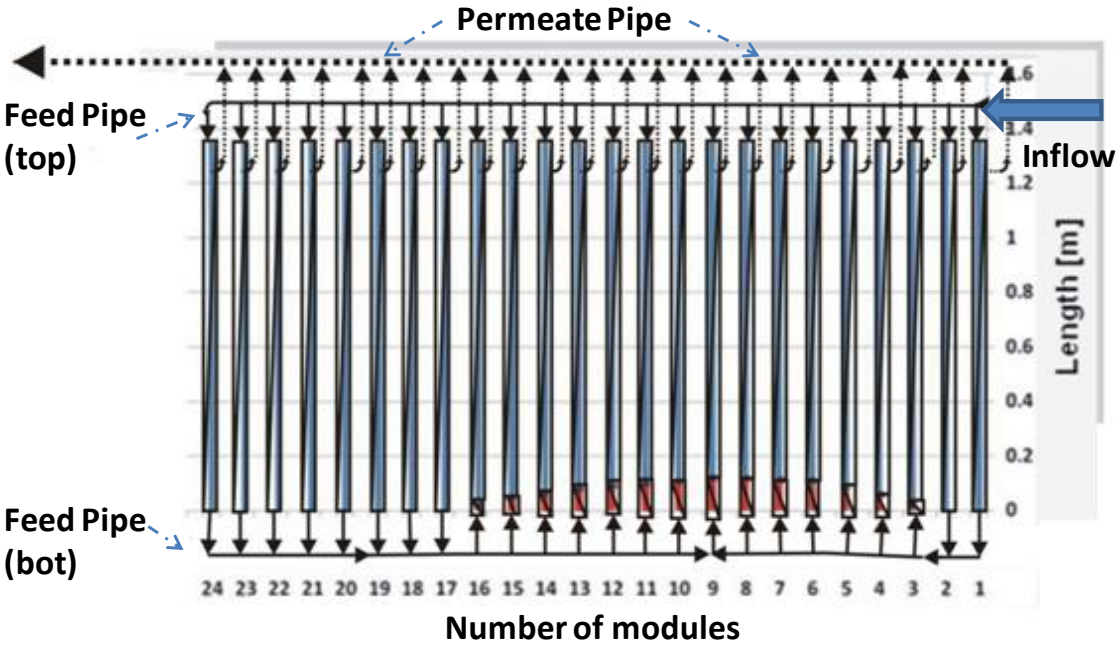

Figure 4.2.6 Simulation results: the flow distribution in the capillaries in the 1st row of feed pipes in a 48-modules filtration system with a required volume flow of 240 m³/h

The reason for this volume flow and permeation length distribution is shown in Figure 4.1.8, where the pressure in the top feed pipes has a small decrease and increase along the flow direction, while the pressure in the bottom pipes is nearly constant. This causes changes of pressure differences between the top and bottom side of the modules where the highest pressure difference occurs somewhere nears the middle of the system. However when the number of modules is 48, the influence of bottom pipe is very small to the pressure distribution in the pipes which is shown in Figure 4.2.7. The largest difference of the pressure inside the top side feed pipe between the system with and without bottom pipe is only 1 mbar which can be neglected. The pressure of top feed pipe at the right side of Figure 4.2.7 can be considered as required driving pressure here. It means that the bottom pipe has no influence for a 48-modules system when the required volume flow is 240 m³/h.

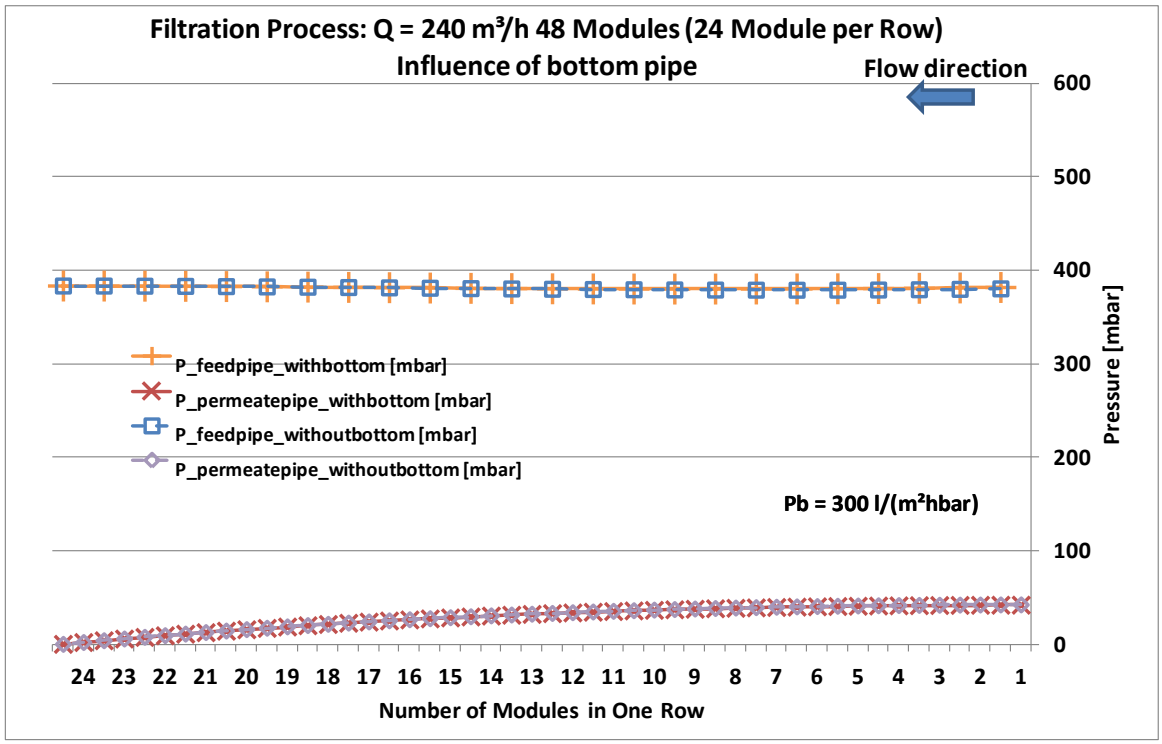

Figure 4.2.7 Simulation results: pressure distribution inside pipes in 48-modules filtration system with and without bottom pipes in the filtration process (Pb_{mem} = 300 l/(m²barh))

But when the number of modules is larger, the situation becomes changed. A filtration system with 96-modules is simulated to show the influence of bottom pipe. The detailed analysis of pressure in pipes is shown in Figure 4.2.8. It is clear to see that the required driving pressure is higher when the system is operated without bottom pipes. In the 96-modules system, the required driving pressure is 575 mbar; this is 9% more than 527 mbar of the system with bottom pipe. The pressure loss in the feed pipe of the system without bottom pipe from the position of module 1 to 20 is higher than that of the system with bottom pipe. The reason is that the water will partly flow into the bottom pipe from the top pipe through the modules near the inflow position. Because the friction in the pipes is proportional to the velocity, lower amount of water in feed pipe leads to low pressure loss due to the friction.

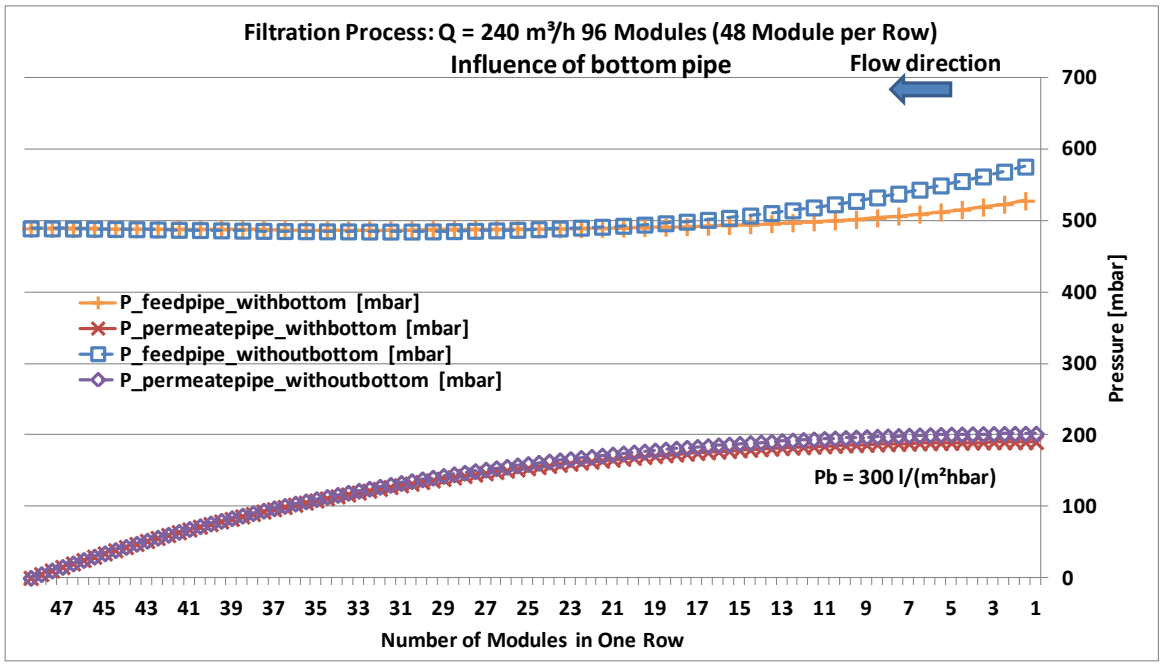

Figure 4.2.8 Simulation results: pressure distribution inside pipes in 96-modules filtration system with and without bottom pipes in the filtration process (Pb: 300 l/(m²hbar))

As is shown in Figure 4.2.9, the performance homogeneity of the system with bottom pipe will be worse than that of the system without bottom pipe when the number of module is 96. With bottom pipe the difference between Q_{rack1} and Q_{rack2} is 10%, while without bottom pipe it becomes 6%.

The TMP distribution is shown in Figure 4.2.10. In a 96-modules system, the maximum TMP of module without bottom pipe is 422 mbar, 20 mbar less than that of module with bottom pipe. The minimum TMP of module without bottom pipe is 294 mbar, 4 mbar more than that of module with bottom pipe.

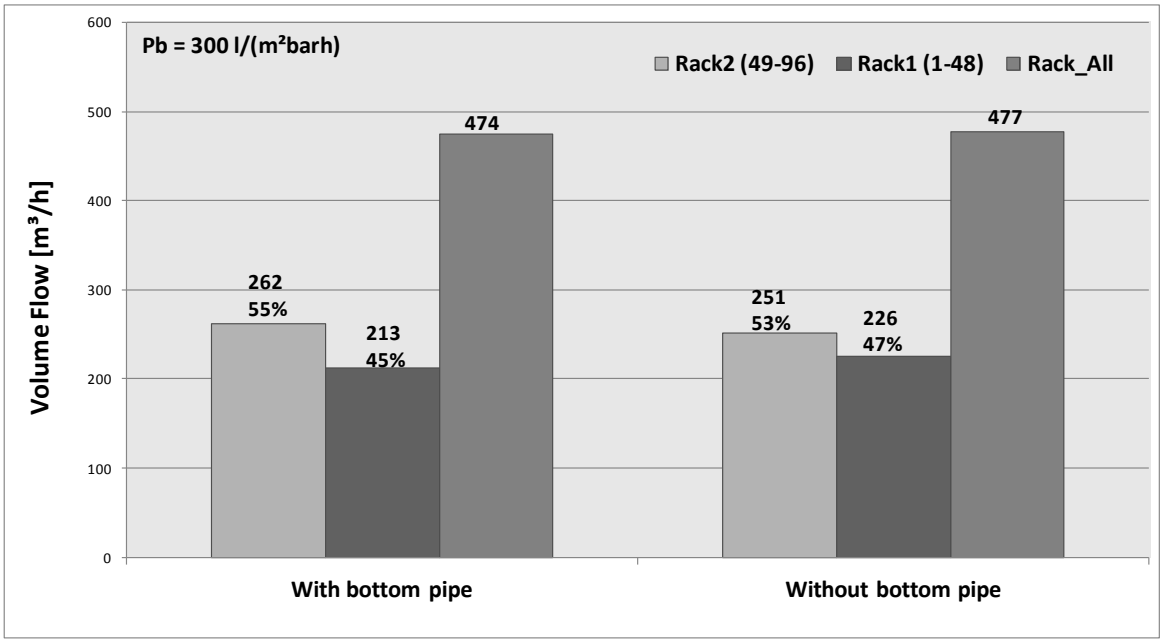

Figure 4.2.9 Simulation results: the sum of permeation volume flow of modules in Rack 1 and Rack 2 in a 96-modules filtration system with and without bottom pipes in the filtration process

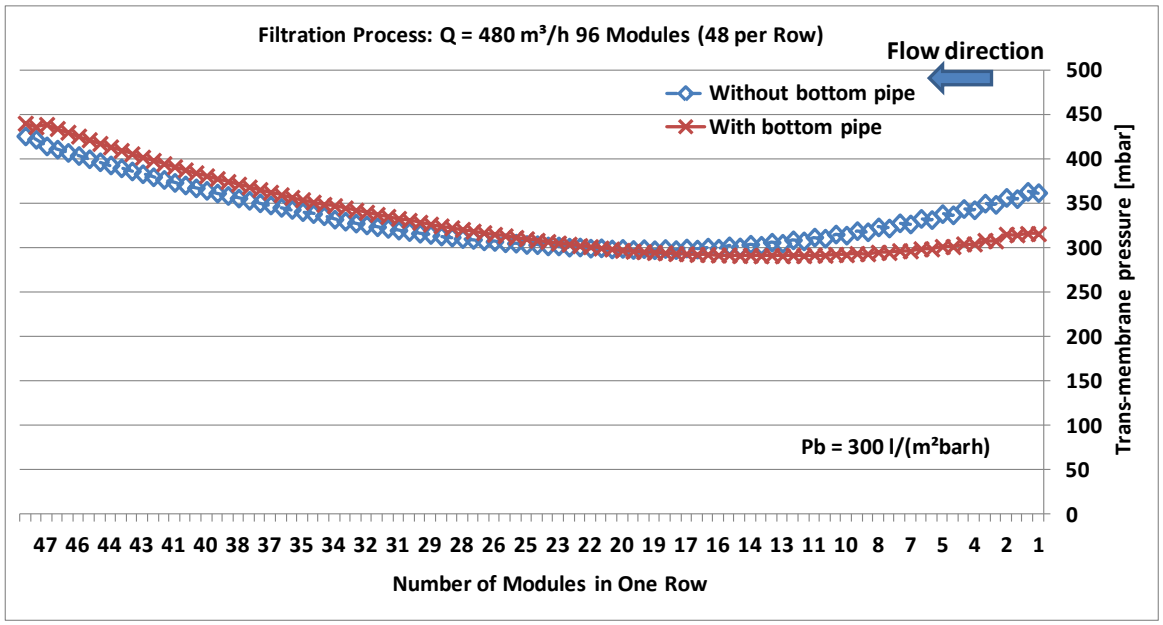

Figure 4.2.10 Simulation results: the TMP distribution in a 96-modules system with and without bottom pipes in the filtration process

Hence, the bottom pipe has nearly no influence to both the performance homogeneity the required driving pressure with the small number of modules system (not more than 48). However in the large number system (equal and larger than 96), the bottom pipe can lead to a lower performance homogeneity while it reduces the energy consumption. So

whether apply bottom pipe in the filtration system with large number of modules is strongly dependent on the specific conditions of the client. For the filtration process, if the client doesn't care about the energy consumption, the system without bottom pipe is a better choice.

4.2.1.5 Feed Position

Larger number of modules per rack increases the system permeation volume flow but decreases the performance homogeneity and causes more energy costs. Is it possible to avoid these disadvantages? Here an optimal operation setup (plant design) is shown to make the system better (see Figure 4.2.11).

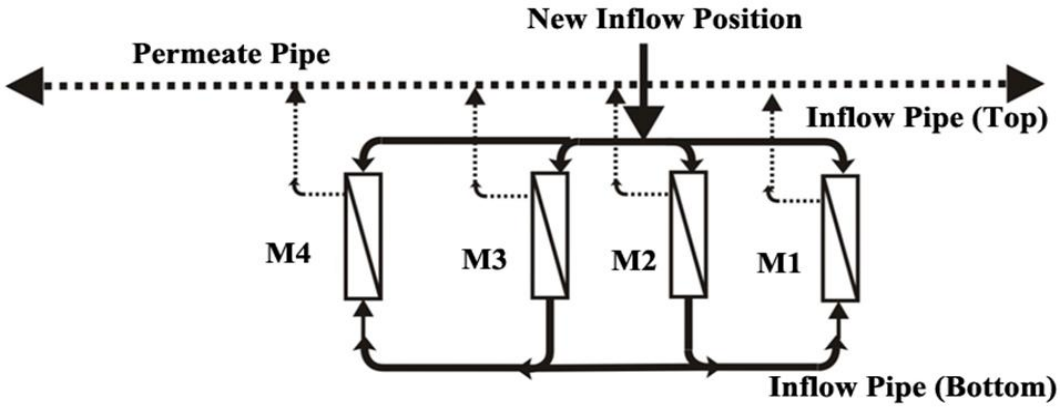

Figure 4.2.11 Optimal setup of inflow position in order to improve the performance homogeneity of the filtration system

The whole T-rack system is built by a number of basic units which contain 8 modules normally. According to this the construction, if the feed pipe inlet is designed in the middle of the system instead of on one side, the system works better from both performance homogeneity and energy consumption point of view. The reason is that this optimal operation setup makes the 96-modules system divided into two 48-modules systems. The 48-modules system has lower operation costs in terms of energy demand and better performance homogeneity.

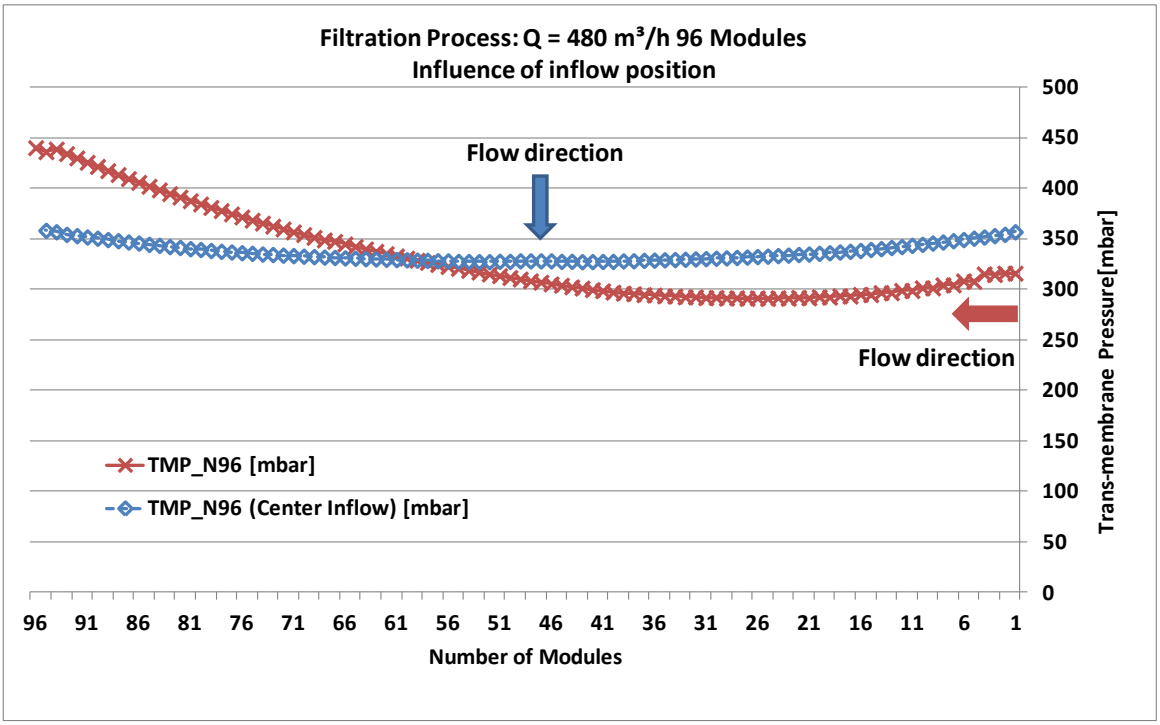

Figure 4.2.12 Simulation results: TMP distribution in a 96-modules filtration system with two different plant designs (inflow from one side and inflow from middle)

As is shown in Figure 4.2.12, with this optimal setup the difference between the highest and lowest TMP of module can be reduced from 147 mbar to 31 mbar. In the simulation, the required driving pressure can be reduced from around 530 mbar to 380 mbar when Pb = 300 l/(m²hbar).

4.2.1.6 Diameter of Feed Pipe and Permeate Pipe

The performance homogeneity of the system and the required driving pressure are strongly influenced by the pressure distribution in the pipes. From theory it is clear that the pressure in the pipes is strongly influenced by the geometry of the system. Considering the two variable diameters, the diameter of the permeate pipe is called PD and the diameter of the feed pipe (inflow pipe) is called FD as shown in Figure 4.2.13.

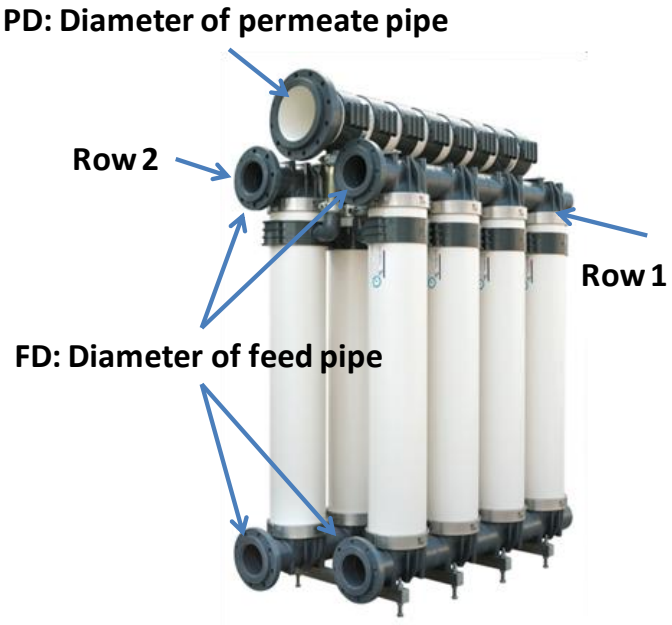

Figure 4.2.13 The Diameters definition of pipes of the T-rack system in the filtration process

As is introduced, for the same volume flow, the increase of diameter makes the friction caused pressure losses smaller according to the Moody chart (see Appendix B, when the diameter D increases then the velocity v decreases). The pressure in the pipes is shown in Figure 4.2.14, from which it is easy to see that a larger PD reduces the pressure drops in the permeate pipe and reduces the required driving pressure. The required driving pressure decreases from 382 to 360 mbar when the PD increases from 235 mm to 380 mm. Due to these, the increase of PD leads to better TMP distribution (see Figure 4.2.15). The TMP difference between the highest performance module to lowest one decrease from 31 mbar to 16 mbar when the PD increases from 235 mm to 380 mm. As it was known, the TMP decides the permeation flow of modules, so smaller TMP difference between modules means better system performance homogeneity.

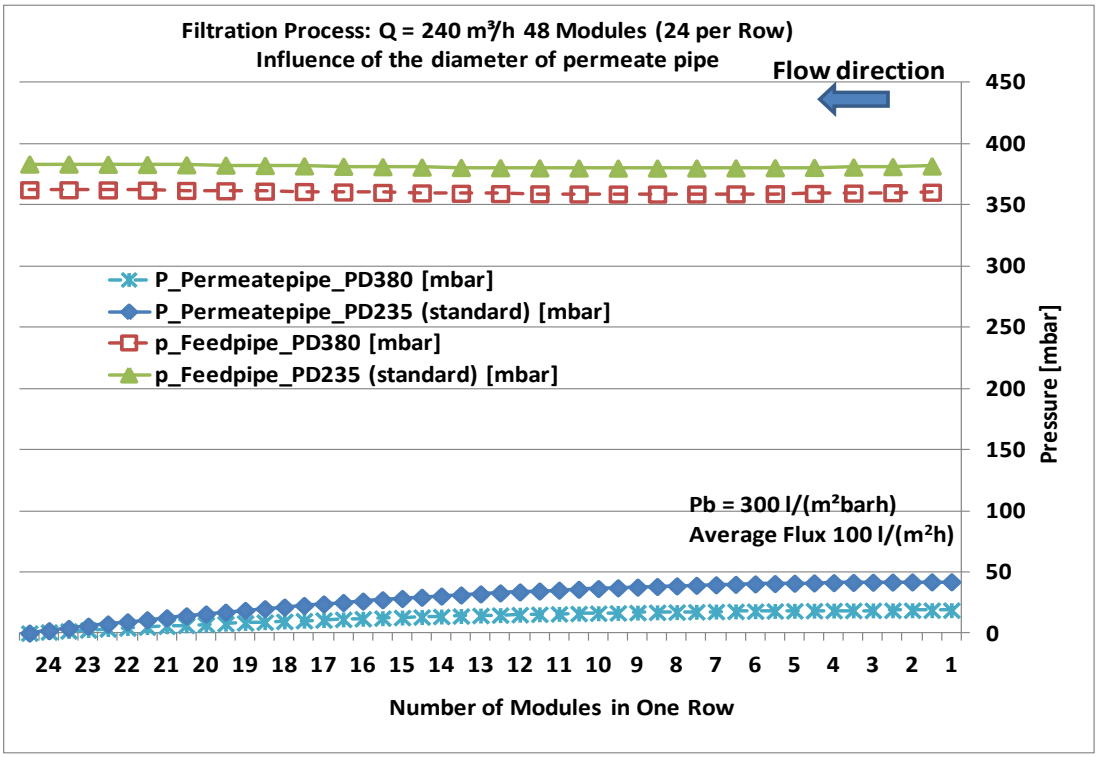

Figure 4.2.14 Simulation results: influence of the diameter of the permeate pipe (PD) on the pressure in the feed and permeate pipes of T-rack system in the filtration process

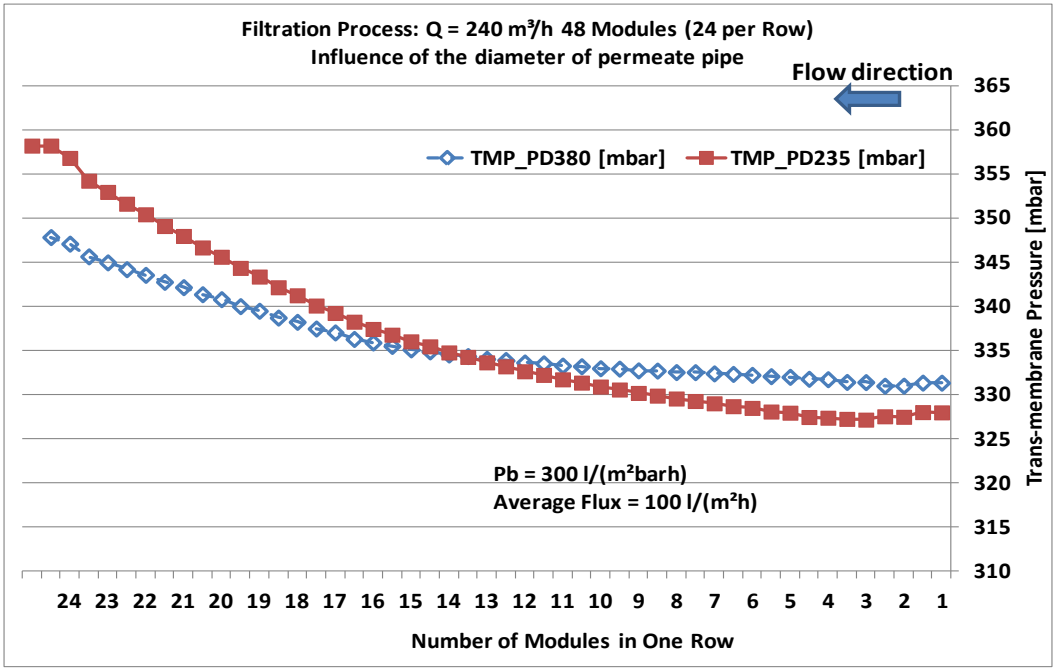

Figure 4.2.15 Simulation results: influence of the diameters of the permeate pipe (PD) on TMP distribution in the T-rack system in the filtration process

The feed pipe diameter (FD) will also influence the system. As is explained in Chapter 3.8.1.1, the pressure difference between the inflow and outflow position of the pipe is decided by the Major and Minor friction loss of the pipe (term $-\frac{\rho {v_1}^2}{2}\left(\frac{\lambda_1 L_1}{d_1}+K_{tot1}\right)-\frac{\rho {v_2}^2}{2}\left(\frac{\lambda_2 L_2}{d_2}+K_{tot2}\right)$ see Equation 3.8.5) and the difference of velocity between inflow and outflow position (term $\frac{\rho {v_1}^2}{2}-\frac{\rho {v_2}^2}{2}$ see Equation 3.8.5). In general, the increase of the pipe diameter will decrease the velocity at the same volume flow which will influence the pressure distribution. For example from inflow of the feed pipe to the dead-end side of feed pipe (velocity is 0), the term $\frac{\rho {v_1}^2}{2}-\frac{\rho {v_2}^2}{2}$ in Equation 3.8.5 is just dependent on the velocity of inflow to be $\frac{\rho {v_{in}}^2}{2}$. With the increase of the feed pipe diameter, the inflow velocity must decrease with same required volume flow which means the term $\frac{\rho {v_{in}}^2}{2}$ decreases. But the simulation results show that the increase of FD has only a very small influence on the pressure distribution in pipes (see Figure 4.2.16).

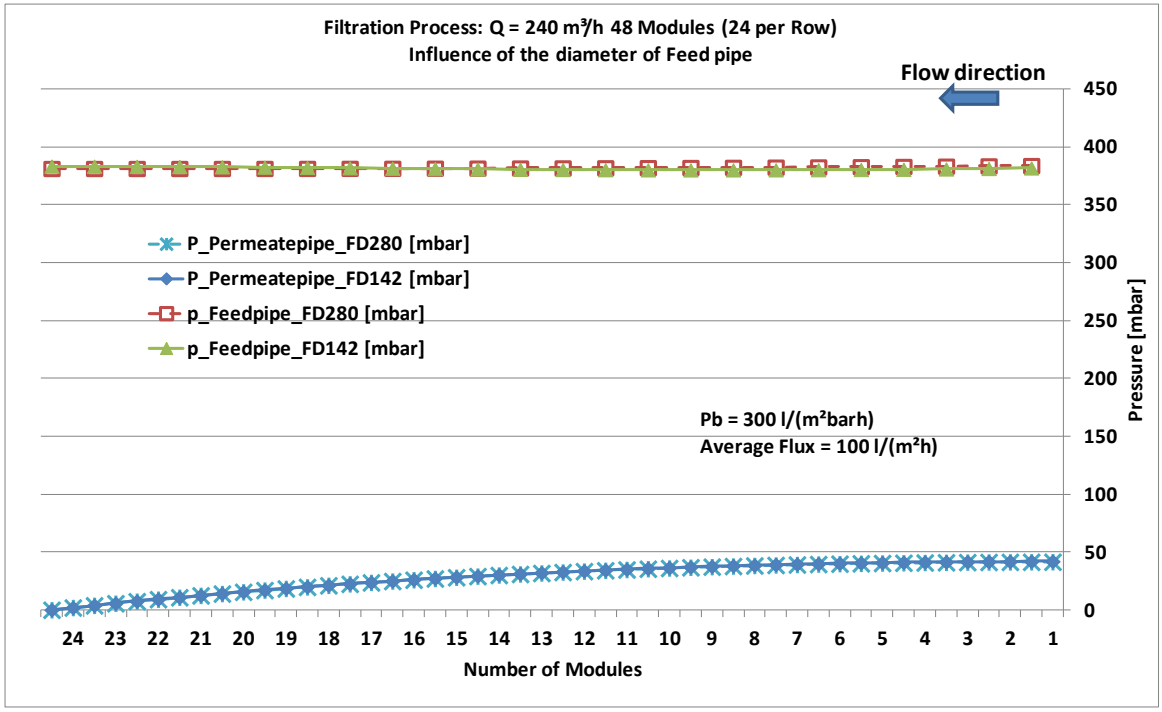

Figure 4.2.16 Simulation results: influence of diameters of feed pipes of T-rack system in the filtration process pressure in pipes

In summary, the simulation results show that in the filtration larger diameter of the permeate pipe (PD) can get better performance homogeneity with lower the required driving energy. The diameter of the feed pipe (FD) doesn't have significant influence on both performance homogeneity and required driving energy.

4.2.2 Influencing Parameters in the Backwash Process

In membrane filtration systems, backwash process is crucial to maintain the permeation performance of the membrane. With the backwash process the fouling layer, which decreases the permeability of membrane system, can be removed. The performance homogeneity of a system is very important in the backwash process, because it determines the efficiency of the backwash cleaning. Under the same pressure conditions, the faster the fluid flows through the module, the better the fouling layer removal efficiency of the backwash. Inhomogeneous volume flow distribution in the modules can lead to bad backwash efficiencies, where one part of the system is clean while the other part is still dirty.

4.2.2.1 Effect of the Membrane Permeability

In the filtration process, the system consisting of membranes with lower permeability leads to better performance homogeneity (see Figure 4.2.2). In the filtration process, the differences between Q_{rack1} and Q_{rack2} with permeability of 500, 400 and 300 l/(m²hbar) are 6%, 5% and 4% (Rack2 – Rack 1) respectively. One has to be aware, that in the back wash process the flow is from the permeate pipe to the feed pipe and from Rack 2 to Rack 1, which is reverse to the filtration process. So while in the filtration process, Q_{rack2} is higher than Q_{rack1}, in the back wash process, Q_{rack1} is higher than Q_{rack2}.

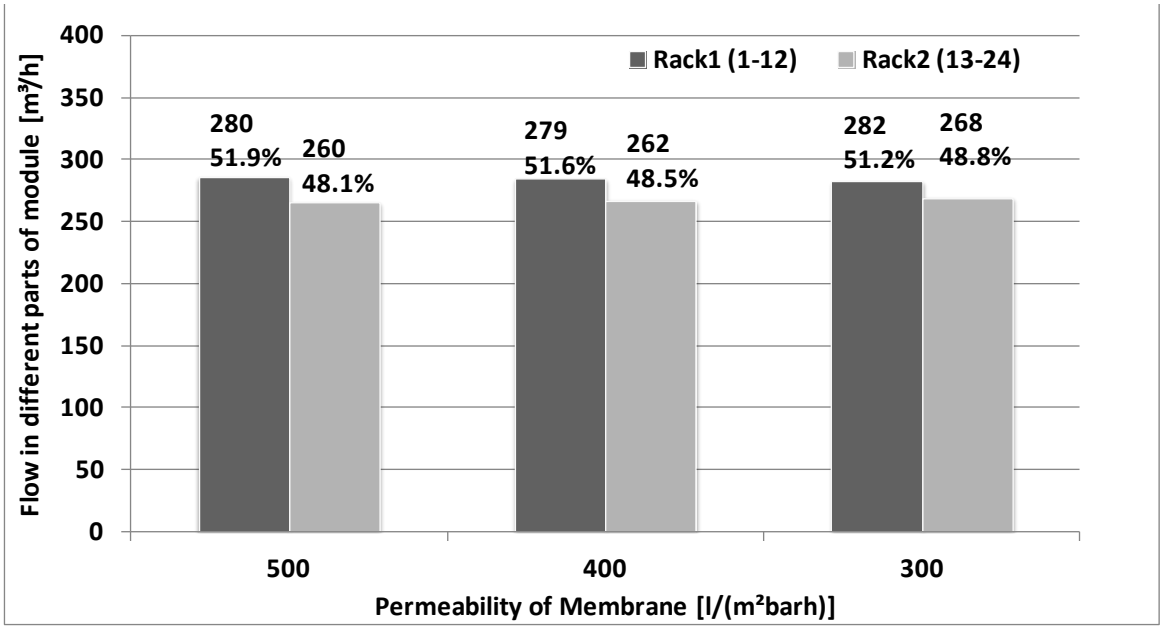

Figure 4.2.17 Simulation results: the sum of the permeation volume flow of modules in Rack 1 and Rack 2 of the T-rack system in the backwash process

Figure 4.2.17 shows that the lower the membrane permeability, the higher the performance homogeneity in the backwash process too. The difference between Q_{rack1} and Q_{rack2} with membrane permeability 500, 400 and 300 l/(m²hbar) are 3.8%, 3.1% and 2.4% respectively. The influence of membrane permeability to the performance homogeneity in the backwash process is smaller than that in the filtration process.

In order to get detailed information of the performance homogeneity, the permeation volume flow of modules in the system along the flow direction was simulated. Along the flow direction in the backwash process, the total permeation volume flow of each module $\dot{V}_{total}$ (see Chapter 3.8.1.2) increases (see Figure 4.2.18). When the permeability is 300 l/(m²hbar), $\dot{V}_{total}$ increases from 11 to 12.3 m³/h along the flow direction, when the permeability is 400 l/(m²hbar), it increases from 10.8 to 12.5 m³/h, and when the permeability is 500 m³/h it increases from 10.6 to 12.8 m³/h. The differences between the highest and lowest permeation modules under different permeability are 1.3 m³/h, 1.7 m³/h and 2.2 m³/h, which are 11.8%, 15.8% and 20.8%

increase respectively.

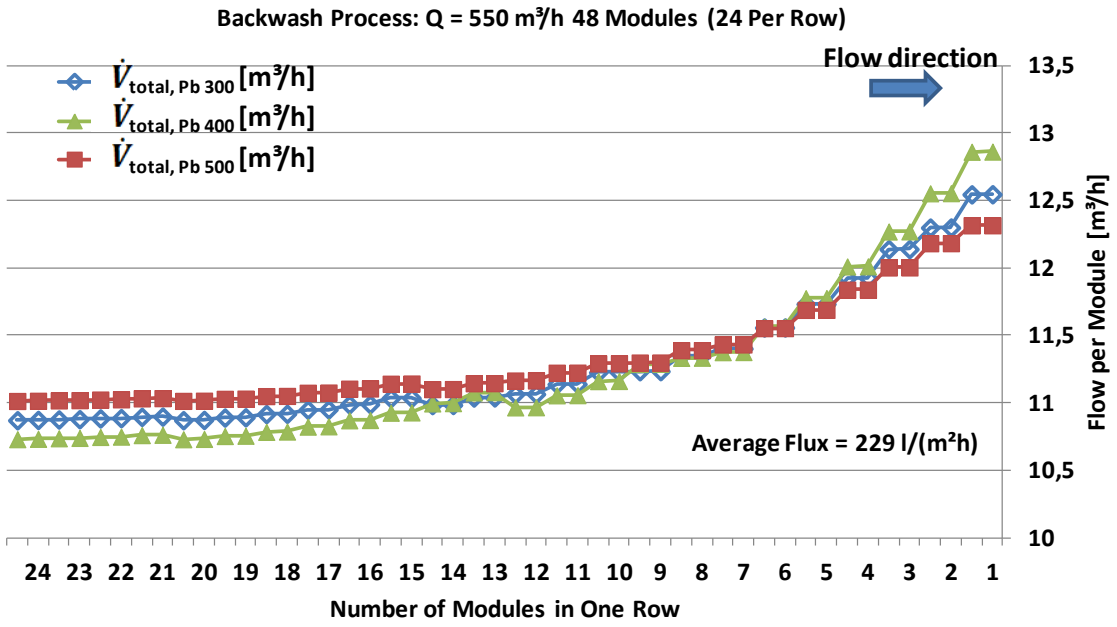

Figure 4.2.18 Simulation results: the total permeation volume flow of modules of T-rack system with different permeability membranes (Pb 300, 400 and 500 l/(m²hbar)) in the backwash process

In order to keep the volume flow of the complete system constant (Q = 550 m³/h always), the filtration system with lower membrane permeability requires larger TMP and required driving pressure in the backwash process. Figure 4.2.19 also indicates the energy required of the systems with different permeability membranes in the backwash process. The required driving pressure for a system with 300 l/(m²hbar) membrane permeability is 1.4 times than that with 500 l/(m²hbar) membrane (1095 mbar to 788 mbar). The required driving pressure with 400 l/(m²hbar) membrane is 1.2 times than that with 500 l/(m²hbar) membrane (903 mbar to 788 mbar). The system permeability is increased (209 l/(m²hbar) to 253.6 l/(m²hbar) and 290.5 l/(m²hbar)) with the increase of membrane permeability while the ratio of the system permeability to membrane permeability decreases (69.7% to 63.4% and 58.1%), which means the energy consumption caused by overcoming friction loss takes more percentage with the increase of membrane permeability.

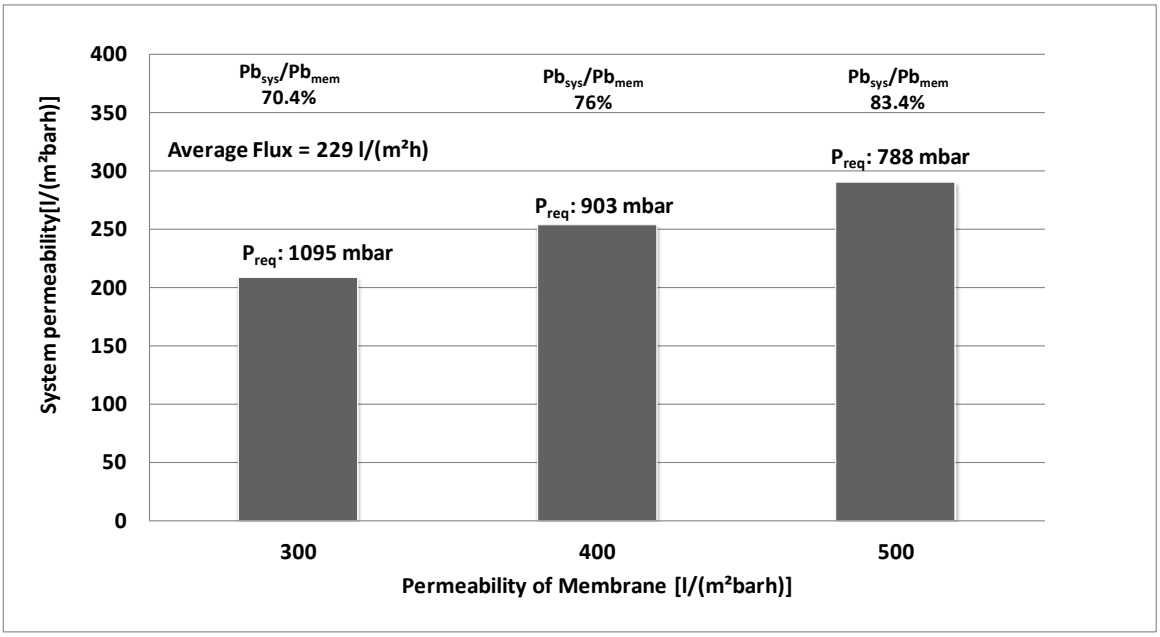

Figure 4.2.19 Simulation results: the system permeability in 48-modules system of different membrane with a required volume flow of 550 m³/h in the backwash process

4.2.2.2 Number of Modules

In Figure 4.2.20, the TMP of modules with different modules number system in the backwash process are shown. The difference between the maximum and the minimum TMP value of modules in the 48-modules system is 87 mbar while that in the 96-modules system becomes 581 mbar and in the 112-modules system becomes 800 mbar. As is mentioned the TMP of modules decides the permeation volume flow of modules. The increasing difference of TMP between modules means worse performance homogeneity. That is with the increase number of modules in the system, the performance homogeneity of the system becomes worse.

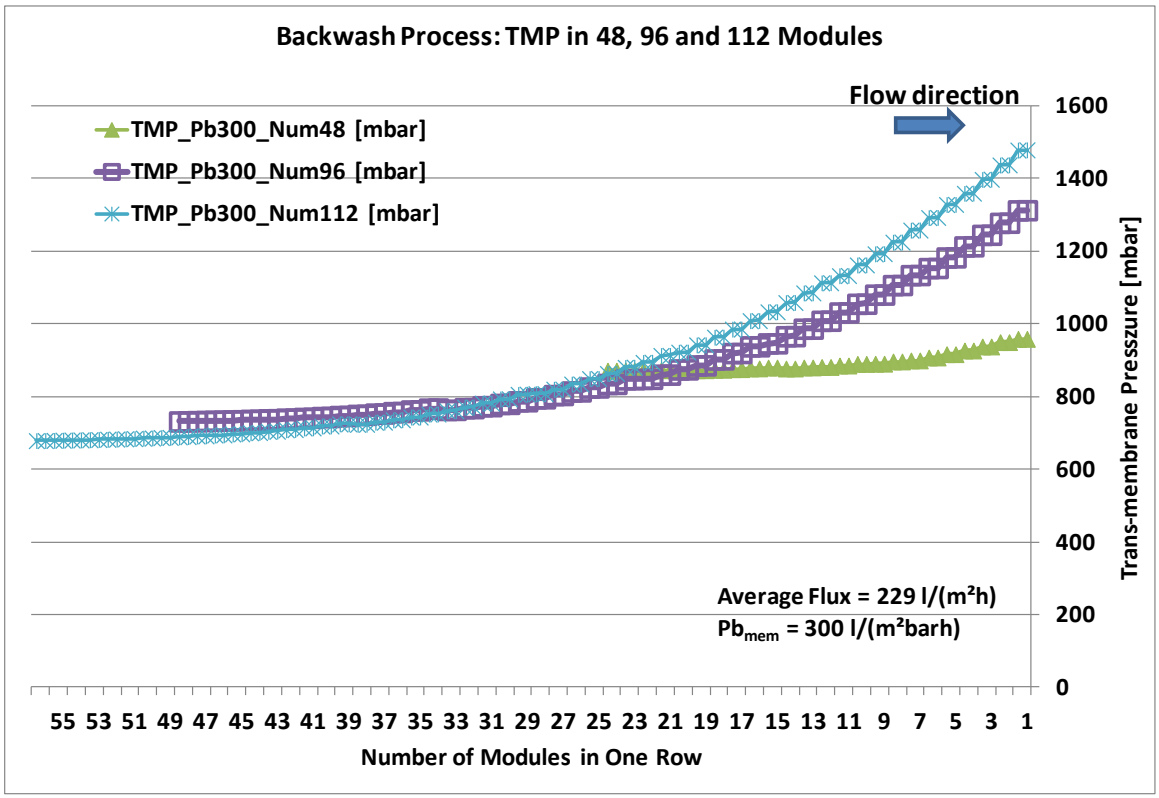

Figure 4.2.20 Simulation results: the TMP distribution in the different number modules system in the backwash process

The sum of the permeation volume flow of modules in the Rack 1 and Rack 2: Q_{rack1} and Q_{rack2} are shown in Figure 4.2.21. The difference between Q_{Rack1} and Q_{Rack2} is 2.4%, 16.2% and 23.5% respectively for 48, 96 and 112-modules systems. It means that the performance homogeneity becomes worse with the increase of the modules's number of modules.

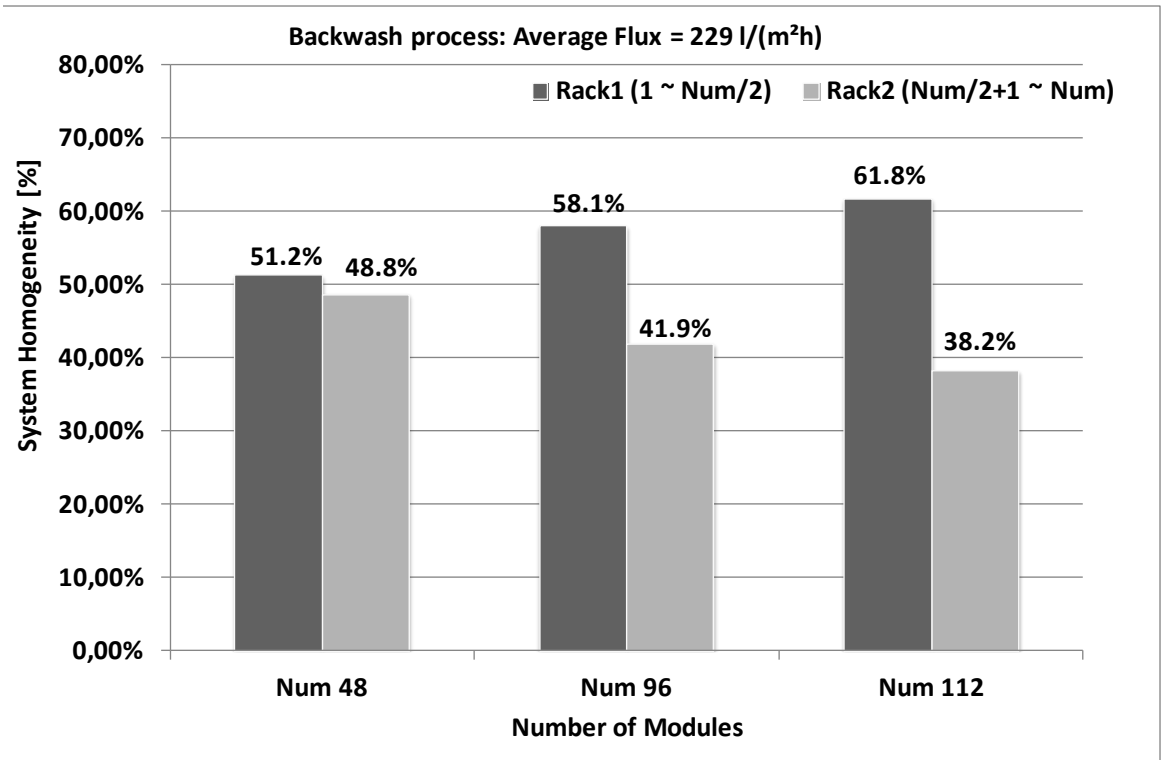

Figure 4.2.21 Simulation results: the sum of permeation volume flow of modules in Rack 1 and Rack 2 of the T-rack system in the backwash process

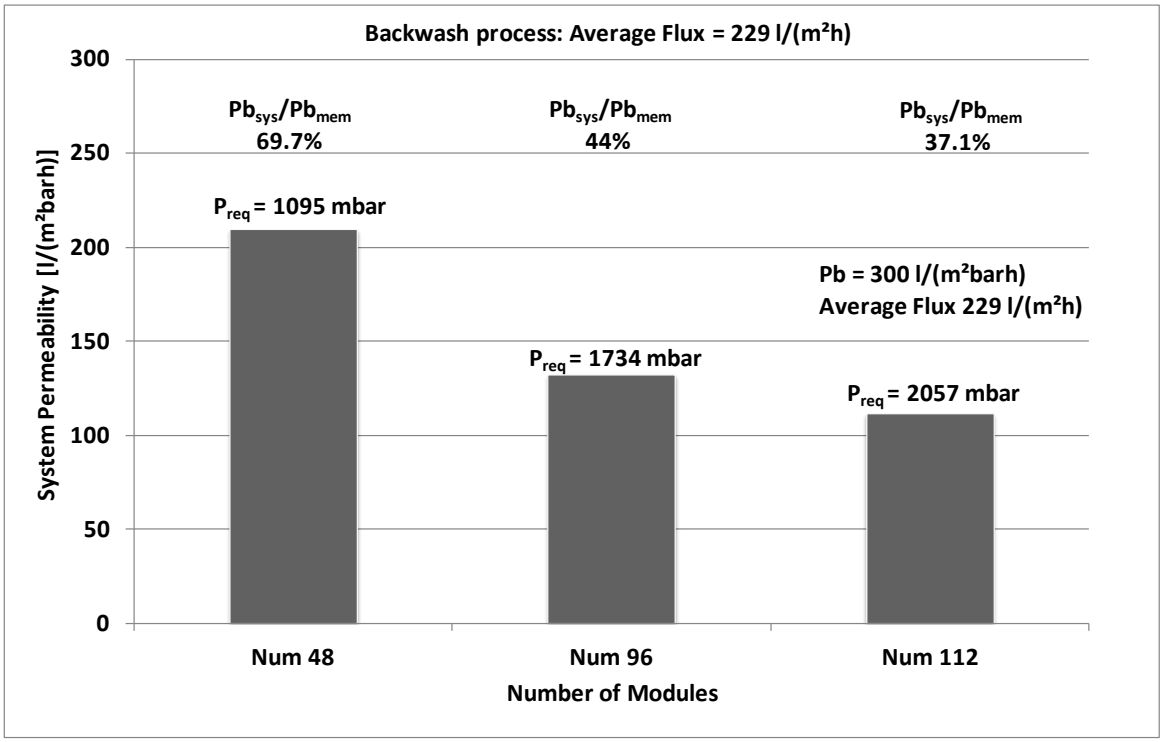

Figure 4.2.22 Simulation results: the system permeability for different number of modules system in the backwash process

The required driving pressure is higher when the number of modules is longer. It is 1095 mbar, 1734 mbar and 2057 mbar for 48, 96, and 112-modules systems respectivly (see Figure 4.2.22). The system permeabilty decreases (209 l/(m²hbar) to 132 l/(m²hbar) and 111 l/(m²hbar)) with the increase of the number of modules. The ratio between the system permeability and the membrane permeablity also decreases (69.1% to 44% and 37.1%) with the increase of the number of modules. More energy is consumed to overcome the friction loss in the system with increase of the number of modules.

4.2.2.3 Feed Position

As is introduced in Chapter 4.2.1.5, in the filtration process, with same number of modules, the system with inflow in the middle can improve the performance homogeneity sharply and meanwhile reduce the required driving pressure. In the backwash process, this optimal operation setup still works. The backwash inflow position is set in the middle of permeate pipe. After permeation, the back wash water will flow out from 2 sides of feed pipe (Figure 4.2.23).

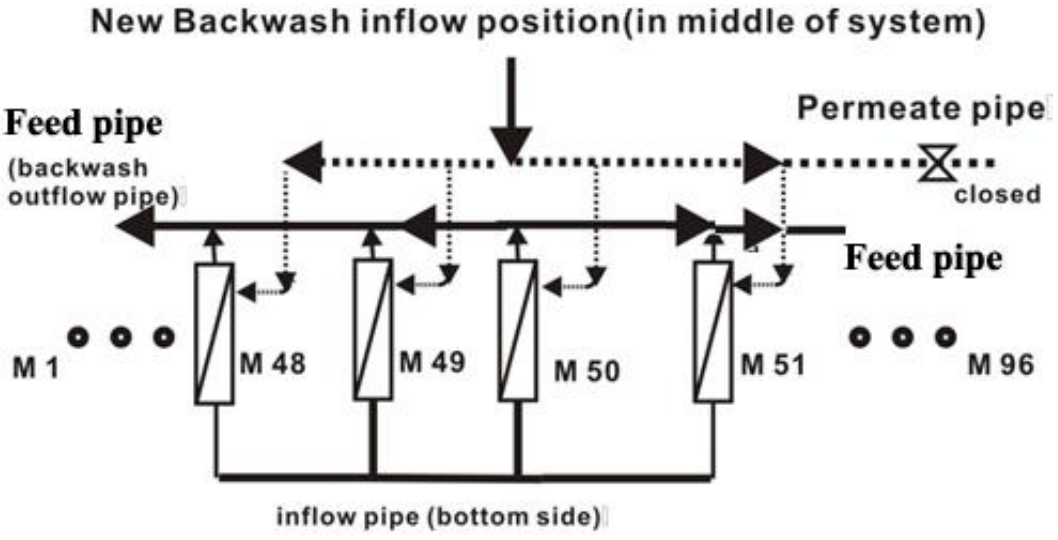

Figure 4.2.23 The optimal setup (plant design) with a volume flow of 550 m³/h in the backwash process

With the optimal setup, a sharp improvement of performance homogeneity is received

and shown in Figure 4.2.24. The TMP difference between the modules with the maximum TMP and the minimum TMP strongly decreases from 581 mbar to 87 mbar comparing with traditional setup to the optimal setup.

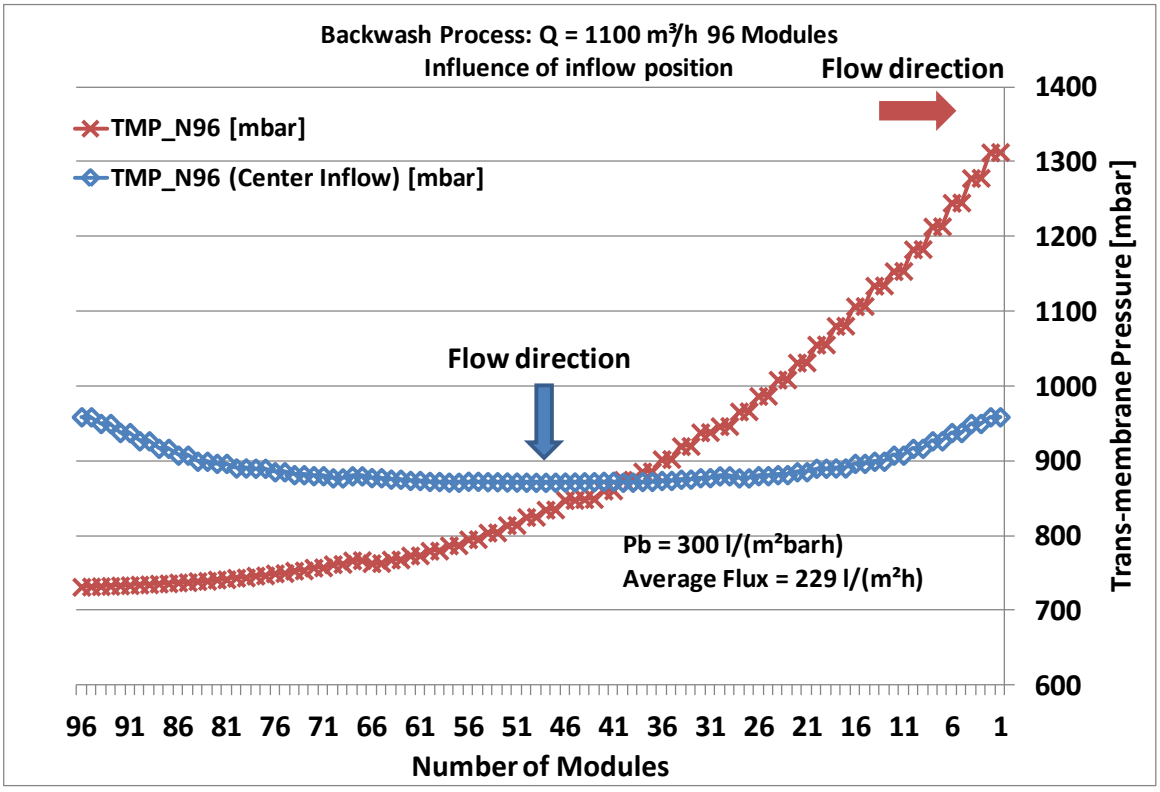

Figure 4.2.24 Simulation results: the TMP of modules in a 96-modules system with two different inflow setup with a volume flow of 1100 m³/h in the backwash process

The required driving pressure is also strongly reduced in the optimal setup. In a traditional 96-modules system the required driving pressure is 1734 mbar and in the optimal setup, this value change to 1059 mbar, 40% smaller when pb_{mem} = 300 l/(m²barh) and average flux = 229 l/(m²h).

4.2.2.4 Diameter of Feed Pipe and Permeate Pipe

The diameter of pipes plays an important role in the backwash process of the membrane system. However the influence of the diameter of the feed pipe (FD) and the permeate pipe (PD) is different to that of the filtration process.

The increase of PD has very small influence to the membrane system in the backwash process (see Figure 4.2.25). It causes maximal 3 mbar TMP difference and 7 mbar lower to the required driving pressure when PD changes from 280 to 380 mm.

The increase of the feed diameter of system in the backwash process can improve the performance homogeneity of the system (see Figure 4.2.25). When FD becomes larger, the friction will be reduced with same volume flow through the pipe, and then the TMP becomes more uniform in the example shown in Figure 4.2.25. When FD increases from 142 to 280 mm, difference between the maximum and minimum TMP decreases from 94 to 9 mbar, and the required driving pressure of system (pressure of pump) also decreases from 1129 to 968 mbar.

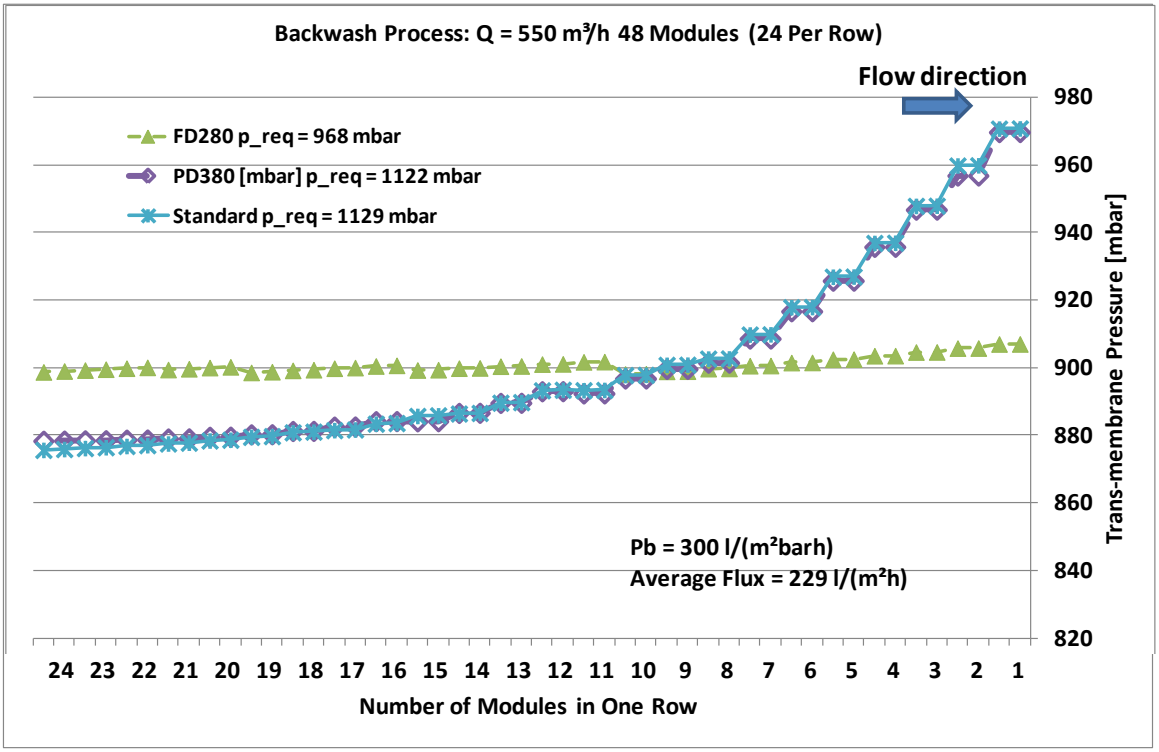

Figure 4.2.25 Simulation results: influence of pipes diameter (FD and PD) with a volume flow of 550 m³/h in the backwash process

4.2.3 Conclusion for T-rack System

From the simulation results, some influencing parameters nearly have the same effect in the filtration or backwash processes, such as lower permeability leads to higher

performance homogeneity of system but more driving pressure is required; high number of modules system has higher permeation volume flow of the complete system but it leads to the lower performance homogeneity and higher required driving pressure. Optimal setup with inflow in the middle of the system improves the performance homogeneity and reduces the required driving pressure in both filtration and backwash processes sharply.

Comparing to the operation parameters, the geometry influence is different in filtration and backwash process. In the filtration process, the increase of PD can improve performance homogeneity of system and reduce the required driving pressure, while in the backwash process it is nearly of no influence. The increase of FD has nearly no influence in the filtration process, while in backwash process it enhances the system performance homogeneity and reduces required driving pressure significantly. The influence of the bottom pipe is not considered in the backwash process. In the filtration process, the bottom pipe shows different influences on systems with less than 48-modules and more than 96-modules system. The bottom pipe has nearly no influence on the performance homogeneity and the required driving pressure in the small number modules system; and it can decrease the performance homogeneity of system and decrease the required driving pressure when the number of modules is large.

5. Summary

T-rack® and BioCel® are trade names both for new and advanced membrane filtration systems created by inge or Microdyn-Nadir respectively. Both systems are complex integrated systems with several substructures and subsystems. The T-rack system for example consists of several piping systems (2 top side inflow pipes, 2 bottom side inflow pipes and 1 outflow pipe), capillary membrane and module systems, special module connectors (so called T-connector), and other pipe connectors. The BioCel® system consists of a suction pipe and several parallel distributed pillow-shaped membrane plates (built by two membrane flat sheets and spacer between them) along the suction pipe. Except the complex structure, the T-rack® and BioCel® system have the same character: they are built by several membrane modules which are connected with pipes.

Simplicity, ease of use, high flexibility and economy are four main advantages of Computation Fluid Dynamic (CFD) tools. These advantages are very important, and helpful in the membrane system analysis and optimization. CFD can be used to analyze different simulation parameters which cover a broad range of different design parameters like geometry of modules, filtration pipe, pipes' connector, membrane permeability and number of modules.

Some special methods like the Calibration-Library-Interpolation method (CLI), the Scale method and the porous media approximation method are developed and employed in this work which are detailed introduced in Appendix A. This strongly simplified the simulation model and the CFD tool could be used with a regular PC. The CLI method could be applied due to the same structures of the typical membrane system character. For varying geometries of modules, module connectors, pipes and pipe connectors, different libraries were created. Comprehensive data bases are filled with different pressure loss and corresponding velocities for all substructures by CFD simulation. In

this way the complete membrane filtration system does not have to be modeled as one integrated 3D model, which cause high time consumption. With the CLI method a system simulation can be done with known parameters like required volume flow or pressure just based on the libraries and an interpolation. Additionally the geometry setup, and other parameters change can be easier carried on than with the traditional CFD simulation method.

The finite segments' quality of the capillaries and pillow-shaped membrane plate is another big challenge because of the dimensions' problem of capillaries and pillow-shaped membrane plate. In order to keep high quality of segments, the equilateral geometry of segments is preferred. Then large memory and long simulation time are needed for the capillaries and pillow-shaped membrane plates. In order to solve this, the Scale method is used here. Scale method is not only used to solve the dimension problem, it can also be used to simulate the geometry change of the pillow-shaped membrane plate caused by pressure difference across membrane. The spacer of the pillow-shaped membrane plate is a porous media which is built by large amount of fibers. The water permeated through the membrane enters into the spacer and changes flow direction from vertical to parallel to the membrane surface rapidly. Here, the porous media approximation method is used to avoid simulating the complex geometry of the spacer.

In the simulation results with CLI method the pressure and pressure loss are shown as mean value. This is a disadvantage of this method as it is only possible to apply to systems, when the permeation calculation based on the mean pressure is not much different to that based on the detailed pressure distribution. In other words, if a system works sensitively to the detailed pressure distribution in one section in the pipes, this CLI method is no longer valid. Luckily, from the validation, it shows that the T-rack and BioCel® membrane filtration systems are not very pressure sensitive. Furthermore, the mean pressure simulation can reduce the requirement of hardware stregnth and time.

In the simulation of T-rack system, the influence of different aspects was shown, e.g. the volume flow of filtration system, permeability of the membrane, number of modules in the system, the bottom pipe, diameter of inflow or permeate pipes and some optimal setups of the system. In the filtration process, larger volume flow leads to larger pressure loss which means larger energy consumption. Lower permeability leads to higher performance homogeneity of system while more driving pressure is required. Large number of modules in one system gets higher permeation flow but need more energy. The system permeability (total flow of the system divided by the total membrane surface area and applied driving pressure) decreases with increasing number of modules. The bottom pipe in the T-rack system has no influence to both the performance homogeneity and the required driving pressure in the small number modules system and it decreases the performance homogeneity and reduces the energy consumption in the large number modules system. A proposed optimal setup with inflow in the middle of the piping system improves the performance homogeneity and reduces the required pressure. Compared with the influence in the filtration process, the parameters nearly have the same effect in the backwash process except the diameter of permeate and feed pipe. In the filtration process, the increase of permeate pipe diameter can improve both performance homogeneity of system and reduce the required driving pressure, while in the backwash process it nearly has no influence. The increase of feed pipe diameter has nearly no influence in the filtration process, while in backwash process it enhances the system performance homogeneity significantly and reduces the required driving pressure.

The same analysis is done to the filtration process of the BioCel® filtration system. The details are shown in Appendix A. In the simulation the geometry influence of a membrane plate is checked and compared. Different designs of suction pipe are compared and analyzed. The quasi-ellipsoid design could be shown to have higher efficiency than the circular design either in the single suction pipe plate or in the double

suction pipes plate. Double suction pipes can also lead to high performance. The geometry change of membrane plate caused by pressure difference across at two sides of the membrane is also considered as a key parameter which can influence the performance of the membrane plate in terms of membrane plate permeability (Volume flow divided by membrane surface area of membrane plate and applied driving pressure). With the geometry change effect and the porous media approximation method, the membrane plate permeability change against the increase of TMP was simulated. The first increase and then decrease of the membrane plate permeability shows that the TMP for the single plate has an optimal value. Different designs of connector between quasi-ellipsoid suction pipes and circular outlet pipe are simulated and compared. The connector with 120 degree (the angle between quasi-ellipsoid pipe and circular pipe) has the lowest Pressure Loss Coefficient and was applied in the integrated system simulation. Two parts of pressure loss were considered in the integrated system simulation: the pressure loss in the piping system (including the connector) and the pressure loss in the membrane plates. The pipe's influence becomes larger with an increase of the numbers of the membrane plates as more permeate is produced and forced through the piping system. When a membrane filtration system is to be built, with help of these rules the suitable value can be setup according to the local conditions.

Both simulations for T-rack and BioCel® system were validated and the difference between simulation and experiment was considered to be acceptable. However, parts of simulation in this work can be done more precisely in future. Because of the assumption of pure water, there are no influences from fouling layer, concentration polarization or osmotic pressure. These can be simulated by the tool if it is necessary. Of course it will make the simulation much more complex.

The presented simulation results shows, that CFD technology is very helpful and useful for the development of membrane filtration system. It can show the influence of

parameters and get the optimal range of these parameters. In general, the new CFD tools can be applied also for other membrane systems given that the systems are built up of identical substructures, the CFD tool itself just needs a slight adaptation. Using the new tool helps saving time and money as expensive tests don´t have to be conducted.

6. Nomenclature

A	Area	[m²]
a	A parameter = $\sqrt{\frac{16}{R_k^3 R_m}}$ in Equation 3.2.9	
A_{ac}	Active permeation area on membrane surface	[m²]
A_{plate}	Membrane surface area of a membrane plate	[m²]
A_k	A parameter = $p_{in} - p_p$ in Equation 3.2.7	[pa/mbar]
A_t	Total permeation area on membrane surface	[m²]
A_{sys}	Total membrane surface in one system	[m²]
A_p	Phenomenological coefficient	
B_k	A parameter = $-\frac{8\eta \dot{V}_{in}}{\pi {R_k}^4}\frac{1}{a}$ in Equation 3.2.8	
C_p	Recovery coefficient	
d	Diameter	[m]
d_{min}	Minimum diameter in sudden contraction situation	[m]
D	Diameter/Hydraulic diameter	[m]
d_i	Diameter at different pipes of system	[m]
F_r	Friction force	[N]
G	Gravity	[N]
g	Gravity acceleration	[m/s^2]

H	Distance between two planes	[mm/m]
$\vec{H}$	Flux on the surface in the conservation equation	
h	Water head	[m]
i	Subscript index (1,2,3,j)	
j	Index: junction point	
J	Permeation Flux	[m/s]
J_w	Water Flux	[m/s]
k_1, k_2	Constant factor	
K	Pressure Loss Coefficient	
K_{SE}	Pressure Loss Coefficient of sudden expansion	
K_{SC}	Pressure Loss Coefficient of sudden contraction	
K_{90}	Pressure Loss Coefficient of 90 angle	
K_{toti}	Total pressure Loss Coefficient at different parts of system	
K_{toti}	Total pressure Loss Coefficient at different parts of system	
K_{porous}	Permeability of porous media	[m²]
l_k	Length of capillary	[m]
L	Length of plane	[m]
L_i	Length of pipe, length of pipe at different parts of system	[m]

$\vec{n}$	Normal direction	
p	pressure	[pa/mbar]
p_{top}	Pressure at the top side feed pipes	[mbar]
p_{bot}	Pressure at the bottom side feed pipes	[mbar]
p_{in}	Pressure at the inflow position of capillaries	[mbar]
p_p	Pressure at the permeate side of membrane	[mbar]
p_{out}	Pressure at the out surface of membrane surface	[mbar]
p_{out}	Pressure of the suction pump	[mbar]
Pb	Permeability	[l/(m²hbar)]
Pb_{sys}	Permeability of the system	[l/(m²hbar)]
Pb_{plate}	Permeability of the membrane plate	[l/(m²hbar)]
Q	Required permeation volume flow of a system	[m³/h]
Q_{rack1}	Sum of permeation flow of modules in Rack 1	[m³/h]
Q_{rack2}	Sum of permeation flow of modules in Rack 2	[m³/h]
Re or Re_d	Reynolds number	
R_m	Resistance of membrane	[1/m]
R_f	Resistance of fouling layer	[1/m]
R_{cp}	Resistance of concentration polarization layer	[1/m]

R_{tot}	Total Resistance	[1/m]
R_k	Radius of capillary	[m]
r	Radial direction in cylindrical coordinate	
$\vec{S}$	Conservation source	
TMP	Trans Membrane Pressure	[mbar]
$\vec{U}$	Conservation parameter	
v	Velocity	[m/s]
v_{in}	The inflow velocity of T-connector	[m/s]
v_i	Velocity at different part of system	[m/s]
v_{outp}	The velocity at the outflow (pipe) of T-connector	[m/s]
v_{outm}	The velocity at the outflow (module) of T-connector	[m/s]
v_x	Superficial velocity in the x direction (free fluid)	[m/s]
v_x^*	velocity of fluid in porous media (2 phases) in the x direction	[m/s]
v_y	Velocity in the y direction	[m/s]
v_z	Velocity in the z direction	[m/s]
v_p	permeation flux in the capillary	[m/s]
$\overline{v_z}$	Mean velocity in the z direction	[m/s]
V	Volume	[m^3]

$\dot{V}$	Volume flow	[m³/h]
$\dot{V}_{in}$	Volume flow at the inlet of capillaries	[m³/h]
$\dot{V}_{total}$	Total permeation flow of a module	[m³/h]
$\dot{V}_{top}$	Volume flow entering module from top feed pipes	[m³/h]
$\dot{V}_{bot}$	Volume flow entering module from bottom feed pipes	[m³/h]
$\dot{V}_3{}'$	Calculated volume flow from T-connector to module	[m³/h]
$\dot{V}_{plate}$	Permeation volume flow of single plate	[m³/h]
$\frac{dX}{dx}$	Gradient of X (pressure, concentration...) in x direction	
x,y,z	Direction in Cartesian coordinate	[m]
z_i	height water head	[m]
α	Dimensionless constant	
π	pi = 3.1415926	
η	Dynamic viscosity	[pa.s]
η_ε	Effective dynamic viscosity	[pa.s]
ρ	Density of fluid	[kg/m³]
ϵ	Porosity of porous media	[%]
λ	Friction factor	
λ_s	Scale factor	

ε	Roughness	[mm]
δ	Thickness of plate	[mm]
τ_w	Wall shear stress	[pa]
Δh	Water head loss	[m]
Δh_m	Water head loss caused by the minor friction loss	[m]
Δh_{total}	Total Water head loss caused by the friction loss	[m]
Δh_λ	Water head loss caused by the major friction loss	[m]
$\Delta p_{critical}$	The critical pressure difference between the top and bottom side of module	[mbar]
Δp_m	The pressure difference between the inlet of the pipe and the outlet to the Module	[mbar]
Δp_p	The pressure difference between the inlet and the outlet of the pipe	[mbar]

7. Reference

[1] F. M. White, "Fluid Mechanics", McGraw- Hill Education, 5th edition, (1998) chapter. 2

[2] F. M. White, "Fluid Mechanics", McGraw- Hill Education, 5th edition, (1998) chapter. 6

[3] S. Schütz, M. Pirsche, "CFD in der mechanischen Trenntechnik", Chemie Ingenieur Vol.79, N0.11 (2007), pg. 1777-1796

[4] P. R. Bandyopadhyay, "Aspects of the Equilibrium Puff in Translational Pipe Flow", *J. Fluid Mech*., Vol. 163, (1986), pg. 439-458

[5] D. A. Siginer, S. I. Bakhtiyarov, "Flow in Porous Media of Variable Permeability and Novel Effects", Vol. 68, (2001)

[6] A. Lerch, "Fouling layer formation by flocs in inside-out driving capillary ultrafiltration membranes", PhD Dissertation, Universität Duisburg Essen, (2008)

[7] M. M. Hafez, "Computational Fluid Dynamics for the 21st Century", Notes on Numerical Fluid Mechanics, Vol. 78, Springer, Berlin, (2001), pg. 117.

[8] P. Angot, "Analysis of Singular Perturbations on the Brinkman Problem for Fictitious Domain Models of Viscous Flow". Mathematical Methods in the Applied Sciences Vol. 22, (1999), pg. 1395–1412.

[9] S.Panglisch, "Zur Bildung und Vermeidung schwer entfernbarer Partikelablagerungen in Kapillarmembranen bei der Dead – End Filtration", PhD Dissertation, Universität Duisburg Essen (2001).

[10] S. O'Callaghan, M. Walsh, T McGloughlin, "Comparison of finite volume, finite

element and theoretical predictions of blood flow through and idealised femoral artery", Summer Bioengineering Conference (2003)

[11] P. Angot, C.H. Bruneau and P. Fabrie, "A Penalization Method to Take into Account Obstacles in Incompressible Viscous Flows". Numerische Mathematik Vol. 81, (1999), pg. 497–520.

[12] S. P. Beier, "Pressure Driving Membrane Process", 2nd edition, Student support, ISBN 87-7681- 152-2, (2007).

[13] H. Schade, E. Kunz, "Strömungslehre", Hrsg.: Water de Gruyter. 2. Aufl., Berlin, New York, (1989).

[14] H. Richter, "Rohrhydraulik: Ein Handbuch zur praktischen Strömungsberechnung", 5. Aufl., Berlin, Springer Verlag, (1971)

[15] S. Panglisch, O. Kiepke, W. Dautzenberg, R. Gimbel, J. Gebel, A. Kirsch, M. Exner, "Ultra- and Microfiltration pilot plant investigation to treat reservoir water", Desalination, Vol. 119, (1998), pg. 277-287

[16] G. Belfort; N. Nagata; "Fluid mechanics and cross-flow filtration: some thoughts", Desalination, Vol. 53, (1985), pg. 57 -79

[17] G. S. Beavers, D. D. Joseph; "Boundary conditions at a naturally permeable wall", J Fluid Mech, (1967), Nr 30 (1), pg. 197-207

[18] I. N. Bronstein, K. A. Semendjajew; "Handbook of mathematics", 18 edition, Frankfurt/Main, Harri Deutsch Verlag, (1979)

[19] C. F. Colebrook; "Turbulent Flow in Pipes, with Particular Reference to the Transition between the Smooth and rough Pipe Laws", J. Inst. Civ. Eng. Lond., Vol. 11, (1938-1939), pg. 133-156.

[20] H. Rouse and S. Ince, "History of hydraulics", Iowa Institute of Hydraulic Research, New York: Dover Publications. Inc. (1957)

[21] J. Nicuradse, "Strömungsgesetze in Rauhen Rohren", VDI Forschungsh. 361, (1933)

[22] L. F. Moody, "Friciton Factor for Pipe Flow", ASME Trans., Vol. 66, (1944), pg. 671-684

[23] "Flow of Fluids through Valves, Fittings, and Pipe", Crane Co, Tech. Pap. 410, Chicago, (1957)

[24] "Pipe Friction Manual", 3rd ed., the hydraulic Institute, New York, (1961)

[25] J. L. Lyons, "Lyons' Valve Designers Handbook", Van Nostrand Reinhold, New York, (1982)

[26] R. D. Blecins, "Applied Fluid Dynamics handbook", Van Nostrand Reinhold, New York, (1984)

[27] I. E. Idelchik, "handbook of Hydraulic Resistance", 3rd ed., CRC Press, Boca Raton, FL, (1993)

[28] P. W. Runstadler, Jr., et al., "Diffusser Data Book", Creare Inc. Tech. Note 186, Hannover, NH, (1975)

[29] H. Darcy, "Les Fontaines Publiques de la Ville de Dijon", Dalmont, Paris (1856)

[30] M. Shakaib, S. M. F. Hasani, M. Mahmood, "Study on the effects of spacer geometry in membrane feed channels using three dimensional computational flow modeling", Journal of Membrane Scientce Vol. 297, (2007), pg. 74- 89

[31] H. C. Brinkman, "A calculation of the viscous force exerted by a flowing fluid on a dense swarm of particles". Appl. Sci. Res. A **1** (1947), pg. 27–33.

[32] A. Nahrstedt, R. Gimbel, "zum dynamischen Filtrationsverhalten von Schüttschichten aus Permeablen Synthetischen Kollektoren aus Permeablen Synthetischen Kollektoren bei der Trübstoffabscheidung aus wäßrigen Susupensionen", Dissertationen aus dem IWW, Universität Duisburg Essen (1998)

[33] J. Kozeny, "Über kapillare Leitung des Wassers im Boden (Aufstieg, Versickerung und Anwendung auf die Bewässerung)", Sitzungsberichte d. Mathem. –naturw. KL. Abt. IIa, Wien Akad., (1927), Nr. 136, pg. 271- 206.

[34] C. A. J. Fletcher, "Computational Techniques for Fluid Dynamics", ISBN 3-540-53058-4 2nd Edition, Springer (1991).

[35] F. Stern, R.V. Wilson, H. Coleman, E. Paterson, "Verification and Validation of CFD simulations", Iowa Institute of Hydraulic Research. The University of Iowa. IIHR Report No. 407 (1999)

[36] P. C. Carman, "Fluid Flow through Granular Beds", Trans. Amer. Inst. Chem. Engrs. Vol. 15 (1937), pg. 150 – 166.

[37] F. Löffler, J. Raasch, "Grundlagen der Mechanischen Verfahrenstechnik", Vieweg Verlag. Wiesbaden (1992).

[38] S. Ergun, "Fluid Flow through Packed Columns", Chem. Eng. Progr. Vol. 48 (1952), pg. 89-94

[39] I. F. Macdonald, M. S. EL-sayed, K. Mow, F. A. L.Dullien, "Flow through Porous Media-the Ergun Equation Revisited" Ind. Eng. Chem. Fundam. Vol. 18 (1979), pg. 199

[40] T. Mulder, "Untersuchungen zur Entwicklung Permeabler Hohlkörperkollektoren zur Trübstoffabscheidung aus wäßrigen Lösungen in Schüttbettfiltern", Dissertationen aus dem IWW, Universität Duisburg Essen (1990)

[41] A. Subramani, S. Kim, E. Hoek, "Pressure, flow, and concentration profiles in open and spacer-filled membrane channels", Journal of Membrane Science Vol. 277 (2006) pg. 7-17

[42] A. Berman, "Laminar flow in channels with porous walls". J. Appl. Phys. Vol. 24 (1953) pg. 1232

[43] S.K. Karode, "Laminar flow in channel with porous walls", J. Membr. Sci. Vol. 191 (2001) pg. 237

[44] G. Neale, W. Nader, "Practical Significance of Brinkman's Extension of Darcy's Law: Coupled Parallel Flows within a Channel and a Bounding Porous Medium", The Canadian J. of Chemical Engineering, Vol. 52, (1974), pg. 475-478.

[45] N. Martys, D. P. Bentz, and E. J. Garboczi, "Computer simulation study of the effective viscosity in Brinkman's equation", Phys. Fluids Vol. 6, (1994) pg. 1434-1994.

[46] N. Martys, "Improved approximation of the Brinkman equation using a lattice Boltzmann method", Physics of Fluids, Vol. 13, No. 6, (2001), pg. 1807-1810.

[47] V. Laptev, "Numerical Solution of Coupled Flow in Plain and Porous Media". PhD Dissertation, Universität Kaiserslautern, (2003), pg. 27

[48] D. A. Nield, A. Bejan: "Convection in Porous Media". Springer-Verlag, New York, (1999), pg. 13

[49] K. Khadra, P. Angot, S. Parneix and J.P. Caltagirone: "Fictitious Domain Approach for Numerical Modelling of Navier-Stokes Equations". International Journal for Numerical Methods in Fluids Vol. 34, (2000), pg. 651–684.

8. Appendix A

A.1 Introduction

Microdyn-Nadir GmbH designed a new special membrane filtration system in order to get more market share. They successfully build a compact system named BioCel® membrane filtration system with Microfiltration pillow-shaped membrane plates. The membranes with a pure water permeability of around 500 l/(m²hbar) are employed in the system. Pillow-shaped membrane plates are constructed by two flat sheet membranes and one permeate spacer between them. The membrane plates are used in a submerged mode with vacuum pressure, hence the filtration direction is outside/in. One or more suction pipes are integrated on both sides of an element (see Figure A.1.1). Shape, number, and location of the suction pipe had to be optimized by the CFD tool. A basic membrane filtration module is built up by several plates connected with seals and arranged in a box with an aeration chamber at the bottom. The box has one dead-end side and one suction port where the connection to the piping system takes place (see Figure A.1.1). The shape of the pipe connector had to be optimized by the CFD tool too.

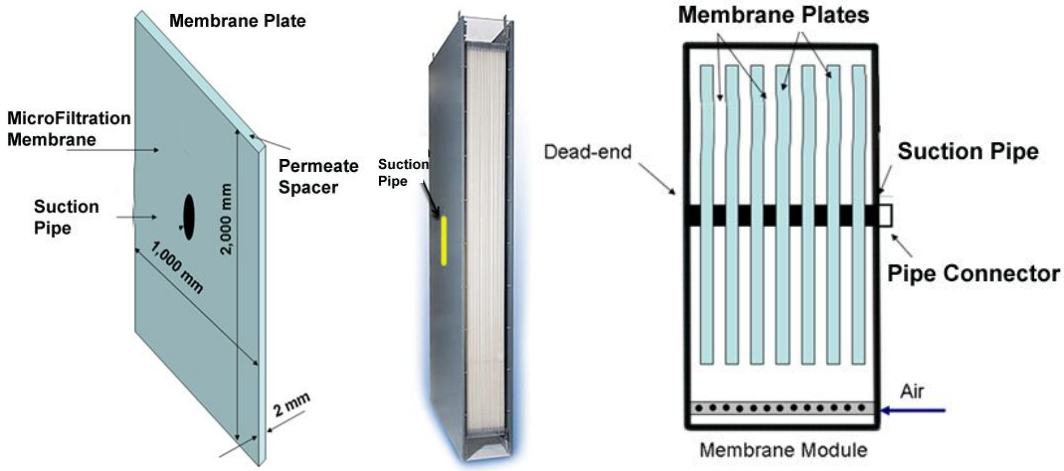

Figure A.1.1 BioCel® membrane filtration system with quasi-ellipsoid suction pipe built by Microdyn-Nadir GmbH

Thickness of the membrane plate is only 2 mm while it has a width of 1000 mm and a

height of 2000 mm. In order to get higher permeation efficiency, different designs of suction pipe are employed and compared. Three predefined quasi-ellipsoid designs are employed; radius R at two sides is 15 mm, 20mm and 30 mm, the length of rectangle between half circles L is 300 mm, 211 mm and 115 mm respectively (see Figure A.1.2). One traditional circular suction pipe design with radius 54.2 mm which has same section area as the ellipse design R15L300 is also considered in this work. The comparison of two designs suction pipe shows the advantage of quasi-ellipsoid design.

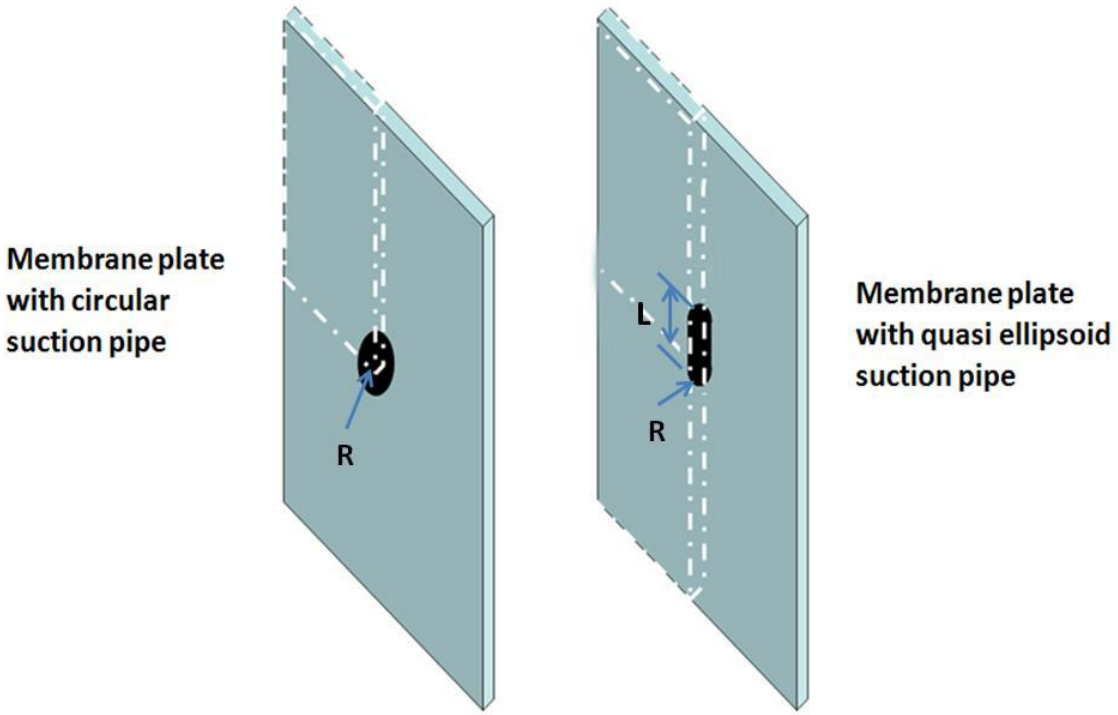

Figure A.1.2 The traditional circular suction pipe design plate and the new quasi-ellipsoid suction pipe plate (From Nadir).

The spacer of the pillow-shaped membrane plate is 2 mm width and consists of large amount of fibers (see Figure A.1.3). The fibers between membrane sheets can be compressed due to different pressure between inside and outside of the membrane sheets. It means the thickness of membrane plate will be smaller than 2 mm during the operation. This thickness will be changed with different applied operation pressure.

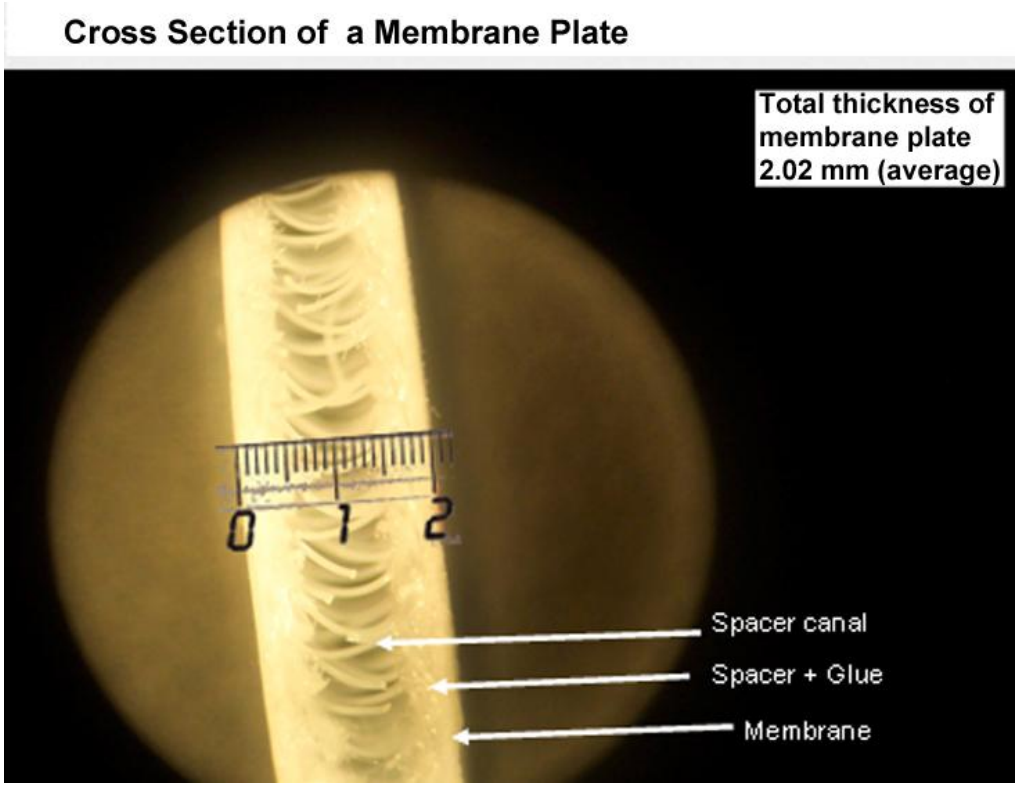

Figure A.1.3 Construction of membrane plate in pillow-shaped membrane plate system from Microdyn-Nadir GmbH

A.2 Characterization of the Permeability of Spacer

In this work, the permeability of porous media K_{porous} is determined by experiments from Microdyn-Nadir. In the experiments, a series of pressure measuring points were built on the surface of plate. Water was set to flow in from one side of plate and flow out from the center suction pipe. There is no permeation occurring through the surface of the plate. The pressure drop caused by the spacer can be shown by the measurements of different points and the known flux. The setup is shown in Figure A.2.1:

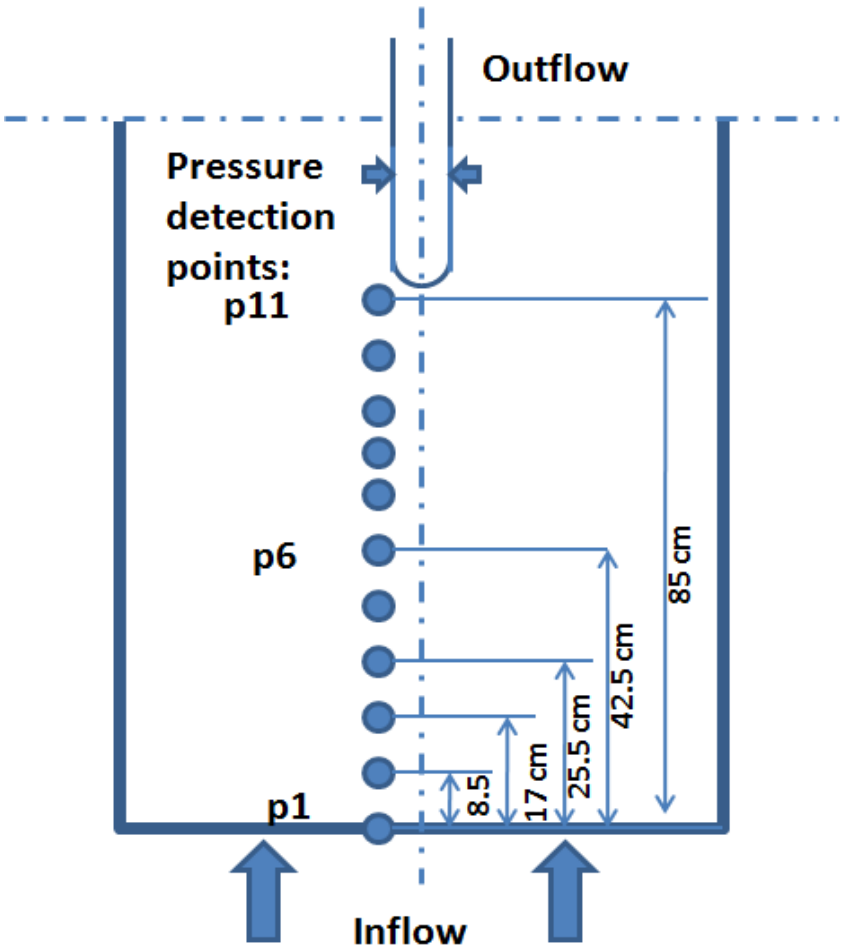

Figure A.2.1 Membrane pressure detection experiment setup built by Microdyn-Nadir.

From these experiments the pressure at different positions in the membrane is plotted against flow velocity (see Figure A.2.2). The pressure detection points are shown in Figure A.2.1. There are 11 points along the flow direction, and the distance between each other is 8.5 cm. A series of experiments with different inflow velocity are done, the pressure at the points are detected and compared. The inflow is at the bottom side of the plate, so there is no velocity direction change and the flow was controlled in laminar state which means the convective acceleration term in Modified Navier Equation can be neglected. In the laminar state the pressure loss caused by the viscosity is proportion to the flow velocity (see Figure 3.3.3) which can be described as permeation term in Brinkmans' Equation. In order to simplify the simulation, the calculation of the

permeability of spacer based on the results of this experiment can be just calculated from the Darcy' Law.

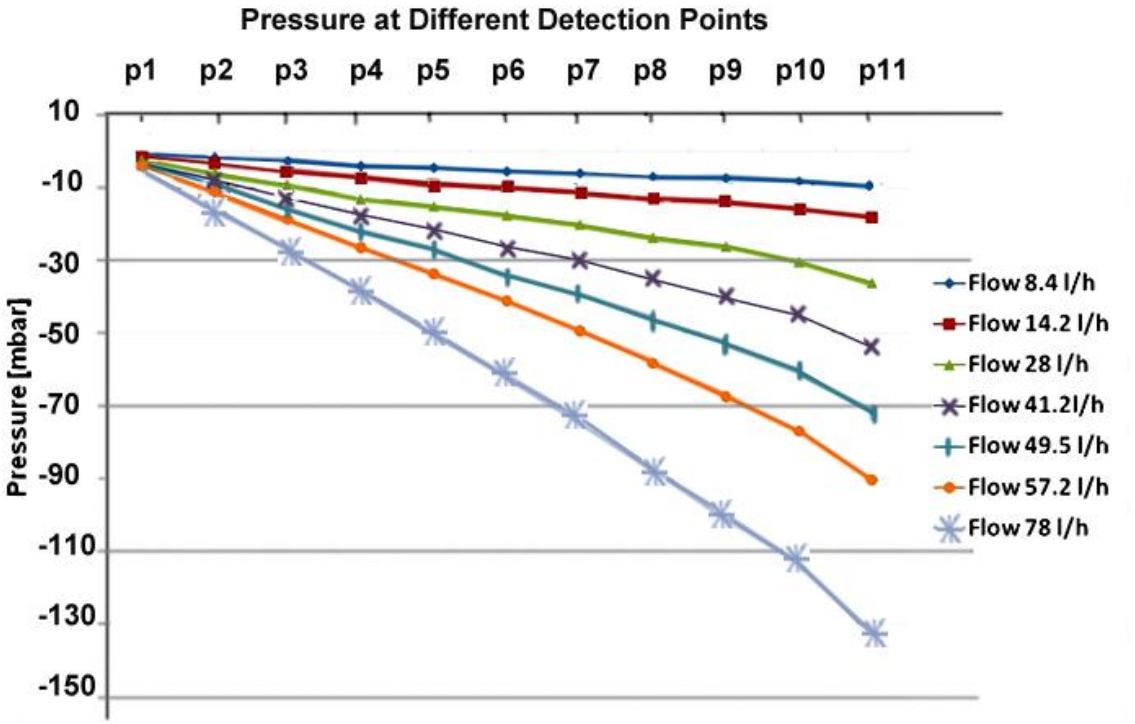

Figure A.2.2 Pressure drops along the membrane with different flow rate

Then two series of pressure drops with corresponding velocities are considered here to calculate the permeability of the porous media. One is the pressure drops from p1 to p6 and the other is from p1 to p11. Then the calculation results of the porous media permeability of the spacer are shown in Figure A.2.3.

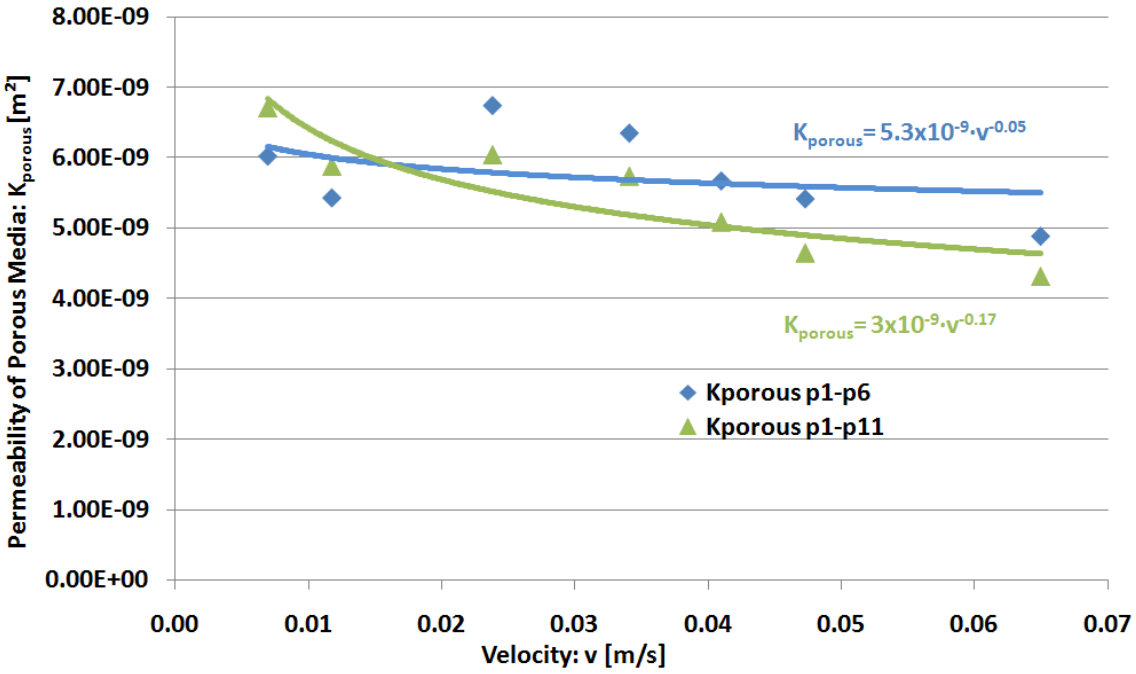

Figure A.2.3 The porous media permeability of spacer generated from experiments

In order to avoid the influence of the suction pipes (around the suction pipe the water is gathered and the velocity is higher), the porous media permeability is calculated from p1 to p6. Using results from the experiments p1 to p6 is more suitable to the Darcy's Law, which takes the permeability to be independent from the velocity. Neglecting the $v^{-0.05}$ term, the porous media permeability $5.3x10^{-9}$ m² is considered as the standard permeability of spacer $K_{porous\_standard}$ in the simulation.

Additionally, even the spacer is used to maintain the stability of membrane plates, a compression caused by the pressure difference between the inside and outside of the membrane plate was induced (see Figure A.2.4). Hence the relationship between the porosity of the spacer and the corresponding pressure difference was considered and modeled in this work.

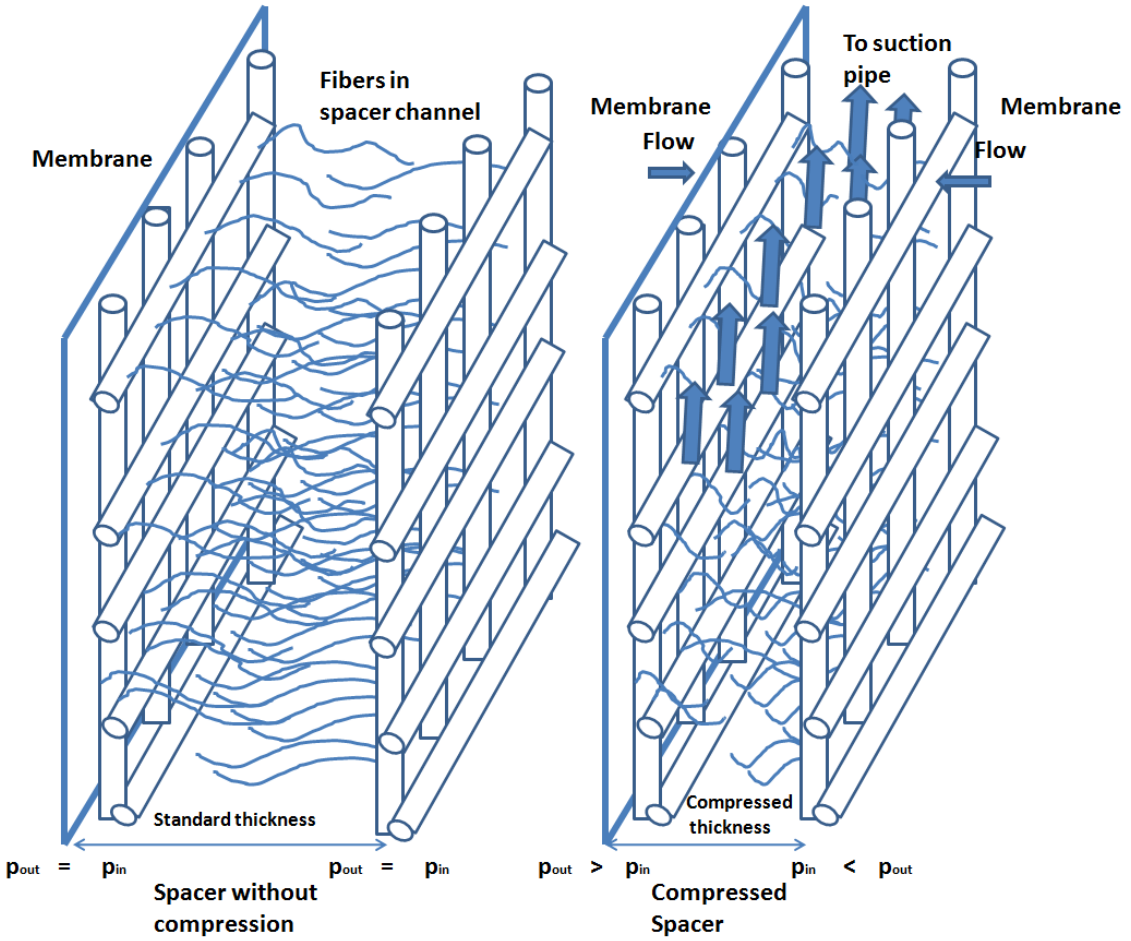

a) b)

Figure A.2.4 Example of spacer employed in the BioCel® system: a) without compression; b) compressed

From the experimental results, the relationship between the thickness of spacer and applied trans-membrane pressure (TMP) is shown in Figure A.2.5. The membrane plate employed in this work is built by the submerged MF membrane, hence the TMP is predefined between 100 to 500 mbar. In this TMP range, the relation between the thickness of plate δ [mm] and TMP [mbar] can be described as:

$$\delta = -\frac{3}{8000} \times \mathrm{TMP} + 2 \qquad \textbf{Equation A.2.1}$$

Here with thickness in mm and TMP in mbar.

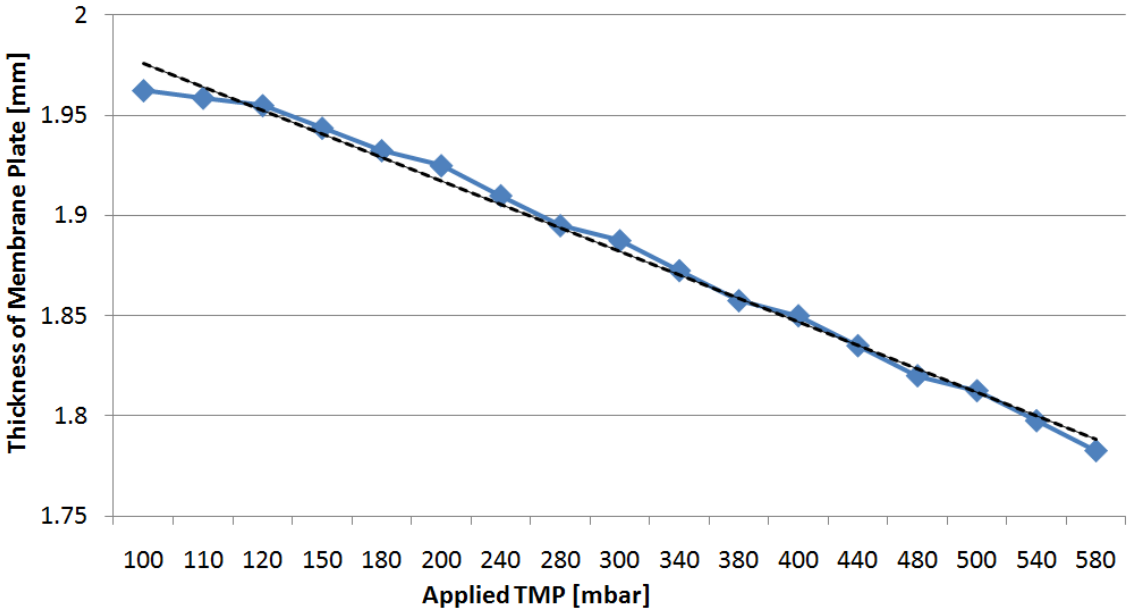

Figure A.2.5 The relationship between the compression of membrane spacer and applied TMP from Microdyn Nadir

The compression of membrane plate will change the porosity of spacer, which subsequently influences the permeability of the membrane plate. From Carman equations [33], the relationship between pressure gradient in x direction and porosity can be written as:

$$\frac{\partial \mathrm{p}}{\partial \mathrm{x}} = \mathrm{k}_1 \cdot \frac{(1-\epsilon)^2}{\epsilon^3} \cdot \frac{\eta \mathrm{v}_\mathrm{x}}{\bar{\mathrm{d}}_\mathrm{k}{}^2} \qquad \textbf{Equation A.2.2}$$

Where $\mathrm{v_x}$ is the superficial velocity of fluid in x direction, $\frac{\partial p}{\partial x}$ is the pressure gradient, ϵ is the porosity of porous media, η is dynamic viscosity, $\overline{d_k}$ is the mean diameter of granular porous media which can be also applied for the fiber diameter of the spacer [32], and k_1 is a factor which equals to 64 at laminar mode.

In 1952, Ergun [38] developed this theory with the additional energy loss caused by turbulent flow and derived a new universal equation to describe the relationship between pressure gradient and porosity of porous media. Later in 1980, Löffer [37] rewrote this equation:

$$\frac{\partial p}{\partial x} = \frac{\rho \cdot v_x^{\,2}}{\bar{d}_k} \cdot \left[\frac{1-\epsilon}{\epsilon^3}\right] \cdot \left[k_1 \cdot \frac{(1-\epsilon)}{Re} + k_2\right] \qquad \textbf{Equation A.2.3}$$

where Reynolds number is defined here as

$$Re = \frac{\rho \cdot \bar{d}_k \cdot v_x}{\eta} \qquad \textbf{Equation A.2.4}$$

k_1 and k_2 are shown in the following table for different situations.

Table A.2.1 k_1 and k_2 value from different authors with different conditions for Equation A.2.2 and A.2.3

Author	Conditions	k_1	k_2
KONZENY (1927)	Laminar flow through porous media	64	0
CARMAN (1937)	Laminar flow through granular system	180	0
ERGUN (1952)	Porous granular system in all range of Re number	150	1.75
MACDONALD et al. (1979)	Granular system in all range of Re number for gas	180	1.8

In order to simplify the simulation model, the original Carman parameter is selected here. If Equation 3.5.1 and A.2.3 are combined, the relation between permeability of porous media and porosity can be written as:

$$\frac{K_{porous}}{K_{porous\_standard}} = 1/\left(\left(\frac{(1-\epsilon)}{1-\epsilon_{standard}}\right)^2 \cdot \left(\frac{\epsilon_{standard}}{\epsilon}\right)^3\right) \qquad \textbf{Equation A.2.5}$$

where $K_{porous\_standard}$ is the standard permeability with the original thickness of spacer, $\epsilon_{standard}$ is the standard porosity with the original thickness. The term K_{porous} is the permeability after compression, and ϵ is the porosity after the compression. As is known, the volume of fiber is constant whatever the spacer is compressed or not, so one equation can be derived:

$$(1-\epsilon) * \delta = (1-\epsilon_{standard}) * \delta_{standard} \qquad \textbf{Equation A.2.6}$$

which means:

$$\epsilon = 1 - (1 - \epsilon_{standard}) * \delta_{standard}/\delta \qquad \textbf{Equation A.2.7}$$

With this equation, the permeability of the spacer can be calculated from Equation A.2.5 when the plate is compressed.

A.3 BioCel® System Simulation

A.3.1 Plate Membrane Model

In Chapter 2.1.2, the structure of the pillow-shaped membrane plate is introduced which is built by two membrane sheets and one spacer between them. Normally the thickness of membrane plate is millimeter range, while the length and width of membrane is meter range. With help of the scale method (see Chapter 3.7), the membrane plate can be simulated based on the porous media approximation method. The simulation model is shown in the Figure A.3.1.

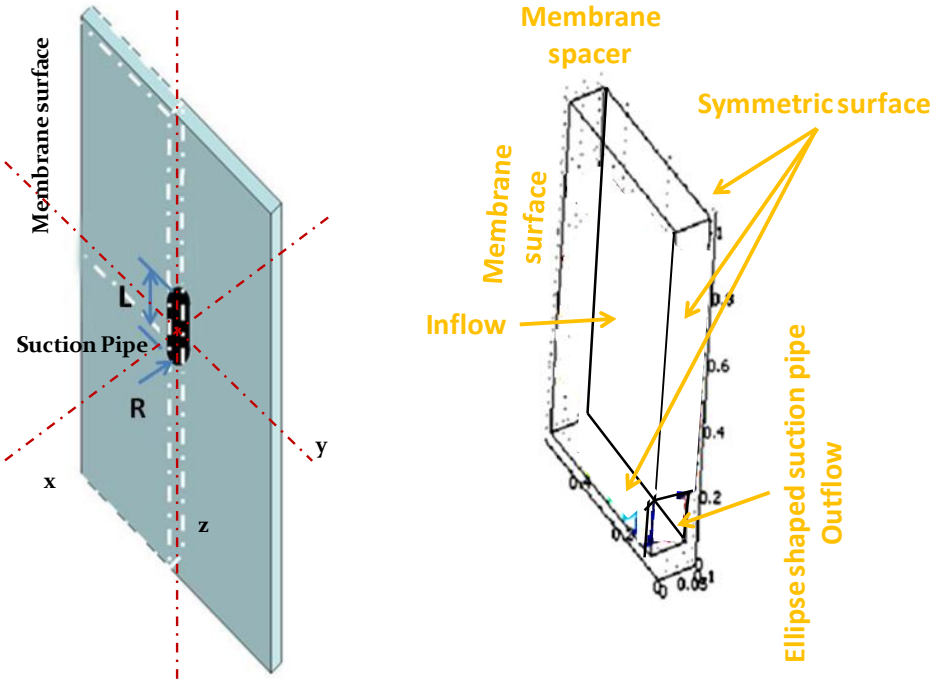

Figure A.3.1 The model setup of plate membrane of BioCel® system

Then this membrane plate simulation model can be combined into the model of the integrated BioCel® system.

A.3.2 Pipe Connector Model

Compared to the T-rack system simulation, the piping system of BioCel® system is nearly same except the different geometry and an additional pipe connector between the different geometry pipes. The pipe connecting membrane plates is quasi-ellipsoid while the outflow pipe of the system is circular. In order to find out the best design of a pipe connector between the different geometry pipes, four different designs are modeled and simulated here shown in following figures.

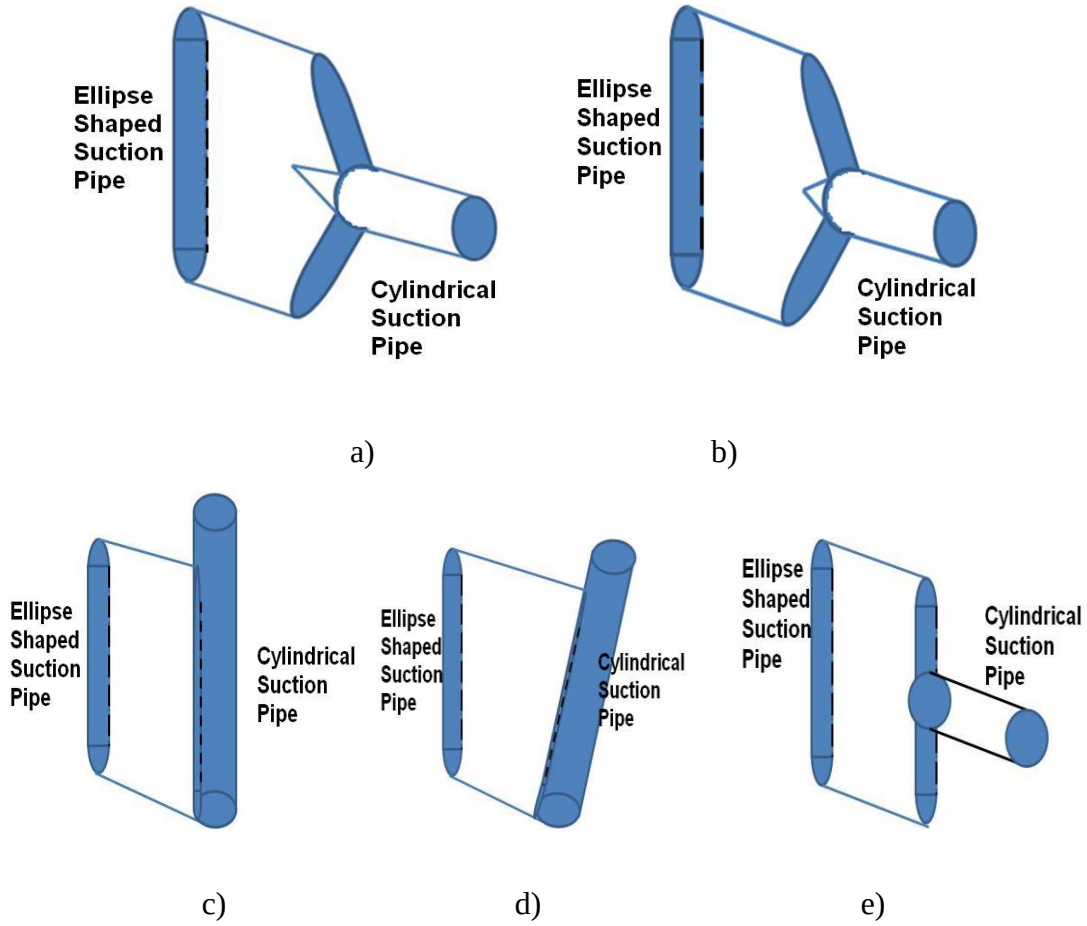

Figure A.3.2 Different designs of connectors between quasi-ellipsoid pipe (D = 30 mm, L = 300 mm) and circular pipe (D = 120 mm)

A.3.3 General Logical Diagramm of BioCel® System Simulation

The simulation model of BioCel® System consists of the membrane plates simulation

model, permeate pipes simulation model and connectors simulation model (see Figure A.3.3). The main logical diagram is necessary to be introduced, before the simulation results are shown.

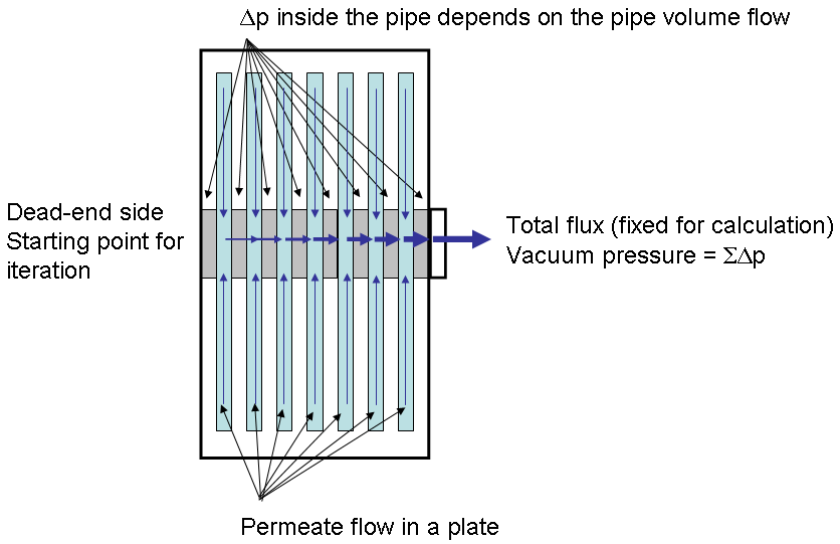

Figure A.3.3 Flow distribution of the pillow-shaped membrane plate filtration system of BioCel® system

Similar to the T-rack system, the iterations also start from the dead-end side of the permeate pipe.

- Assume the pressure in the dead-end of permeate pipe;
- Calculate the flow permeation from the membrane plate, with help of CLI method;
- Calculate the pressure loss inside of the permeate pipe and do the step 1 and 2 again until getting the pressure at the outlet of the permeate pipe;
- Compare the calculated outlet pressure to demanded pressure. If they are not same, reassume the pressure in the dead-end of the permeate pipe and do the steps 1 to 3 again.

The detail diagram is shown in the Figure A.3.4.

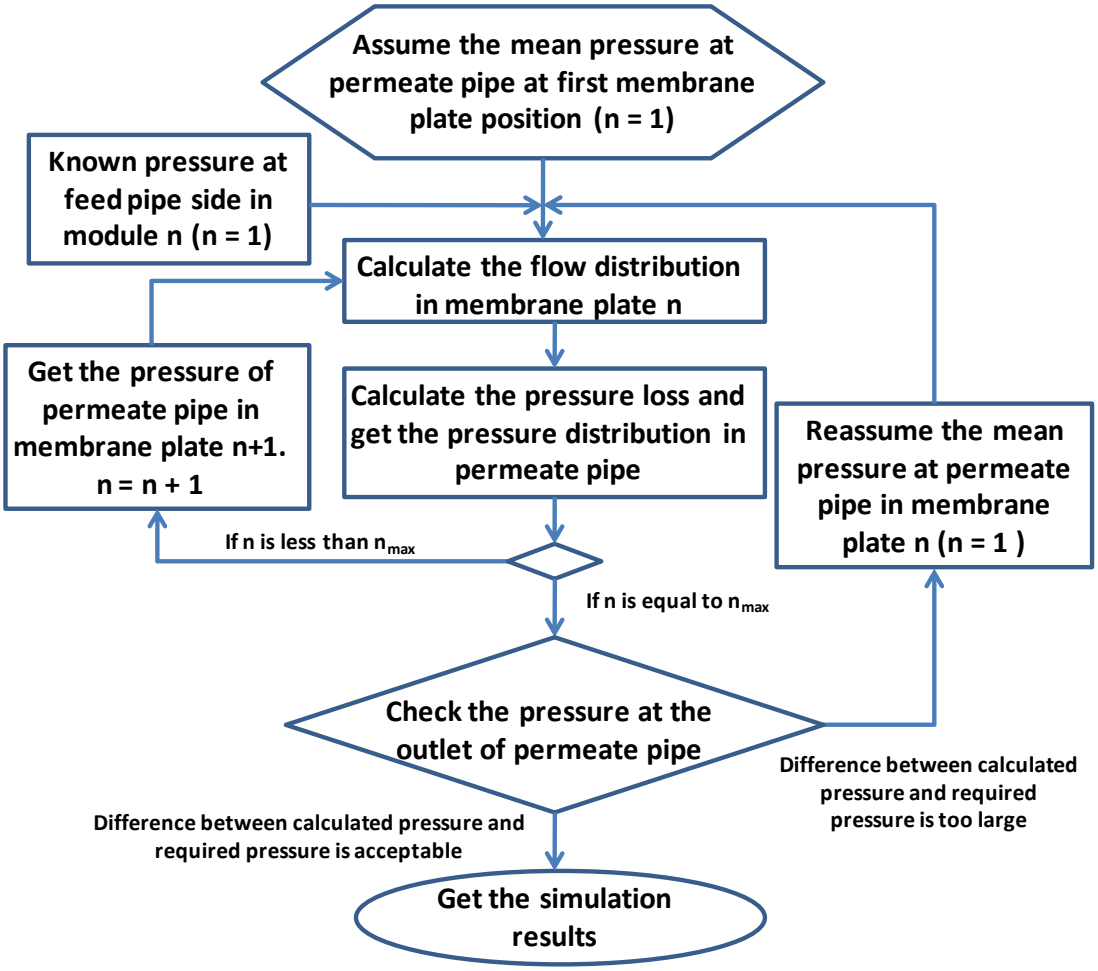

Figure A.3.4 The Logical diagram of the plate membrane filtration system simulation

A.4 Validation of BioCel® System

For the validation, the theoretical results were compared to the experimental results. Although in reality the pure water permeability of the different plates is not uniform, in the simulation the average value was assumed to be 530 l/(m²hbar) which is just the average permeability of membrane in experiment. No fouling layer formation was considered. The pressure out of plate was set to constant 1 bar. The filtration system consisted of with 50 plates in one module. The total experiment was about 2 hours long. The simulation results were expressed as TMP and compared with the average TMP provided from the experiment. As is shown in Figure A.4.1, the smallest difference between simulation and experiment is 3% and the largest difference is 20 %. Taking into

account the effects caused by fouling or by inhomogeneous permeability of the membranes, this difference was seen to be acceptable. Hence, the model was used for further analysis.

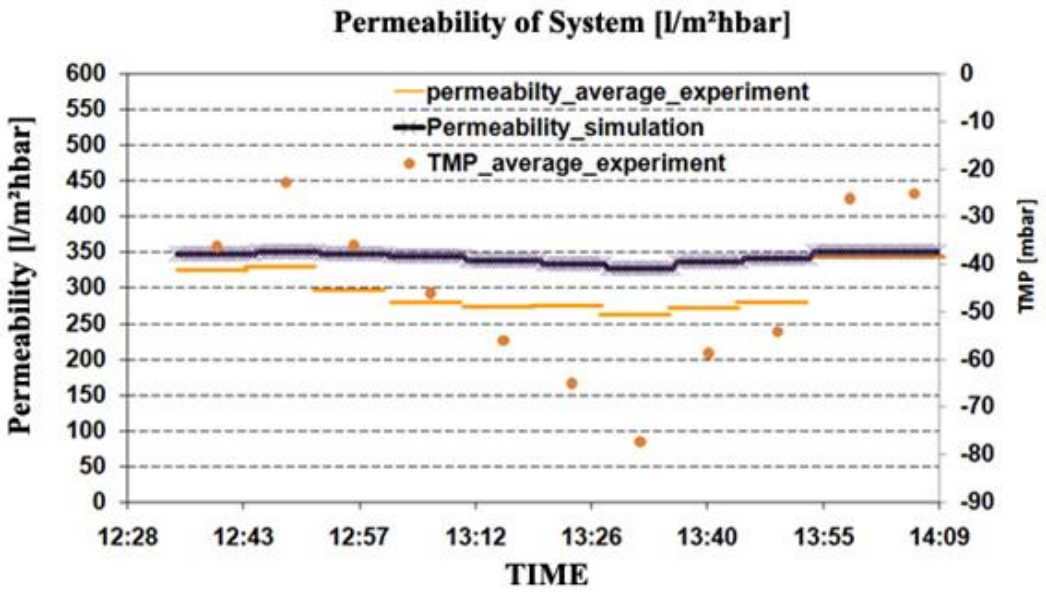

Figure A.4.1 Validation of plate simulation model with experiment system which has 1 module consists of 50 plates and the mean permeability of membrane is about 530 l/(m²hbar).

A.5 Simulation of BioCel® System

A.5.1 Single Plate simulation Results with Different Geometry and Membrane Permeability

A.5.1.1 Simulation of Membrane Plate

The membrane surface simulation is based on Darcy's Law. The permeation flux through the membrane surface is sensitive to the TMP. The pressure at the permeation side of the membrane is set constant to 1 bar, while the pressure in the plate is strongly dependent on the spacer resistant and the flow velocity.

The membrane plate model considers the membrane surface as an inflow boundary condition and the suction pipe as outflow condition. In Figure A.5.1, it shows an example

of a simulation results in terms of pressure distribution inside a plate with circular suction pipe. The colored surfaces in the plate describe isobaric planes. Near the suction pipe, where the vacuum pressure is the highest (means absolute pressure is the lowest) the color of the surface is blue and near the upper edge where vacuum pressure is the lowest (means absolute pressure is the highest) the color is dark red. Streamlines of the permeate flowing in the plate in direction of the suction pipe are always rectangular to the isobaric planes. This CFD model was then used to calculate the pressure loss for different permeate fluxes or TMP respectively. The results were saved into the library for the simulation of a total module.

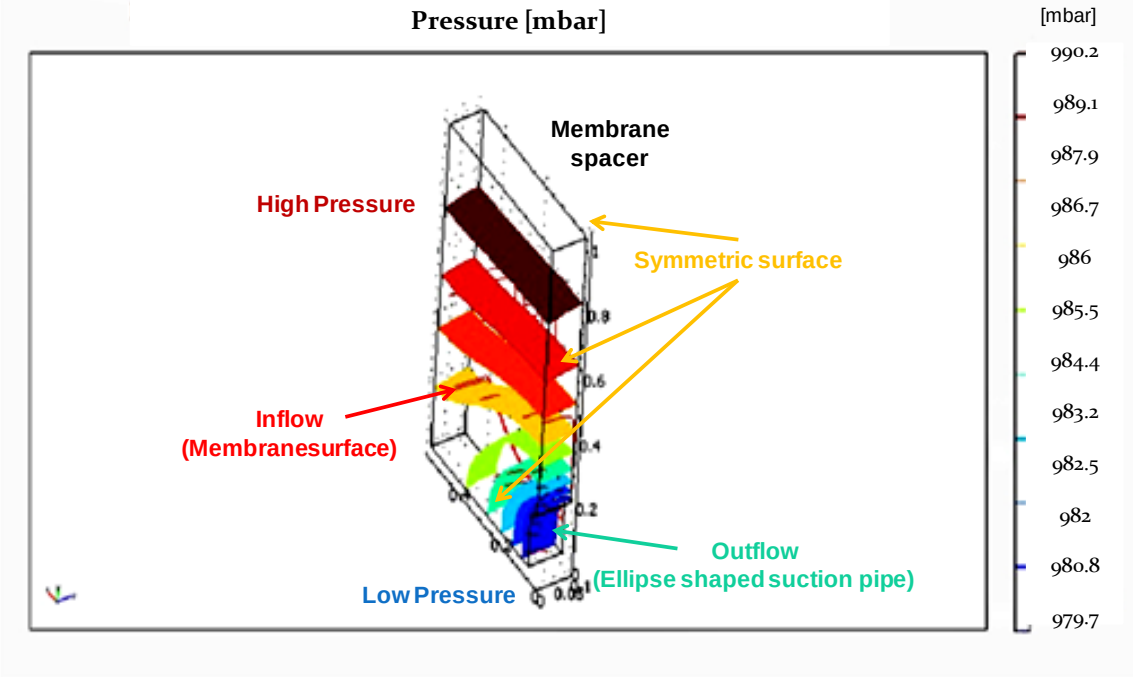

Figure A.5.1 Simulation results: The pressure distribution with the BioCel® plate membrane model with quasi-ellipsoid suction pipe

In order to test the permeation of membrane plate under different working conditions, the parameter named permeability of membrane plate is employed. It is defined as the permeation volume flow of single plate $\dot{V}_{plate}$ divided by membrane surface (A_{plate}) and pressure difference between outside and suction pipe (pump).

$$Pb_{plate} = \frac{\dot{V}_{plate}}{A_{plate} \cdot (p_{out} - p_{pump})}$$ **Equation A.5.1**

Three predefined quasi-ellipsoid designs were surveyed; radius for the two semi-circles has been 15 mm, 20 mm and 30 mm, the length of rectangle between semi-circles has been 300 mm 211 mm and 115 mm respectively. As is introduced the length and height of the plate are 2000 mm and 1000 mm. From these geometric data the indications were derived 2000x1000xR15L300, 2000x1000xR20L211 and 2000x1000xR30L115 or R15L300, R20L211 and R30L115. One circular suction pipe design with a radius of 54.2 mm with the same section area as the quasi-ellipsoid design 2000x1000xR15L300 was also considered.

The permeability of a plate (Pb_{plate}, See Equation A.5.1) for different TMP with different suction pipe design is shown in the Figure A.5.2. TMP was expressed as the difference between the pump pressure p_{pump} and the pressure in the tank p_{out} (p_{out} was considered to be constant). The difference between permeability of membrane plate and that of membrane is due to the pressure loss in the plate caused by the spacer. Following the CFD modeling, the 2000x1000xR15L300 quasi-ellipsoid design has the highest performance in terms of permeability. For a TMP of 40 mbar the plate permeability is 370 l/(m²hbar) which is 70% of the membrane permeability. The maximum permeability of 2000x1000xR20L211 is 355 l/(m²hbar) or 67% of the membrane permeability and that of 2000x1000xR30L115 is 345 l/(m²hbar) 65% of the membrane permeability. The permeability of a single plate in all considered cases increases firstly and decreases later after a TMP of 40 mbar. This TMP can be considered as the critical pressure point for the maximal performance of the system.

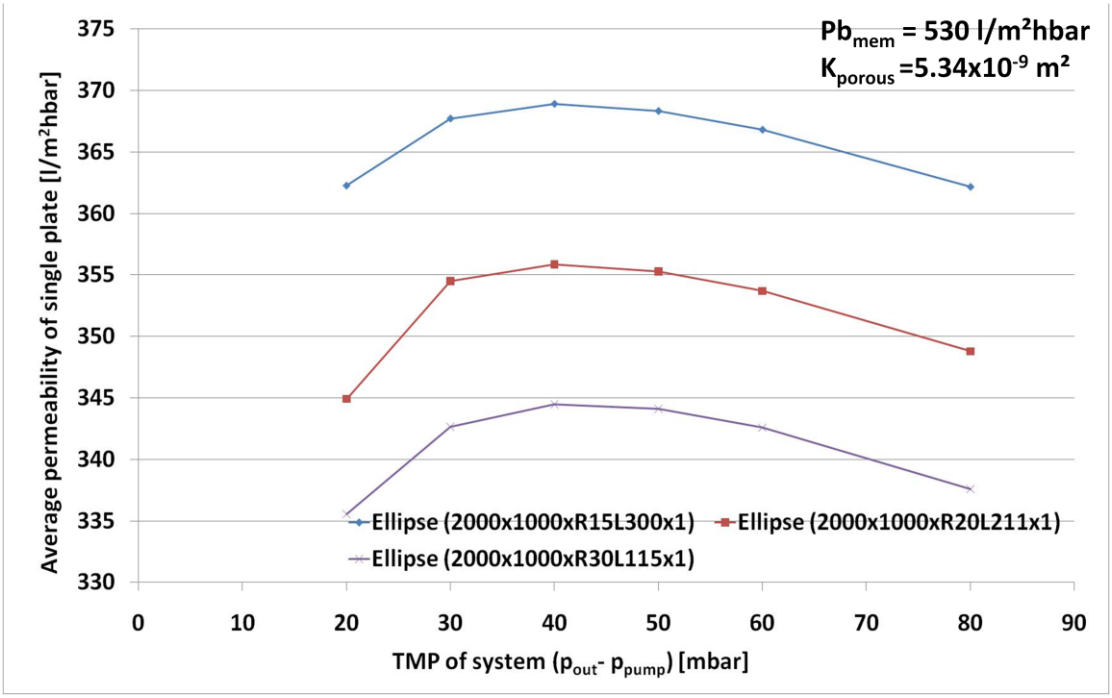

Figure A.5.2 Simulation results: The permeability of membrane plate under different TMP

This calculated maximum of permeability is due to an incomplete exploitation of the total membrane surface of the plate for TMP below the critical TMP (40 mbar in Figure A.5.2). If the TMP is too low it could happen theoretically that the pressure loss caused by the permeation flow in the spacer is too high to overcome. It results in that the flow only permeates in one part of the membrane surface which is named active permeation area. For TMP larger than the critical TMP, the increase of TMP means a higher flux or higher velocity through membrane and spacer, which cause higher pressure loss in the plates. When the active area is equal to the total membrane surface, the permeability of membrane plate starts to decrease due to the additional pressure loss caused in the plate.

With a TMP smaller than the critical TMP condition, e.g. the pressure of suction pipe is only 99320 Pa (TMP = 7.8 mbar), only a part of the membrane surface is permeated. This permeation area is here named active permeation area (see Figure A.5.3).

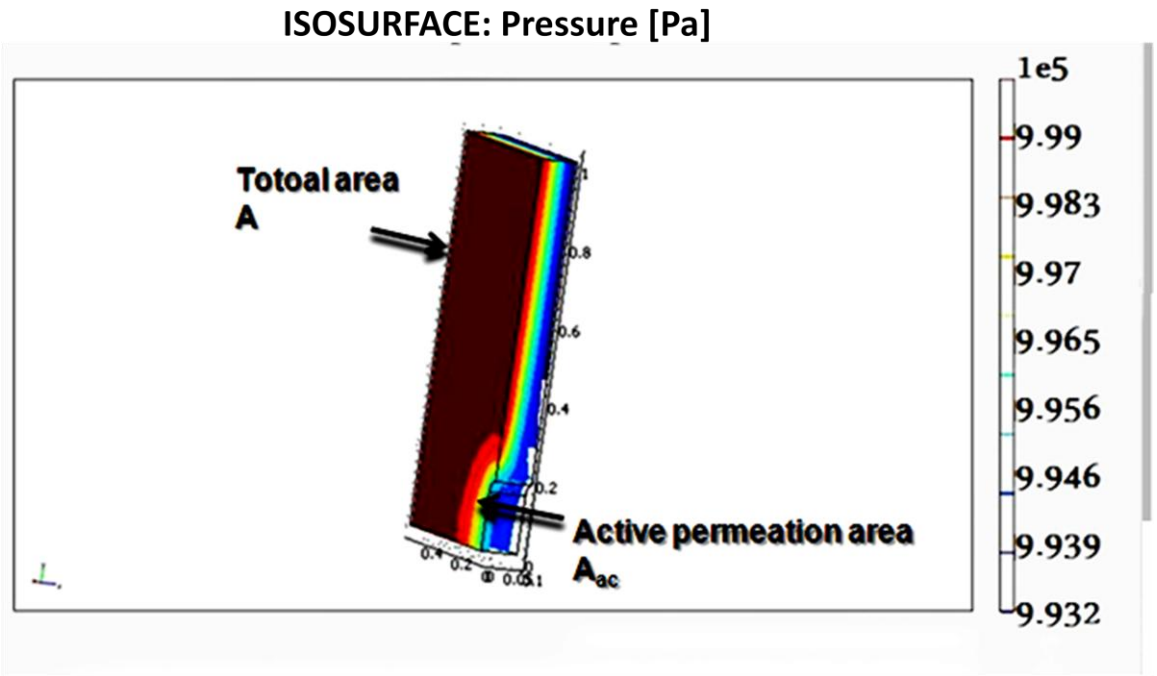

Figure A.5.3 Simulation results: The active permeation area with low TMP while the calculation of the permeability of the plate is based on the total Area of the membrane surface.

The simulation of the membrane plate with circular suction pipe design was done for comparison. Again, the permeability of membrane plate increases to a maximum value and then decreases, while the maximum value of circular pipe design shown at a TMP of 50 mbar. By comparing the permeability of membrane plate with a circular suction pipe with the same area than quasi-ellipsoid design it can be shown, that the permeability for the circular design is about 10% lower (see Figure A.5.4).

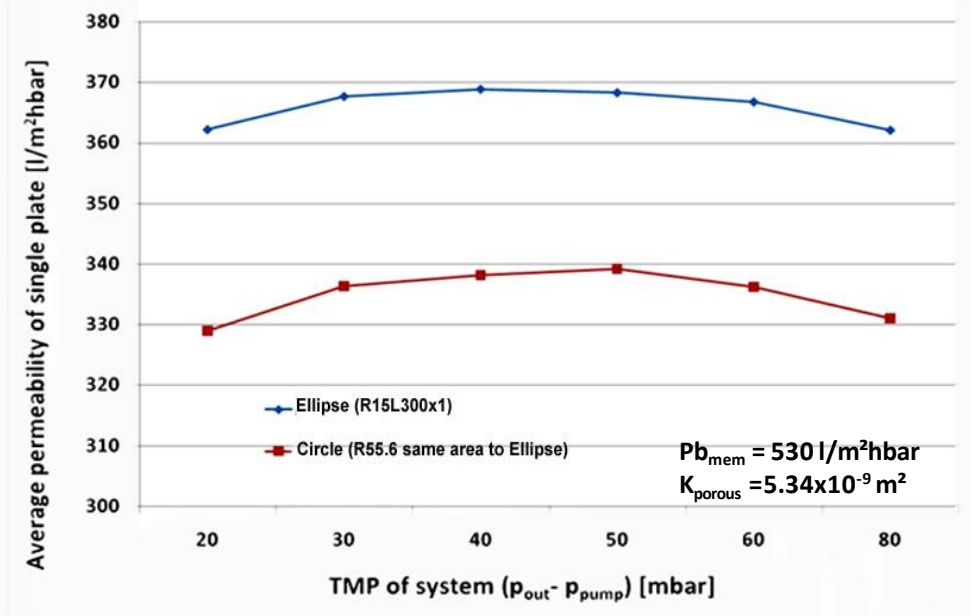

Figure A.5.4 Simulation results: The Permeability of membrane plate of quasi-ellipsoid design R15L300 and same area circular design R55.6 model under different TMP of plate

According to the simulation results for the BioCel® system, the maximal permeability of membrane plate with one suction pipe is about 70% of the permeability of the membrane. In order to improve the performance by a different design, two quasi-ellipsoid and two circular suction pipes respectively in one plate were simulated (see Figure A.5.5). From the simulation results, the advantage of the two suction pipes design can be seen. The performance of the plate with two quasi-ellipsoid suction pipes is the best with a permeability of membrane plate about 81% of the membrane permeability then followed by the two circle suction pipes design with a permeability of membrane plate about 77% of the membrane permeability. The design with just one quasi-ellipsoid suction pipe performs the worst compared to the other designs. However, the excess of production costs especially for the total system for a two suction pipe design devours the benefit of a lower permeability loss.

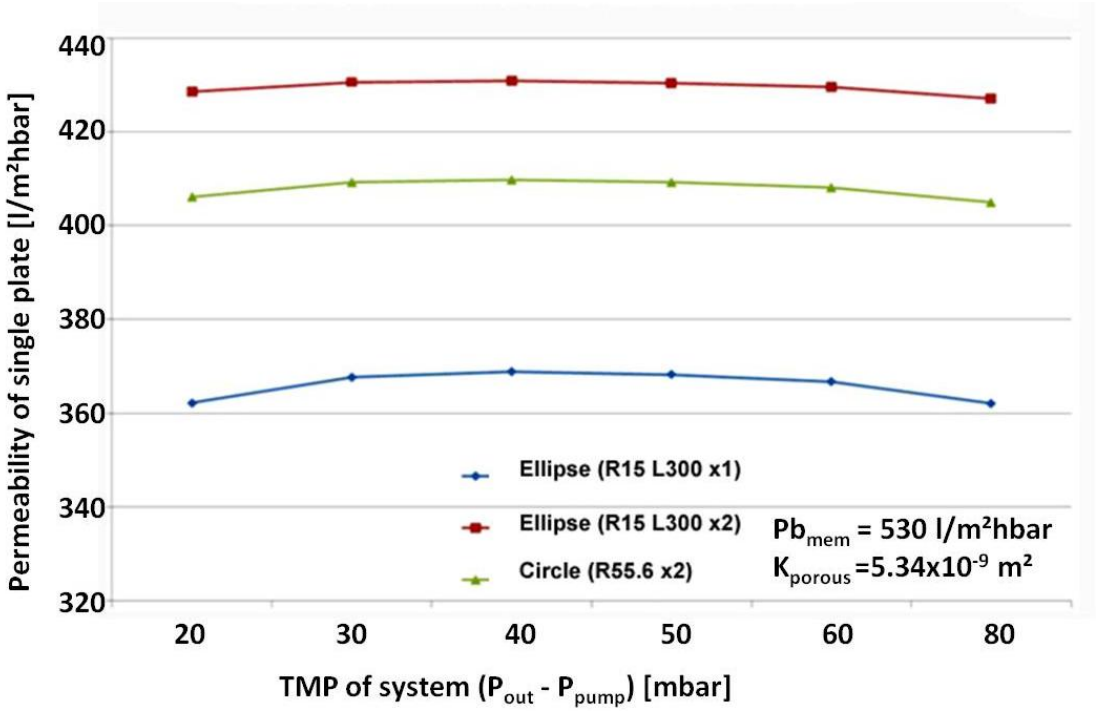

Figure A.5.5 Simulation results: The permeability of membrane plate of 1 or 2 suction pipes with different shape design.

A.5.2 Simulation and Optimization of the Pipe Connector in BioCel® System

The simulation results have shown the advantage of the plate with quasi-ellipsoid design suction pipe. But the filtration system can't take the quasi-ellipsoid design in all piping system, the connector between the quasi-ellipsoid pipe and circular pipe must be considered and the pressure loss caused by this connector must be known. There are 5 different designs of connector considered here. The parameter Pressure Loss Coefficient (see Equation 3.3.4) is employed here to compare the designs. The Pressure Loss Coefficients of different valves are shown in Table 1.1.1.

The 5 designs are shown in Figure A.5.6. Design a) is a combination of a gradual contraction and a longer gradual conical expansion connector. The design b) has the same gradual contraction but a shorter gradual conical expansion. The design c) and d) are the design without contraction or expansion but with 90 or 120 ° bend. The design e)

shows the design which 2 pipes are directly connected.

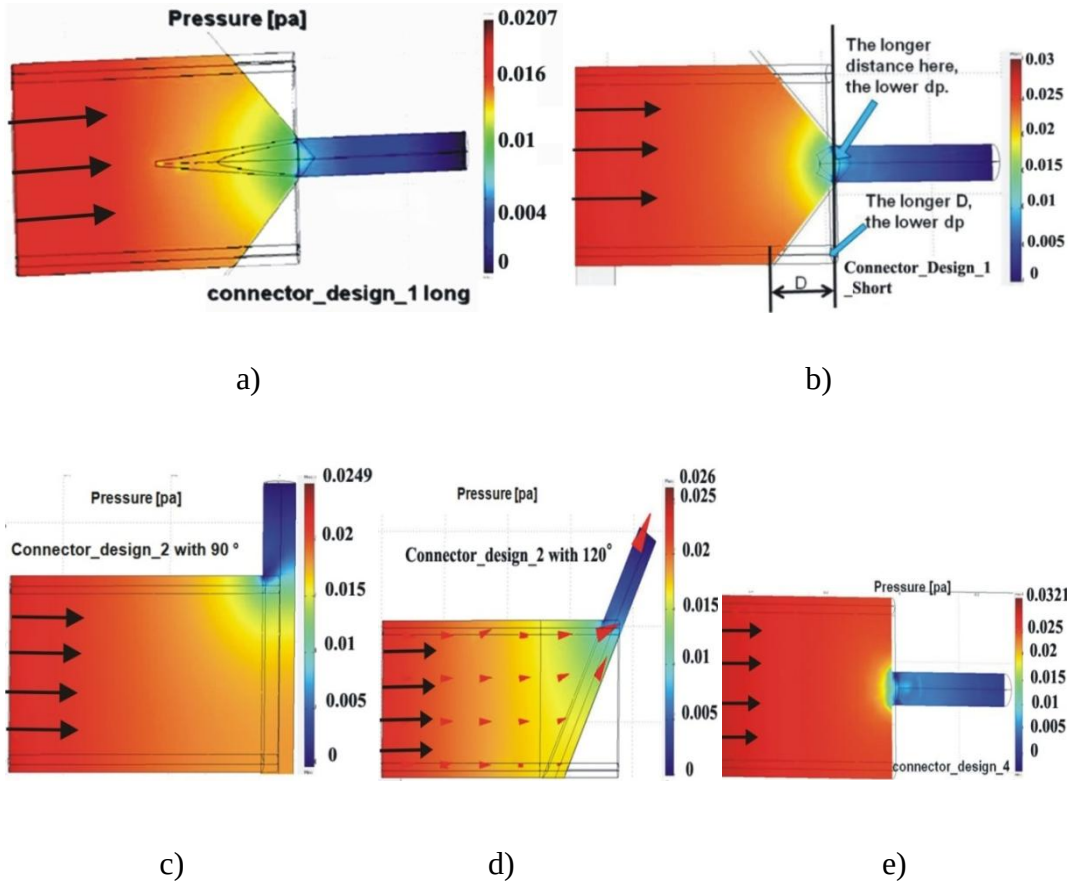

Figure A.5.6 Simulation results: The 5 different design of pipe connector between the quasi-ellipsoid pipe (R15L300) and circle pipe R32 mm; the pressure decreases along the flow direction

The connector with 120 ° bend shown in Figure A.5.6 d) has the lowest Pressure Loss Coefficient here which means lower pressure loss caused with same flow condition. The Pressure Loss Coefficient value is 38 here. Then is the connector with a combination of a gradual contraction and a gradual conical longer expansion which value is 41. The worst performance is the directly connected design which value is 62. From the comparison, the design of 120 ° bend is suggested to be applied in the filtration system.

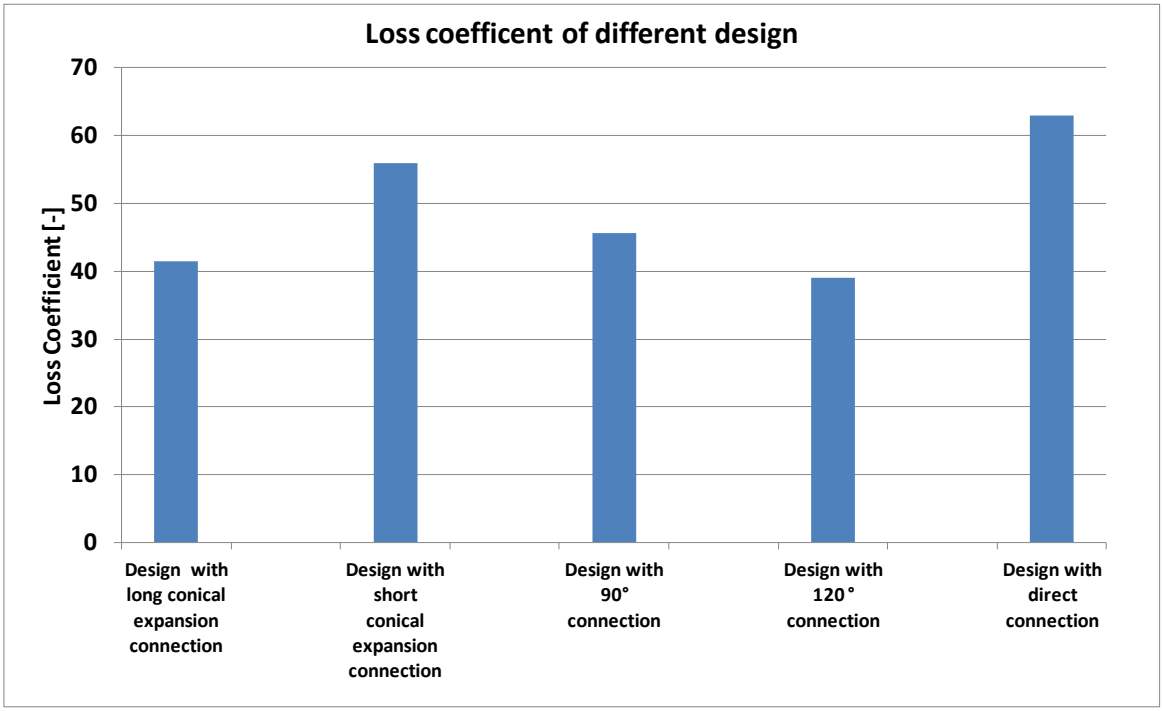

Figure A.5.7 Simulation results: The Pressure Loss coefficient of different design of connectors with same length of ellipse part and circle pipe part

A.5.3 Simulation and Optimization of the Integrated BioCel® System

After the buildup of single membrane plate and pipe connector's model, the integrated BioCel® membrane filtration system is preferred to be simulated. The model consists of a number of plates in one module and connecting piping system. The membrane permeability is set to 530 l/(m²hbar) which is the mean permeability in the real system. The Pressure Loss Coefficient of connector is from the 120° bend design, which is 38 in the R15L300 design.

A.5.3.1 Permeability of Integrated BioCel® System

In order to show the influence of plates' number in the system, the permeability of the system is used to show the different permeation of total system with different TMP.

$$Pb_{sys} = \frac{\mathrm{Q}}{A_{total}(p_{out} - p_{pump})} \qquad \textbf{Equation A.5.3}$$

Here the p_{out} is the pressure at the outside of membrane surface, and p_{pump} is the

suction pump pressure.

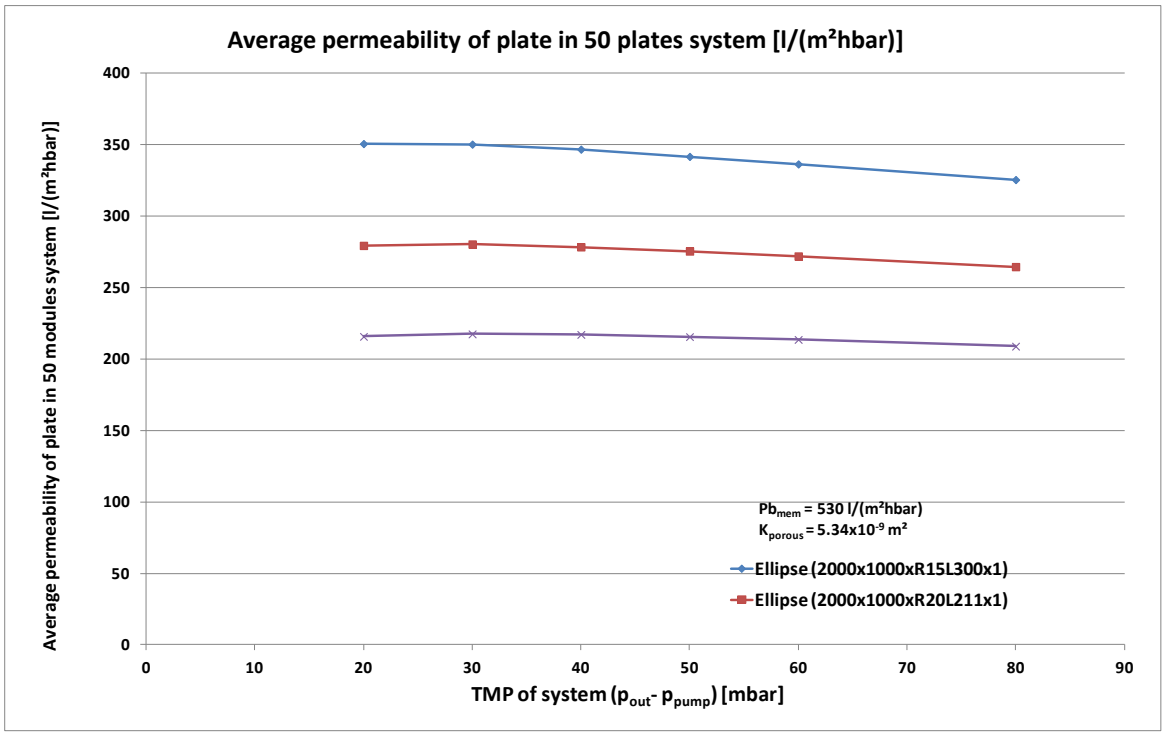

Figure A.5.8 Simulation results: The permeability of system with different TMP of 50 plates system

Compared to the single plate simulation, the permeability of the system with quasi-ellipsoid R15L300 suction pipe is also the highest. However the permeability always decreases with an increase in TMP. The decrease of permeability of system becomes larger with the increase of TMP. The maximum permeability of the system is 350 l/(m²hbar) shown when the TMP is 20 mbar. With 2000x1000xR20L211 design, the maximum permeability of the system is 280 l/(m²hbar) which is only 80% of R15L300 design. The 2000x1000xR30L115 system has 215 l/(m²hbar) maximum permeability of the system shown at TMP 30 mbar, which is only 61% of 2000x1000xR15L300 design. As is introduced in Figure A.5.2, the maximum permeability of the membrane plate occurs at 30 mbar suction pressure while the maximum permeability of the system occurs at 20 mbar in the system which consists of 50 plates in a system. The reason can be known from the two permeability calculation equations (See Equation A.5.1 and A.5.3). The maximum permeability of the system occurs with lower pressure which is

due to the additional pressure loss in the pipe. Lower suction pressure leads to lower permeation and lower pressure loss in the suction pipe, even there is smaller active permeation area.

A.5.3.2 Pressure Loss in the Piping system (including connectors)

As is introduced, a BioCel® system consists of membrane plates, suction pipe connecting the plates and the connector connecting the suction pipe to the outlet pipe. Under same average permeation flux in each plate, more plates in one system cause more fluid permeation and in consequence a higher volume flow through the piping system. From the fluid friction calculation, the pressure loss in the piping system increases due to the increase of velocity and increase of the pipe length. Due to Equation A.5.3, larger pressure loss in the piping system means lower permeability of system. Figure A.5.9 shows the permeability of the system in the module consists of 50 plates is only 97% of that of single plate and then decreases to 90% in that of 100 plates , 75% in that of 150 plates and 65% in that of 200 plates.

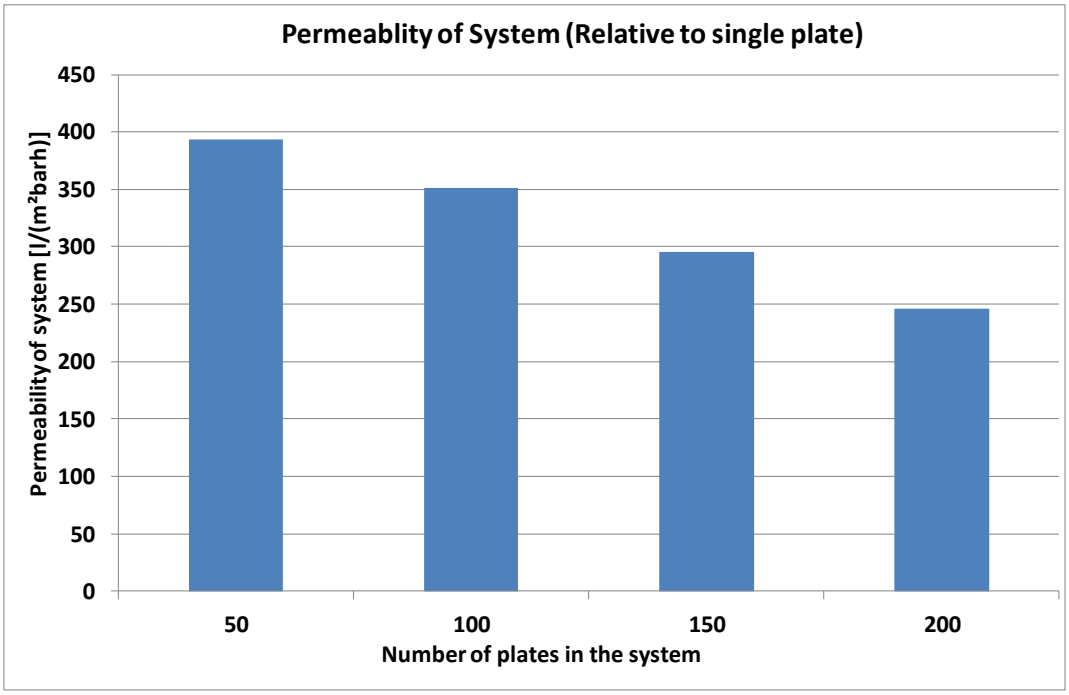

Figure A.5.9 Simulation results: permeability of system Pb_{sys} and Pb_{sys} /Pb_{plate} in the system consists of different number of plates when TMP is 20 mbar.

Figure A.5.10 shows the pressure distribution inside the piping system. The pressure decreases from 1st plate to the outlet. The pressure loss in the piping system is classified into two parts, one is caused by pipe and the other is caused by the pipe connector.

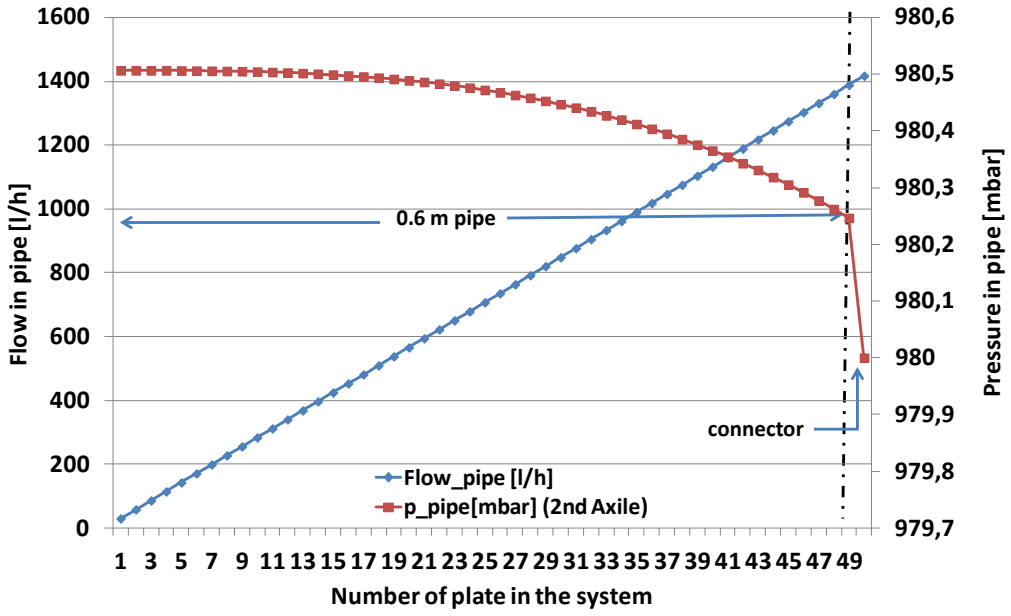

Figure A.5.10 Simulation results: The pressure and flow distribution in the 50 plates system, the TMP is 20 mbar.

In the 50 plates system, the pressure loss caused by pipe friction is only 0.23 mbar which is 45% of total pressure loss in the piping system, while the pressure loss caused by pipe connector is 55%. However compare the pressure loss inside the piping system to TMP on the membrane plate, it is only ~ 2.5% which means the influence of pressure loss in the piping system to the system performance is very small when the number of plates is 50.

The details of pressure loss at different parts of piping system are shown in Figure A.5.11. The pressure loss caused in the pipe becomes higher with the increase of the number of plates. In the system consists of 100 plates, the pressure loss caused by the piping system takes 65% of the total pressure loss. This value becomes 68% with the module consists of 150 plates and 70% with 200 plates.

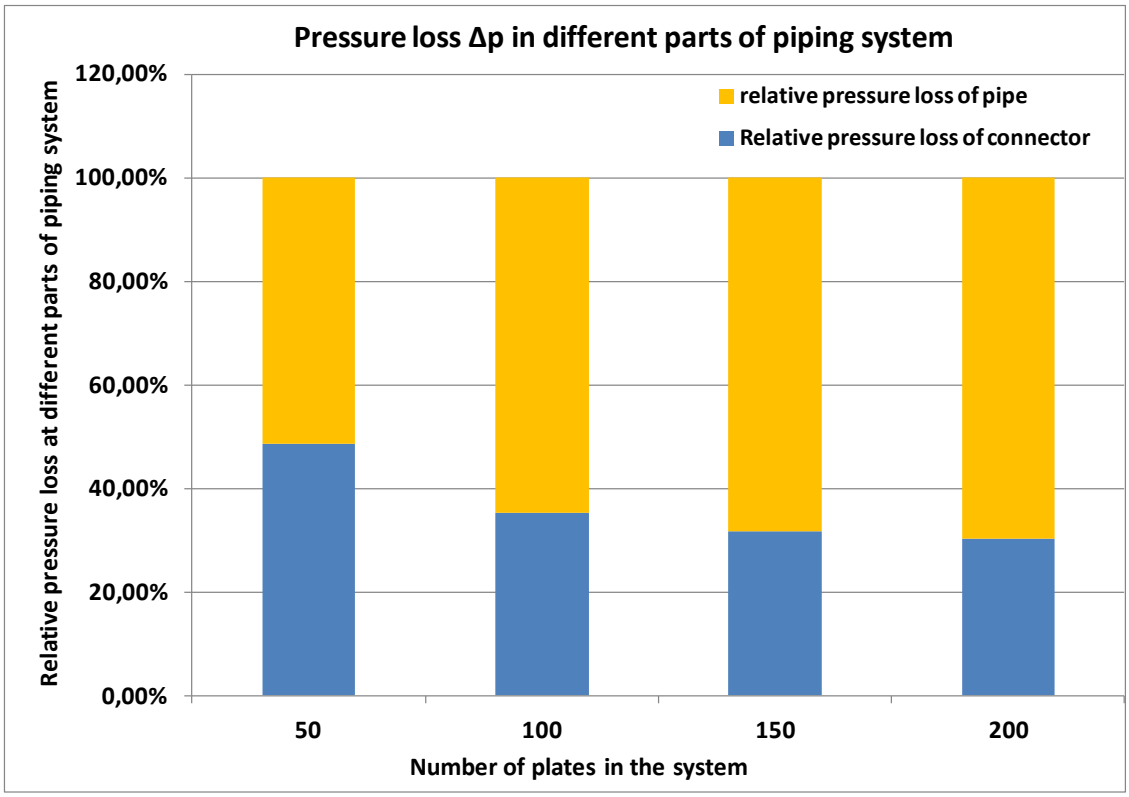

Figure A.5.11 Simulation results: The percentage of pressure loss at different parts of the system with different number plates with 20 mbar TMP

Figure A.5.12 shows the absolute value of the pressure loss caused by the piping system with different number plates. When the number of plates in the system increases 2 times,

from 50 to 100, the total pressure loss increases from 0.5 to 2.5, 5 times increases. From 100 to 200, also 2 times more, the pressure loss increases 3.2 times. From 150 to 200, 1.3 times more, the pressure loss increases to 1.5 times. When the system has 200 plates, the pressure drops caused by the pipe is 8.2 mbar, while the total TMP of system is just 20 mbar. The pressure loss takes 41%. It means that the permeation in 1st plate and last plate along the pipe has 41% difference. The performance of last plate is only about 60% of that of the first plate.

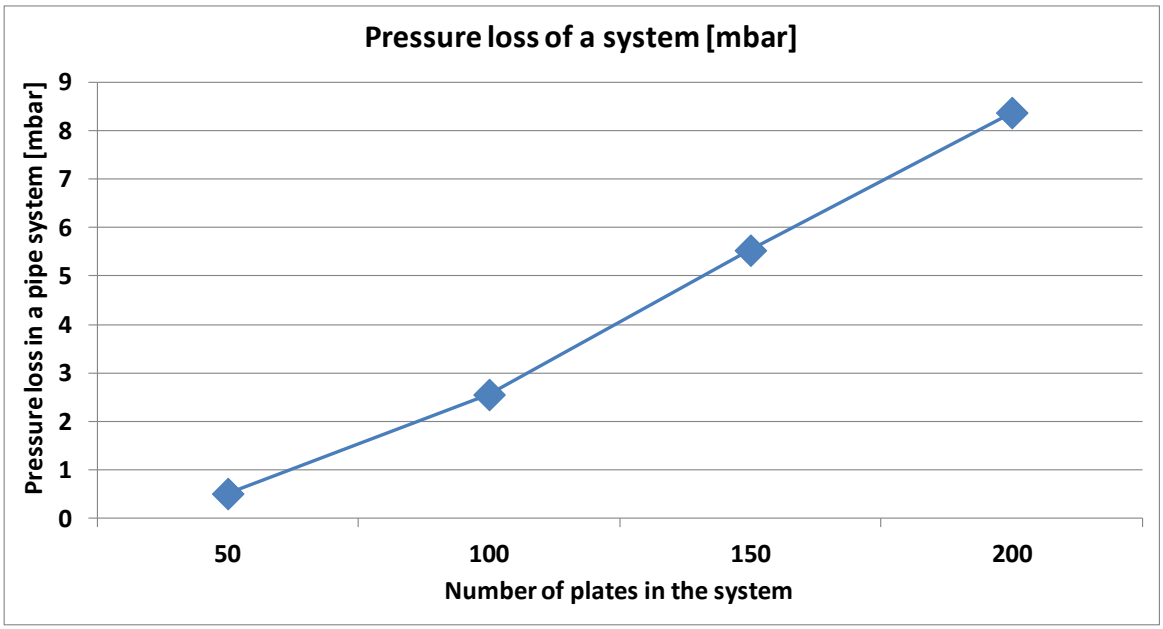

Figure A.5.12 Simulation results: The absolute total pressure loss value of piping system in the system with different number plates with 20 mbar TMP.

A.6 Conclusion

The pillow-shaped membrane filtration system from Microdyn-Nadir was simulated.

Even it is an integrated complex membrane filtration system which consists of pipes system (different shape), pipe connectors, and pillow-shaped membrane plates. With help of porous media approximation method, Calibration-Library-Interpolation method and scale method, the CFD simulation can be done in a low time and hardware cost way.

The geometry influence of plate is checked and compared. Different designs of suction pipe are compared and analyzed. The ellipsoid design has obvious high efficiency whether in the single suction pipe plate or in the double suction pipes plate. Double suction pipes can also lead to high permeation flow with same suction pipe design.

The compression of spacer is also considered as a key parameter which can influence the permeation of the membrane plate. With the compression effect and the porous media approximation method, the permeability change against the increase of TMP is simulated. The first increase and then decrease shows that the TMP for the single plate has an optimized value.

Different designs of connector between ellipsoid suction pipes and circular out let pipe are simulated and compared. The connector with 120 degree has the lower Pressure Loss Coefficient and was applied in the integrated system simulation.

Two parts of pressure loss were shown in the integrated system simulation: the pressure loss in the piping system (including the connector) and the pressure loss in the membrane plates. The piping system’s influence becomes larger with an increase of the numbers of the membrane plates as more permeate is produced and forced through the piping system. The simulation of integrated system is validated and the difference between simulation and experiment is considered acceptable.

9. Appendix B

Moody Chart:

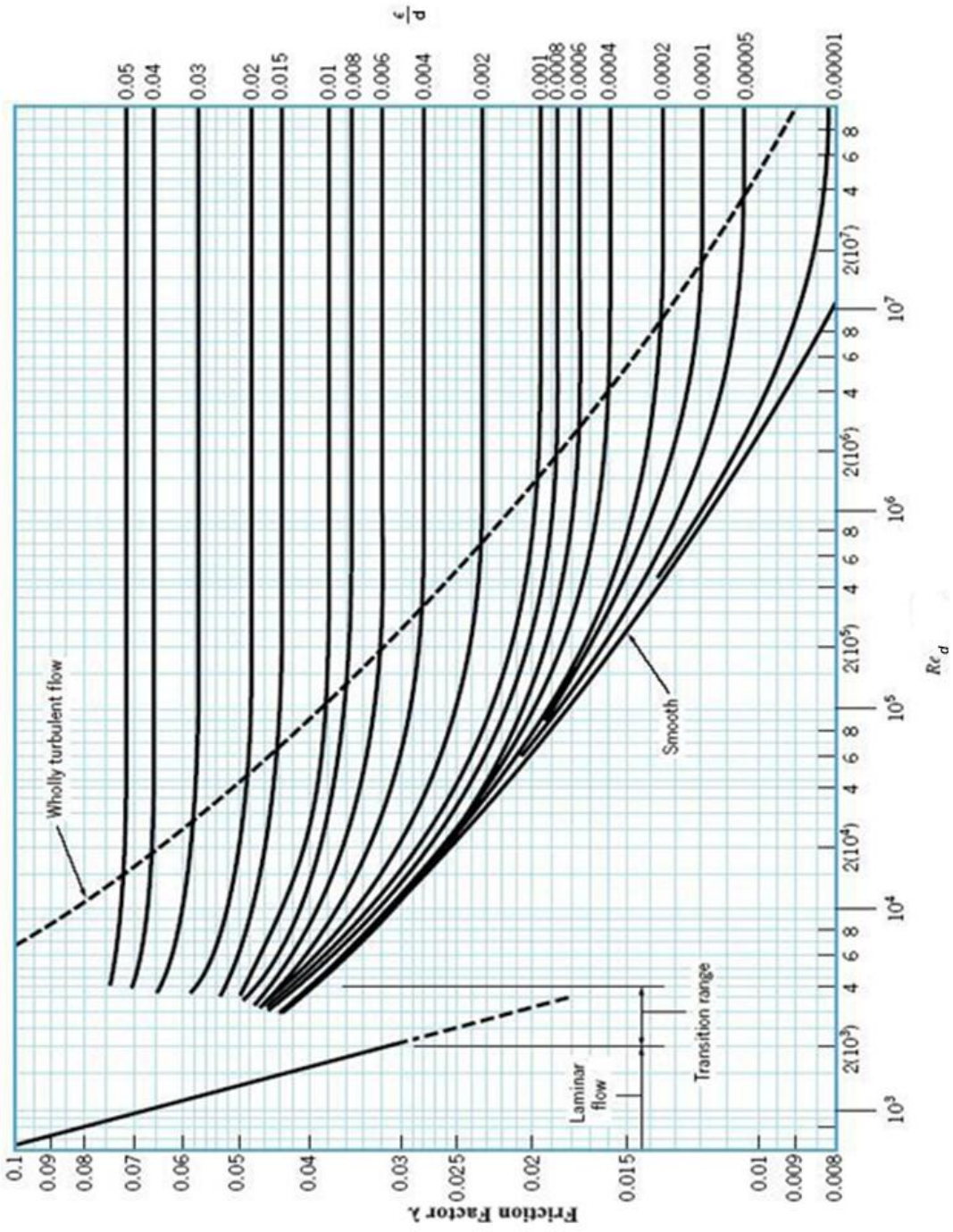

10. Appendix C

Denotation employed in simulation model for inge:

First index:

el = element

pipe = collecting pipe (T-connectors in case of T-rack)

feedpipe = collecting feed pipe (index used for pressure)

permeatepipe = collecting permeate pipe (index used for pressure)

el,feed = element feed side (index used for pressure)

el,permeate = element permeate side (index used for pressure)

mem = on membrane surface (for pressure)

Second index:

top for top;

bot for bottom;

Third index:

r for row, el for element;

r_2,el_3 means third element in the second row

for single collecting pipes with symmetric row arrangement: 1-1 means location in pipe besides element r_1,el_1 and r_2,el_1

fourth index:

flow in: in

flow out: out